Marquette University

e-Publications@Marquette

Dissertations, Theses, and Professional
Projects

Improved Management of Recalcitrant Nutrient Species: Transformation and Adsorption

Synthia Parveen Mallick
Marquette University

IMPROVED MANAGEMENT OF RECALCITRANT NUTRIENT SPECIES:
TRANSFORMATION AND ADSORPTION

by

Synthia Parveen Mallick

A Dissertation submitted to the Faculty of the Graduate School,
Marquette University,
in Partial Fulfillment of the Requirements for
the Degree of Doctor of Philosophy

Milwaukee, WI

August 2022

ABSTRACT
IMPROVED MANAGEMENT OF RECALCITRANT NUTRIENT SPECIES:
TRANSFORMATION AND ADSORPTION

Synthia Parveen Mallick

Marquette University, 2022

Soluble non-reactive nutrient species, i.e., dissolved organic nitrogen (DON) and soluble non-reactive phosphorus (sNRP), are not effectively removed and recovered. Unfortunately, the non-reactive species can cause eutrophication in receiving waterbodies. Thus, removal and recovery of soluble non-reactive nutrients is critical for reducing nutrient discharge and advancing the national goal of enhanced nutrient recovery.

Transformation of non-reactive nutrients to more readily removable/recoverable species using ozonation and UV/H_2O_2 for enhanced nutrient recovery has been reported in literature. Electrooxidation (EO) may outperform these processes in transforming nutrients as EO can utilize multiple oxidation pathways, e.g., in-situ generated oxidants or direct electron transfer (DET). This research evaluated EO for DON and sNRP transformation into more reactive dissolved inorganic nitrogen and soluble reactive phosphorus, respectively.

The efficacy of EO for DON and sNRP transformation into more reactive species was first evaluated in synthetic water matrices. Transformation using EO increased with current density. DON showed less susceptibility towards EO-based transformation compared to sNRP; accordingly, subsequent EO tests focused on sNRP. Compared to UV/H_2O_2, EO transformation consumed up to 2.4 times less energy.

The role of sorbed and dissolved in-situ generated oxidants in EO-based transformation was investigated using quenchers. These results, along with chronoamperometry tests, confirmed that DET was the dominant mechanism for EO-based nutrient transformation. Removal of sNRP using ion exchange improved up to 1.6 times after EO treatment. However, the ion exchanger's affinity for EO-treated sNRP did not improve, suggesting that centrate sNRP removal improved after EO due to decreased organics after EO treatment.

Since EO can be highly energy demanding, selective adsorption might be beneficial for enhanced nutrient recovery. Previous studies reported highly selective orthophosphate adsorption on a phosphate-binding protein (PBP), but sNRP adsorption on PBP has not yet been studied. Thus, adsorption of sNRP using PBP was assessed, showing that 95% of equilibrium sNRP adsorption on PBP takes place within 4 minutes. The sNRP compounds likely bind at PBP's phosphate-selective binding site, and compounds with higher P content were removed to a greater extent.

ACKNOWLEDGEMENTS

Synthia Parveen Mallick

TABLE OF CONTENTS

LIST OF TABLES

LIST OF FIGURES

1. INTRODUCTION

A wide range of treatment processes are available for nitrogen (N) and phosphorus (P) treatment. Conventional treatment processes including biological N removal, enhanced biological P removal, chemical precipitation, coagulation/flocculation/sedimentation, ion exchange, micro- or ultra-filtration, and adsorption generally remove dissolved inorganic N (DIN) and reactive P (Henze, 1991; Venkiteshwaran et al., 2018a). However, dissolved organic N (DON) and soluble non-reactive P (sNRP) are generally not effectively removed in conventional treatment processes, e.g., <40% sNRP removal (Gu et al., 2011; Henze, 1991). The organic fraction of dissolved N is defined as DON while the soluble fraction of P not detectable in a colorimetric test is defined as sNRP (APHA, 2012). Transformation of DON and sNRP to more readily removable/recoverable DIN and soluble reactive P (sRP), respectively, can help utilities meet stringent N and P regulations. Additionally, recovery of the transformed DON and sNRP species will help to advance sustainable nutrient management goals. In addition to transformation of the recalcitrant nutrient species, selective adsorption can enhance nutrient removal and recovery from wastewater.

Transformation of non-reactive nutrients is not widely studied yet. A single recent study reported up to 48% tertiary effluent DON to DIN transformation applying 3 mg/L ozone dose (Ahmadi, 2017). The only two sNRP transformation studies identified in the literature reported greater than 90% transformation of the sNRP compound triethyl phosphate (TEP) to orthophosphate using 100 mg/L H_2O_2 and 28.5 J/cm^2 ultraviolet (UV) fluence and up to $38.1 \pm 2.9\%$ transformation of beta-glycerol phosphate using 0.43 J/cm^2 UV fluence (Sindelar et al., 2016; Venkiteshwaran et al., 2021a). These DON and

sNRP transformation studies (Ahmadi 2017; Sindelar et al., 2016; Venkiteshwaran et al., 2021a), demonstrated that advanced oxidation processes (AOPs) can potentially transform DON and sNRP compounds. However, the extent of transformation and controlling parameters for AOP-based nutrient transformation are yet to be studied to further develop this treatment strategy.

Preliminary results from this research showed that UV/H_2O_2 cannot effectively transform DON compounds as detectable transformation of DON compounds was not achieved. Other AOPs such as electrooxidation (EO) may be advantageous over UV/H_2O_2. EO may leverage a combination of anodic oxidation, oxidation utilizing highly reactive radicals (HO• radicals and others), and direct electron transfer, whereas UV/H_2O_2 processes primarily rely on oxidation via indirect or direct HO• radicals. Degradation of refractory compounds such as emerging contaminants has been reported using EO. For example, 62.5 mg/L of 4-aminoantipyrine (a DON compound) was removed using EO at pH 3.5 with 77.5 mA/cm^2 current density for 7 minutes (da Silva et al., 2018). However, EO can be energy intensive at high applied current, whereas low applied current slows the process.

Greater understanding of the efficiency of transformation using promising AOPs such as EO is needed to assess process feasibility. Additionally, selective adsorption of partially or un-transformed non-reactive nutrients can be helpful for achieving enhanced nutrient recovery while limiting energy inputs.

The objectives of this research were to:

1)   Evaluate electrooxidation for transformation of dissolved organic nitrogen and soluble non-reactive phosphorus to more readily removable and recoverable forms.

Compared to UV/H$_2$O$_2$, EO can utilize multiple pathways for transformation as stated earlier. Therefore, the hypothesis of Objective 1 was that EO would transform DON and sNRP more efficiently, with less energy input, compared to AOPs such as UV/H$_2$O$_2$. The efficacy of EO for transformation of DON and sNRP into DIN and sRP, respectively, was assessed in batch experiments under different EO operating conditions, i.e., current density, mixing speed, electrolyte composition, and solution pH. Transformation of DON and sNRP was assessed in synthetic and wastewater effluent matrices. Each synthetic water matrix contained one of four DON compounds or one of five sNRP compounds representing a range of chemical structures (compounds used in this study are shown in Figure 4.1). The degree of transformation and energy consumption for EO-based transformation was compared with UV/H$_2$O$_2$-based transformation. This objective is presented in Chapter 4.

2)   Assess the mechanism of electrooxidation-based transformation of recalcitrant phosphorus and recoverability of centrate phosphorus after electrooxidation.

Transformation of nutrients may be achieved via multiple EO pathways, e.g., sorbed or dissolved in-situ generated oxidants or direct electron transfer (DET). The oxidation pathways for nutrient transformation were investigated in this objective. Two quenchers were used to distinguish the roles of sorbed and

dissolved oxidants in transformation. Chronoamperometry tests were conducted to evaluate DET of nutrients.

Since EO is an energy intensive process, if partially transformed nutrients can be recovered using ion exchangers, the high energy input needed for achieving complete oxidation might be circumvented. Therefore, recovery of EO-treated sNRP compounds in synthetic and wastewater (e.g., centrate) matrices was assessed in batch LayneRT^{TM} ion exchange experiments with the hypothesis that EO would improve the recoverability of sNRP compounds using ion exchange. This objective is presented in Chapter 5.

3) Evaluate adsorption of recalcitrant phosphorus compounds using the phosphate-selective binding-protein PstS.

Another sNRP recovery pathway could be to adsorb sNRP compounds (without any AOP-based transformation to avoid an energy-intensive AOP) using phosphorus-selective adsorbents. Immobilized phosphate-selective proteins such as PstS, or phosphate-binding protein, (called PBP hereafter), have shown strong performance for adsorption of orthophosphate (Venkiteshwaran et al., 2020). However, PBP adsorption for sNRP removal is yet to be evaluated.

Orthophosphate binds with PBP using 12 strong hydrogen bonds formed between the phosphate molecule's 4 oxygen atoms and the PBP's amino acid residues (Luecke and Quiocho, 1990). Therefore, it was hypothesized that PBP would adsorb sNRP compounds with accessible phosphate functional groups. Batch adsorption experiments were conducted to assess kinetics and isotherm properties of sNRP adsorption on PBP. The affinity of PBP for sNRP adsorption was

assessed using isothermal titration calorimetry (ITC). Competition between orthophosphate and sNRP compounds was also assessed. The controlled release of adsorbed sNRP compounds was evaluated under different pH conditions. This objective is presented in Chapter 6.

In addition to the brief introductions in Chapters 4 – 6, an in-depth review of the literature relevant to DON and sNRP treatment technologies is provided in Chapter 2 and 3, respectively.

2. LITERATURE REVIEW: META-ANALYSIS OF THE PREVALENCE OF DISSOLVED ORGANIC NITROGEN (DON) IN WATER AND WASTEWATER AND REVIEW OF DON REMOVAL AND RECOVERY STRATEGIES

This work was previously published as:

> Mallick, S.P., Mallick, Z., Mayer, B.K., 2022. Meta-analysis of the prevalence of dissolved organic nitrogen (DON) in water and wastewater and review of DON removal and recovery strategies. *Science of the Total Environment, 828,* 154476.

It is republished here, with minor adjustments, with permission from the journal.

2.1. Nitrogen forms and their behavior in aquatic ecosystems and wastewater treatment plants

2.1.1. The importance of nitrogen removal and recovery from wastewater

Nitrogen (N) is one of the key nutrients needed to sustain all living beings. However, excess inputs of nutrients, i.e., N and phosphorus (P) lead to eutrophication and greenhouse gas emissions (Beaulieu et al., 2019). In nutrient management, the emphasis is often on P discharge regulations as P is considered the limiting nutrient in many ecosystems. However, freshwater and coastal waters may be limited by N or co-limited by both N and P under certain conditions, including seasonal and spatial variation (Conley, 1999). Thus, excess N can lead to eutrophication and hypoxic conditions in a range of surface waters (Seitzinger et al., 2002).

Future projections suggest that anthropogenic N inputs to freshwater systems will increase due to urban or agricultural run-off or wastewater sources (Seitzinger et al., 2002; Xie and Ringler, 2017). Wastewater-derived N inputs can account for a large fraction of N flows to natural waters. For instance, approximately 19% of the total nitrogen (TN) in the Chesapeake Bay is derived from wastewater (Mesfioui et al., 2012).

Hence, it is crucial to monitor and regulate anthropogenic N inputs such as wastewater. Additionally, N can increase the formation potential of harmful disinfection by-products (DBPs), e.g., N-nitrosodimethylamine (NDMA) (Krasner et al., 2005).

Another aspect of N management is the potential for recovery of N from wastewater as N is imperative for modern agriculture. The use of N fertilizer (primarily in the ammonium, ammonia, or urea form) increased more than 9-fold between 1961 and 2019 to accommodate the food demands of the world's growing population (International Fertilizer Association, 2019). Unfortunately, the industrial Haber-Bosch process traditionally used for synthesis of ammonium from atmospheric N_2 is expensive and energy intensive (van der Hoek et al., 2018). Recovery of N from wastewater can help reduce dependence on the Haber-Bosch process by reusing N from wastewaters as fertilizer/soil amendments or other products such as biofuel feed stock.

2.1.2. Forms of nitrogen and the importance of the dissolved organic nitrogen fraction

While N removal and recovery from wastewater can contribute to sustainable nutrient management, thereby advancing solutions to one of the National Academy of Engineering's Grand Challenges (2019), existing treatment processes may not effectively target all types of N.

Common N species in aquatic systems occur in both oxidized and reduced inorganic forms (e.g., NO_3^-, NO_2^-, NH_4^+, and NH_3), as organic molecules, and in dissolved and particulate forms. The fraction smaller than 0.20 µm is classified as dissolved N, whereas the larger size fraction is particulate N (Jørgensen, 2009) (Figure 2.1). In conventional wastewater treatment facilities, particulate N is generally well removed during primary treatment, with subsequent biological treatment removing the
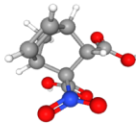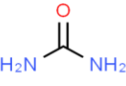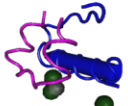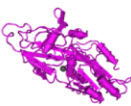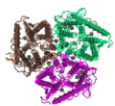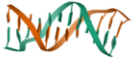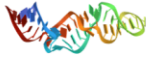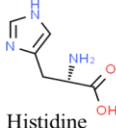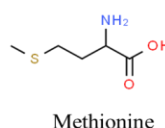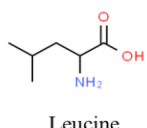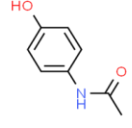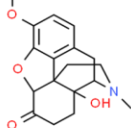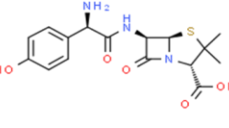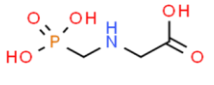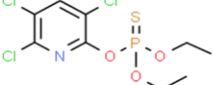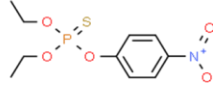
remaining particulate N (Sattayatewa et al., 2010). Among the dissolved species,

dissolved inorganic N (DIN) is most effectively removed in wastewater treatment

facilities. Owing to the lesser extent of DON reactivity, recovery processes also generally

target DIN. However, as dissolved organic N (DON) is more poorly removed/recovered,

it may pass through treatment systems, and can constitute a substantial fraction of

effluent TN.
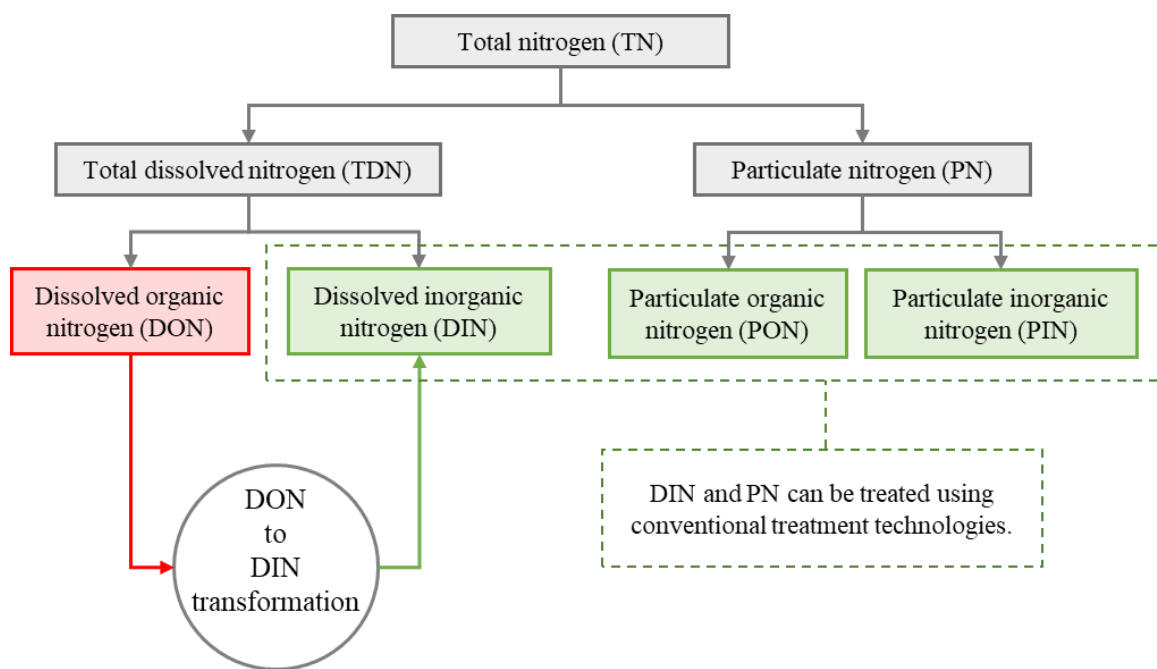
Figure 2.1. Forms of nitrogen (N) in water, modified from APHA (2012). Dissolved inorganic nitrogen (DIN) and particulate N (shaded in green) can be treated effectively using conventional methods, while dissolved organic nitrogen (DON, shaded in red) is not effectively treated with current technologies. Treatment technologies targeting transformation of DON to the more readily removable/recoverable DIN can be employed to achieve effective DON removal and recovery.

Wastewater DON includes proteins, nucleic acids, amino acids, urea, and

micropollutants coming from pharmaceuticals (e.g., flushed medications or release of

pharma compounds through excretion) or agriculture (e.g., pesticides, herbicides,

insecticides, and fertilizer run-off). Examples of wastewater DON compounds are shown

in Figure 2.2.

Figure 2.2. Examples of representative dissolved organic nitrogen (DON) compounds in wastewater. The natural organic matter image was taken from the National Center for Biotechnology Information (2022). Protein and nucleic acid images were taken from the National Institutes of Health (Madej et al., 2014) and RSCB (Berman et al., 2000) databases, respectively, specifically: insulin, PDB ID 1ZNI (Bentley et al., 1976); phosphate binding protein, PDB ID 4OMB (Neznansky et al., 2014); ammonia transporter protein, PDB ID 2B2J (Andrade et al., 2005); DNA, PDB ID 1BNA (Drew et al., 1981); RNA, PDB ID 1CQ5 (Schmitz et al., 1999). All other images were taken from Chemspider.

Anthropogenic sources including wastewater discharges are estimated to contribute 30% of global DON discharge to the environment (Jickells et al., 2017). Thus, treatment processes facilitating wastewater DON removal and recovery can help reduce TN discharge to streams and achieve sustainable nutrient management. The objective of this study was to quantify the occurrence of DON in different water matrices and critically assess currently available N treatment processes in terms of their DON removal and recovery potential.

2.2. Meta-analysis of DON in environmental waters and wastewaters

2.2.1. Occurrence of DON

Understanding the occurrence of DON in environmental waters and wastewater effluents is important for elucidating the potential effects of DON on natural ecosystems. The occurrence of DON and TDN in groundwater, surface water, and wastewater effluent was assessed in this review. Water quality data for groundwaters and surface waters in 2019 were downloaded from the Water Quality Portal (https://www.waterqualitydata.us/portal/; sponsored by the United States Geological Survey [USGS], United States Environmental Protection Agency [EPA], and the National Water Quality Monitoring Council [NWQMC]). This data set includes water quality data collected from more than 400 sites across the United States. The initial search returned more than 630,000 N data points, which were then filtered to include only data for sites reporting both DON and DIN for the sampling event. Most sites did not directly report DON measurements, but for sites reporting dissolved inorganic species (NO_3^-, NO_2^-, and NH_4^+ or DIN) and TDN, DON was calculated as the difference. A full description of the data analysis is available in Section A1 of Appendix A.

For municipal wastewater effluent, discharge data for 2019 was retrieved from the EPA's Enforcement and Compliance History Online (ECHO) website (https://echo.epa.gov/). The initial search returned 72,468 N data points. Like the environmental water data, wastewater effluent data were filtered to include only those with geographic/temporally matched inorganic and organic N measurements, resulting in a total of 168 data points. The ECHO data did not explicitly differentiate between dissolved and particulate species. One-way ANOVA and Tukey post-hoc analyses were performed to determine statistical significance in the datasets using GraphPad Prism 9.3.1 (GraphPad Software, Inc., San Diego, CA).

The variability in TDN and DON in different water matrices is presented in Figure 2.3. The concentration of TDN was significantly higher in wastewater effluent than in groundwater ($p < 0.0001$), which in turn exceeded surface water TDN ($p < 0.0001$). Wastewater effluent TDN was between 0.79 mg N/L and 22.7 mg N/L (median = 4.4 mg N/L, n = 163). Groundwater ranged from 0.1 to 13.7 mg N/L (median = 1.2 mg N/L, n = 106). The concentration of TDN in surface water ranged from 0.011 to 22.8 mg N/L (median = 0.9 mg N/L, n = 11,803). According to the EPA (2013), TDN less than 6 mg N/L does not disrupt environmental ecosystems, although state or regional agencies may impose lower regulations depending on the water quality in local reservoirs. The majority of surface waters assessed here (97%) were below the suggested maximum of 6 mg N/L TDN.

The concentration of DON also varied greatly among the different water matrices, with significantly more DON in wastewater effluent than surface water and groundwater (Figure 2.3b; $p < 0.0001$). Wastewater effluent DON varied from 0.01 to 10.9 mg N/L

(median = 1.1 mg N/L, n = 163). Surface water DON ranged from 0.002 to 14.3 mg N/L

(median = 0.3 mg N/L, n = 11,803), while groundwater DON ranged from 0.005 – 3.24

mg N/L (median = 0.07 mg N/L, n = 106).
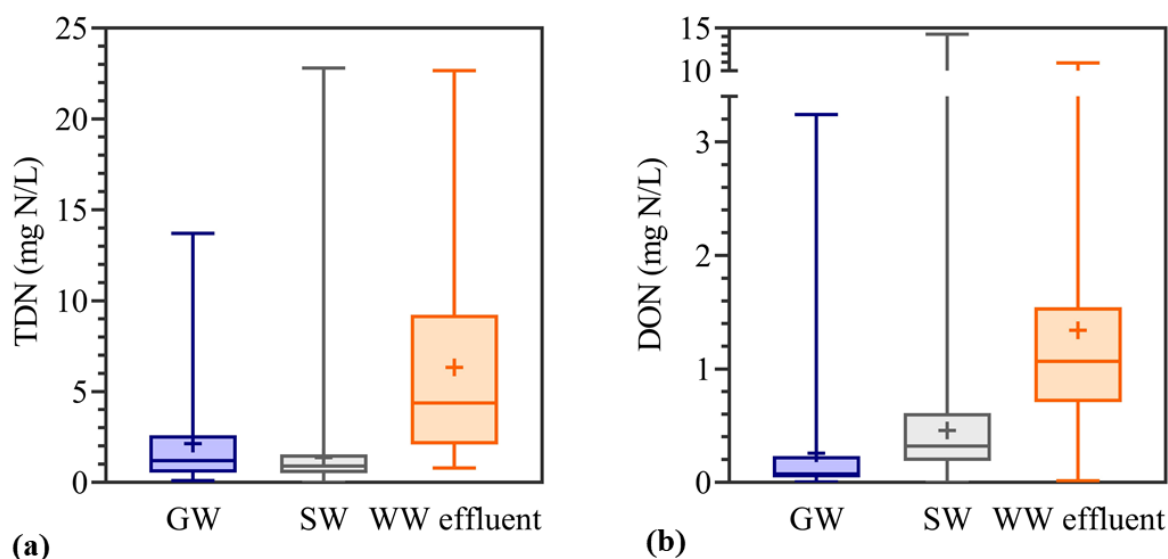
Figure 2.3. Variability of **(a)** total dissolved nitrogen (TDN) and **(b)** dissolved organic nitrogen (DON) concentrations in groundwater (GW), surface water (SW), and wastewater (WW) effluent. Data for groundwater (n = 106 from 75 sites), surface water (n = 11,803 from 1,599 sites), and wastewater effluent (n = 163 from 163 sites) is from the US in 2019. Environmental and wastewater effluent data for these analyses were downloaded from the Water Quality Portal and Enforcement and Compliance History Online (ECHO) websites, respectively. The whiskers represent the minimum and maximum values in the data set, the boxes represent the 25th and 75th percentile values with a median line inside the box, and the mean is shown as a "+" sign.

The ratio of DON to TDN illustrates the prevalence of DON in different water

matrices, where increasing values indicate higher levels of DON relative to DIN.

Generally, in oligotrophic systems where N enrichment is low, DON is the dominant

species, and it may also be an important secondary constituent in enriched hypertrophic

systems (Durand et al., 2011). As shown in Figure 2.4a, the ratio of DON to TDN varied

from 0.3 to 86.7% in groundwater (median = 8.7%, n = 106), 0.1 to 99.7% in surface

water (median = 48.2%, n = 11,803), and 0.07 to 99.7% in wastewater effluent (median = 25.7%, n = 163). The DON to TDN ratio was significantly higher in surface water than in wastewater effluent ($p < 0.0001$), which was in turn greater than groundwater ($p = 0.0047$). The majority of the N was in the DON form for 7.5% of groundwaters, 49.1% of surface waters, and 12.3% of wastewater effluents (Figure 2.4b).
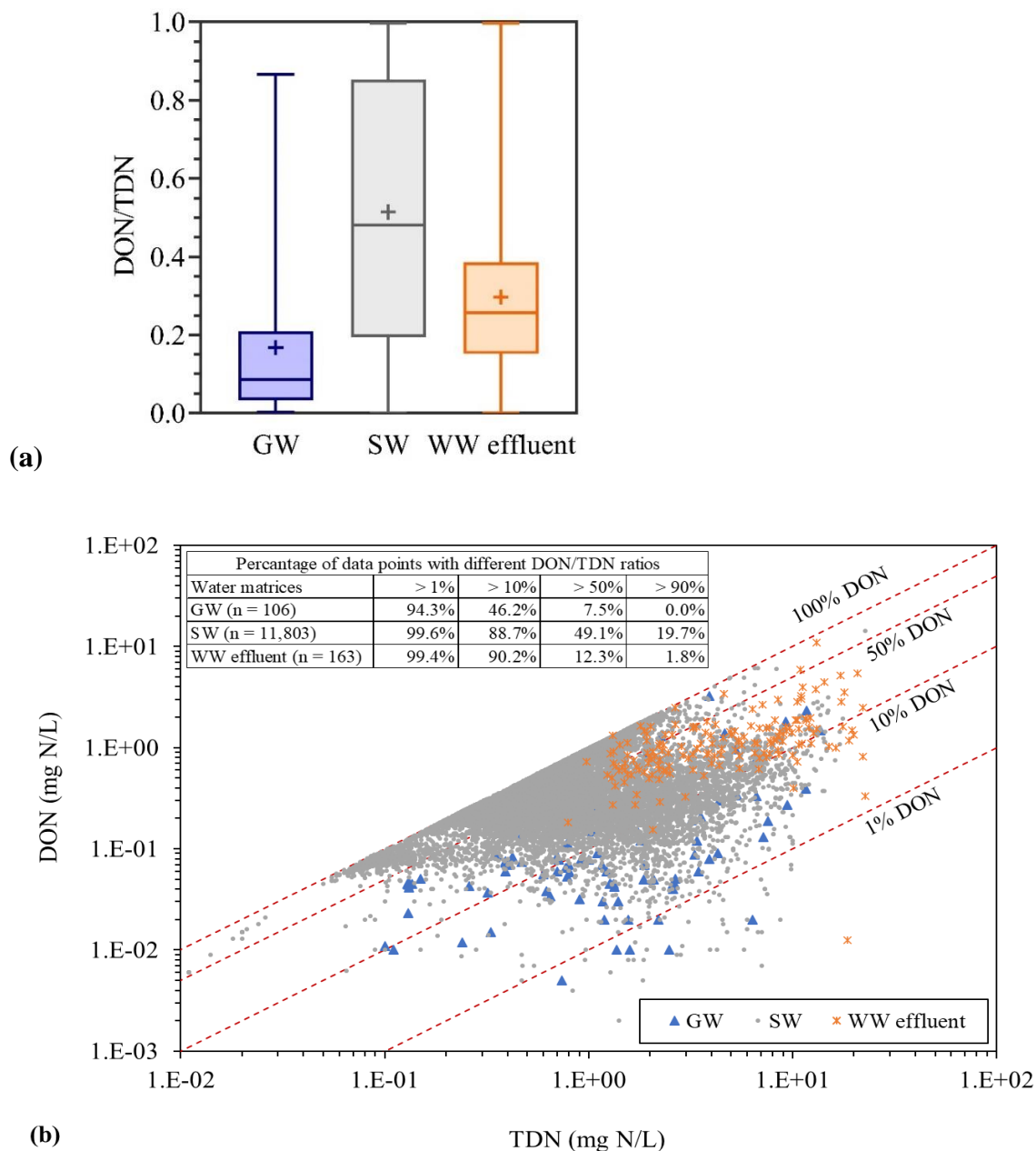
Figure 2.4. (a) Ratio of dissolved organic nitrogen (DON) to total dissolved nitrogen (TDN) in groundwater (GW), surface water (SW), and wastewater (WW) effluents. **(b)** DON versus TDN concentrations in GW, SW, and WW effluent. Data for groundwater (n = 106 from 75 sites), surface water (n = 11,803 from 1,599 sites), and wastewater effluent (n = 163 from 163 sites) includes data points across the US in 2019. Environmental and wastewater effluent data for these analyses were downloaded from the Water Quality Portal and Enforcement and Compliance History Online (ECHO) websites, respectively. The whiskers represent the minimum and maximum values in the data set, the boxes represent the 25th and 75th percentile values with a median line inside the box, and the mean is shown as a "+" sign.

2.2.2. Spatial variation in the occurrence of DON in surface waters in the US

The concentration of TDN, DON, and ratio of DON to TDN in surface water samples varied spatially across the US. Similar analysis was not conducted for groundwater and wastewater, as the datasets had groundwater and wastewater data from only 13 and 8 states, respectively. The TDN and DON analyses are shown in Figure A.1 and Figure A.2 of Appendix A, respectively. Nebraska had significantly higher TDN than all other states ($p \leq 0.0001$) except Iowa ($p = 0.0712$). The highest DON levels, however, were reported in North Dakota ($p \leq 0.0268$). Notably, comparison of DON data among different states is limited as the number of sites with temporally matched DIN, DON, and TDN data varied widely among the states, with some states reporting very few values and others reporting large amounts of data (Figure A.3). Given that organic N is introduced into aquatic and soil ecosystems from terrestrial run-off, leaching, sediment release, active and passive release from phytoplankton, algae, zooplankton, etc. (Berman and Deborah, 2003; Joye and Anderson, 2008), a combination of factors could potentially impact DON prevalence.

The ratio of DON:TDN in surface water for each state is shown in Figure 2.5. Florida reported significantly higher DON:TDN (n = 3,171) than all other states ($p \leq 0.0467$) except for Alaska and Wyoming (which were statistically similar, albeit with much smaller datasets, with 4 and 2 datapoints, respectively). Based on the DON to TDN ratio in the samples, DON accounted for more than 25% of TDN in more than half of the states, while DON constituted the majority of N in almost 20% of the states. Thus, DON can constitute a substantial fraction of TDN in environmental waters and efforts to reduce DON discharges could help to reduce TDN concentrations in environmental waters.
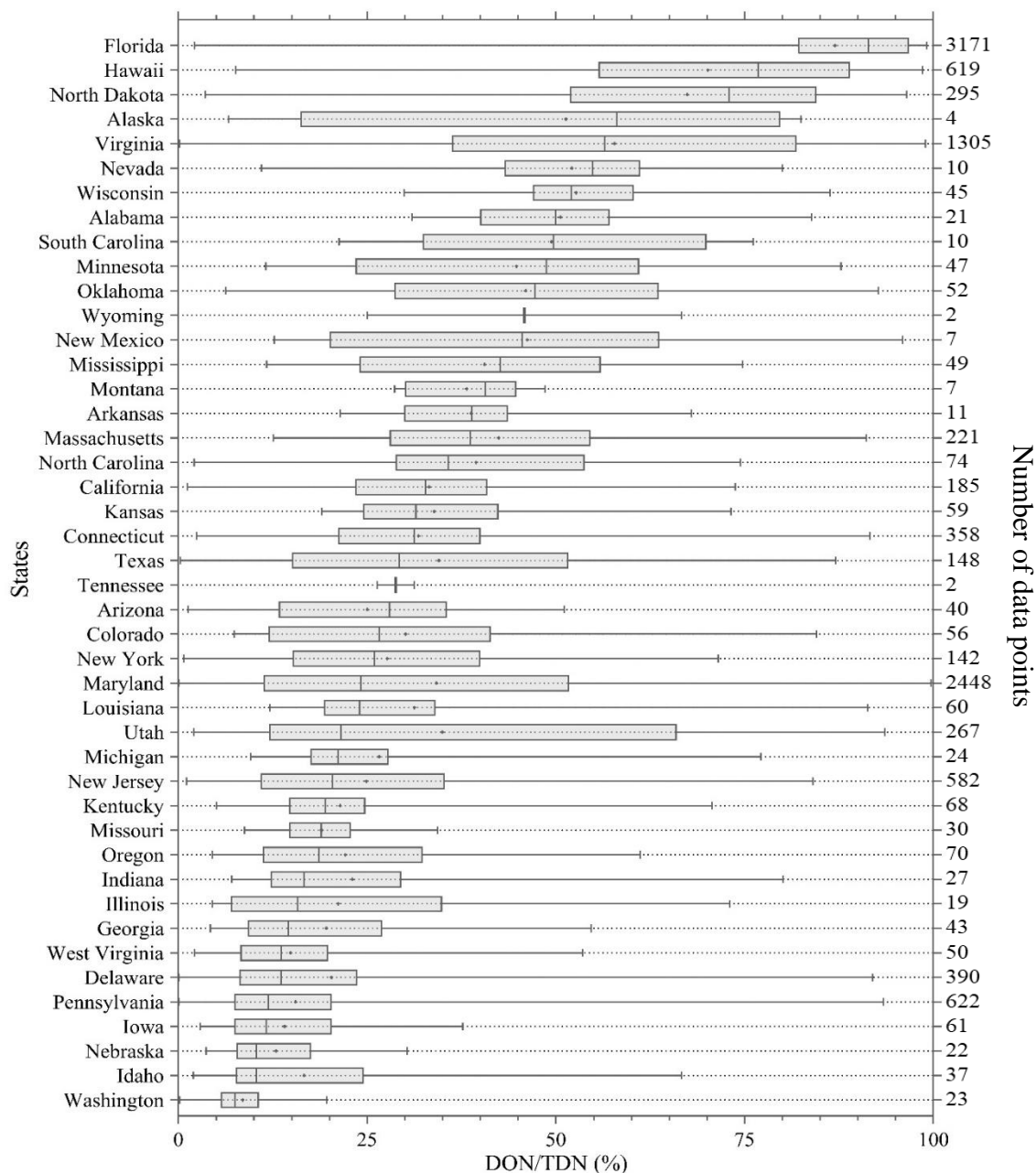
Figure 2.5. Variation of dissolved organic nitrogen (DON) as a fraction of total dissolved nitrogen (TDN) in surface water among 44 different states in the US. Surface water data for these analyses were downloaded from the Water Quality Portal for the year 2019. Data for six states – South Dakota, Ohio, Maine, New Hampshire, Vermont, and Rhode Island – was not available. The whiskers represent the minimum and maximum values in the data set, the boxes represent the 25th and 75th percentile values with a median line inside the box, and the mean is shown with a "•" sign. States are arranged from high to low median DON/TDN (%).

2.3. Significance of DON treatment

2.3.1. DON removal

As shown in Figure 2.4, the majority of the N was present as DON in nearly half of the surface waters analyzed here. Similarly, 60-69% of TDN in rivers, estuaries, and open ocean waters has previously been reported to be DON (Shetye et al., 2019; Sipler and Bronk, 2015). Since DON can bio-assimilate or transform to more bioavailable DIN species over time, it contributes to eutrophication in receiving waters. Moreover, waters with high levels of DON can increase the potential for NDMA or other harmful disinfection by-product formation if the water is used as influent for drinking water treatment purposes. Therefore, DON treatment strategies are important in achieving advanced N management goals.

The degree of eutrophication in an N-limited aquatic system depends on the bioavailability of the N species or the composition of the TN pool. Although DIN is more bioavailable (Ryther and Dunstan, 1971), when DON is present in abundance, it can also be bio-assimilated through several different pathways. For instance, both microbial activity and photochemical reactions (Vähätalo, 2009) can transform DON to bioavailable NH_4^+ and other DIN species. Direct bio-assimilation of DON (without transforming DON to DIN species) is also possible in DIN-scarce aquatic systems, with an estimated 18 – 61% of effluent DON being bioavailable (Urgun-Demirtas et al., 2008). Urgun-Demirtas et al. (2008) observed successful biomass growth utilizing DON as the N source. Additionally, 28 – 61% of effluent DON was assimilated by algae over a 14-day growth period (Qin et al., 2015). Low molecular weight DON compounds like urea and amino acids can also be bio-assimilated by phytoplankton (Bradley et al., 2010).

Wastewater effluent discharge can be one of the major anthropogenic sources of DON release into streams (Hu, et al., 2016). Tertiary effluent DON concentrations typically range from 0.4 – 2.2 mg N/L, often accounting for 65 – 80% of the effluent TDN (Fan et al., 2017) (0.1 to 99.7% in our meta-analysis). Effluent DON contains influent DON that passes through the treatment system as well as microbially-generated DON from microbial growth and biodegradation of organic matter. Microbially-derived DON is released during metabolic processes as well as microbial lysis (Zheng et al., 2021). Differentiating untreated influent DON and microbially-derived DON is difficult, but Hu et al. (2020) recently modeled DON in wastewater and reported that microbially-derived DON theoretically accounts for approximately 50% of total effluent DON.

The bioavailability of N species varies depending on the structure of the compounds. Effluent DON characterization is therefore helpful for understanding bioavailability, and the role of DON in causing eutrophication, which is relevant to selection of effective N treatment strategies (Lee and Westerhoff, 2006). However, effluent DON characterization is challenging, with approximately 70% unidentifiable; thus, effluent DON is often characterized based on size distribution and hydrophobicity (Hu et al., 2016; Yu, 2012). The majority of effluent DON is low molecular weight (67% < 1 kDa), and 93% is hydrophilic (Pehlivanoglu-Mantas and Sedlak, 2006). This low molecular weight, hydrophilic fraction of DON is more bioavailable, and can cause eutrophication (Feng et al., 2019). Additionally, DON compounds may cause hypoxic conditions in aquatic systems by exerting oxygen demand owing to the compounds' bioavailability (Murthy et al., 2006).

In addition to its potential to contribute to eutrophication in receiving waterbodies, DON can also lead to nitrogenous DBP formation, e.g., halonitromethanes, haloacetonitriles, haloacetamides, and N-nitrosamines (Kristiana et al., 2017; Peters et al., 1990). In particular, low molecular weight DON can cause higher NDMA formation (Feng et al., 2019). Speciation of other by-products such as trihalomethanes (THMs) and haloacetic acids (HAAs), both of which are regulated in drinking water in the US, can also be affected by DON. For instance, if the source water contains high levels of DON, HAAs might exceed THMs, and levels of the HAA dihaloacetic acid may increase (Westerhoff and Mash, 2002). Some studies show that HAAs can be more harmful for fetal growth than THMs and dihaloacetic acid may be associated with higher risk for genotoxicity than trihaloacetic acid (Plewa et al., 2010; Porter et al., 2005). Accordingly, wastewater treatment processes capable of removing DON in addition to DIN can help reduce eutrophication and DBP formation potential.

2.3.2. DON recovery

In addition to decreasing anthropogenic N releases to environmental waters, removing N from wastewater offers an opportunity to recover pollutant N as a valuable product, thereby enhancing sustainable nutrient management. Ammonia synthesis constitutes up to 87% of the total energy cost in the fertilizer industry and is also responsible for 1.6 tons of CO_2 emissions and 943 m^3 of natural gas use per ton of ammonia synthesis (Beckinghausen et al., 2020). Reuse of wastewater-derived N can help reduce dependence on energy-intensive industrial ammonia synthesis. Like wastewater N removal, however, DIN species are also the most readily *recoverable* N species as DIN is more reactive than DON. Process selection to encourage DON recovery (in addition to DIN) can therefore help to close the loop for anthropogenic N cycling.

2.4. N treatment processes

Although DON removal and recovery can contribute to sustainable N management goals, typical wastewater N treatment processes (discussed in the following sections) cannot effectively treat DON due to its relative recalcitrance. Table 2.1 summarizes the available N treatment processes and helps shed light on which N species are typically targeted by each process. As shown, no existing processes explicitly target DON removal/recovery, although DON is treated to some extent using several of the technologies.

Table 2.1. Currently available nitrogen (N) treatment technologies and susceptibility of dissolved organic nitrogen (DON) to removal/recovery using these technologies

Technology	Typically targeted N species	Dissolved organic N removal	Current scale of testing	References
Biological Processes				
Biological N removal (BNR)	NH_4^+, NO_3^-	Not targeted, partial removal through hydrolysis	Full-scale	(Eom and Park, 2021)
Anammox, SHARON-Anammox, DEMON-Anammox	NH_4^+, NO_3^-	Not targeted, partial removal through hydrolysis	Full-scale	(Zuo et al., 2020)
Microalgal uptake	NH_4^+, NO_3^-	Not targeted, partial removal through hydrolysis	Full-scale	(Díez-Montero et al., 2020; Nagarajan et al., 2020)
Physicochemical Processes				
Adsorption:				
Layered double hydroxides (LDH)	NH_4^+, NO_3^-, NO_2^-	Up to approximately 1.2 mg DON/g LDH from biochemical leachate tailings	Bench	(Xu et al., 2020)

Technology	Typically targeted N species	Dissolved organic N removal	Current scale of testing	References
Nanomaterials (iron, copper, platinum, manganese, carbon nanotube, nanofibers, nanocomposites such as polymers, graphene-based nanocomposites, Co-Fe_3O_4 activated on peroxymonosulfate)	NH_4^+, NO_3^-	Up to approximately 0.75 mg DON (histidine) / (0.1 g Co-Fe_3O_4 activated on 228 mg peroxymonosulfate)	Bench	(Abdollahbeigi and Asgari, 2020; Han et al., 2021; Luo et al., 2021)
Biochar	NH_4^+, NO_3^-	Significant removal of DON was not reported	Bench	(Clough et al., 2013; Saarela et al., 2020; Zhang et al., 2020)
Activated carbon	NH_4^+, NO_3^-	Up to 72% wastewater effluent DON removal using powdered activated carbon	Full-scale	(Han et al., 2021; Hu et al., 2020; Parkin and McCarty, 1981)
Zeolite, bentonite, natural clay	NH_4^+, NO_3^-	Not reported	Pilot-scale	(Han et al., 2021; Lazaratou et al., 2020)
Metal organic framework (MOF)	NH_4^+, NO_3^-	Up to 95.1 mg DON (bovine serum albumin)/g of MOF-loaded ultrafiltration membrane. Efficiency of ultrafiltration alone was not reported	Bench	(Han et al., 2021; Pishnamazi et al., 2020)
Ion exchange:				
Ion exchange resin	NH_4^+, NO_3^-	10 – 56% DON removal from wastewater effluent	Full-scale	(Czerwionka and Makinia, 2014; Li et al., 2020; Parkin and McCarty, 1981)

Technology	Typically targeted N species	Dissolved organic N removal	Current scale of testing	References
Magnetic ion exchange (MIEX)	NH_4^+, NO_3^-	Up to 0.8 mg DON removal /mL MIEX from wastewater effluent	Bench	(Tang et al., 2021)
Membrane:				
Reverse osmosis (RO)	NH_4^+, NO_3^-, organic	> 90% DON removal from wastewater effluent	Full-scale	(Merlo et al., 2012; Wang et al., 2020; Zheng et al., 2021)
Micro/ultra/nano filtration	NH_4^+, NO_3^-	Limited, as most wastewater DON compounds are less than 1 kDa in molecular weight	Full-scale	(Huang et al., 2021)
Electrochemical:				
Electro-dialysis (ED)	NH_4^+, NO_3^-	Not reported	Pilot-scale	(Mohammadi et al., 2021)
Bio-electrochemical cell (BEC)	NH_4^+, NO_3^-	Up to 37.8 g N/m^2-d urea removal from synthetic wastewater in the absence of competing ions	Pilot-scale	(Arredondo et al., 2015; Sun et al., 2020)
Direct urea fuel cell (DUFC)	Organic N	> 90% urea removal	Bench	(Nangan et al., 2021; Schranck and Doudrick, 2020)
Urea-nitrate fuel cell (UNFC)	Organic N, NO_3^-	Urea removal was reported but not quantified	Bench	(Nangan et al., 2021)
Other physicochemical processes:				
Air stripping	NH_4^+	Up to 7% removal	Full-scale	(Gunes et al., 2020)

Technology	Typically targeted N species	Dissolved organic N removal	Current scale of testing	References
Struvite precipitation	NH_4^+	Not removed as struvite is formed using NH_4^+	Full-scale	(Saerens et al., 2021)
Coagulation	DIN species	Up to 48% removal from river water with $0.25 - 0.35$ mg N/L DON initially	Full-scale	(Lee and Westerhoff, 2006)
Photo-catalysis	NH_4^+, NO_3^-, organic	> 90% removal of nitrobenzene using iron-doped TiO_2	Full-scale	(Feng et al., 2021; Li et al., 2021; Nitoi et al., 2015; Wang et al., 2021)

As shown in Table 2.1, and described in further detail in the following sections, existing full-scale technologies, offer limited DON removal, with the exception of RO and activated carbon. Notably, neither RO nor activated carbon is operated to target DON treatment; thus, limited DON removal may be observed as a byproduct of operation. Bench-scale studies of LDH, ion exchange resin, MOFs, and electrochemical treatments indicate some extent of DON removal, but future research is needed at larger scales in more realistic wastewater matrices.

2.4.1. Biological treatment

In general, the biological processes have limited effectiveness for DON treatment. Some DON is hydrolyzed to NH_4^+ in biological nitrogen removal (BNR) and anammox-based processes (Qian et al., 2017). In typical BNR processes, effluent DON concentrations can range from 1 to 2 mg N/L (Henze, 1991). A survey of four full-scale treatment plants reported that DON decreased from $1 - 3$ mg N/L to $0.69 - 1.42$ mg N/L during BNR (Sattayatewa et al., 2010). Chen et al. (2011) showed that biodegradation

removed up to 39% of DON from wastewater containing an initial concentration of 0.69 – 1.56 mg N/L DON. While biodegradation of DON is possible, it would take place in the absence of DIN species as the DIN species are more easily accessible to microbes. Likewise, removal and recovery of N through microalgal uptake also targets NH_4^+ or NO_3^- in the feedstock as the inorganic N species are more easily bio-assimilated. Microbial uptake of DON is limited to scenarios in which NH_4^+ or NO_3^- are scarce (Díez-Montero et al., 2020; Nagarajan et al., 2020).

2.4.2. Adsorption and ion exchange

Among the different physicochemical processes for N treatment, adsorption is very effective. Parkin and McCarty (1981) reported up to 72% removal of tertiary effluent DON using powdered activated carbon (PAC); however, studies reporting DON recovery using activated carbon are lacking. Moreover, recent reports suggest that wastewater DON is mostly hydrophilic, hence, removal of wastewater DON using activated carbon adsorption might not be effective (Arnaldos and Pagilla, 2010; Pehlivanoglu-Mantas and Sedlak, 2008). Among the various adsorbents, LDHs and nanomaterials reportedly offer potential for organic N adsorption, although no distinction between DON versus PON was reported (Luo et al., 2021; Saarela et al., 2020; Xu et al., 2020; Zhang et al., 2020).

To the author's best knowledge, the only study reporting the use of the emerging metal organic framework (MOF) adsorbent for DON removal showed 98.1% removal of DON (bovine serum albumin) using UiO-66 NH_2 and ZIF-8 MOFs loaded onto polyvinylidene fluoride/chitosan ultrafiltration membranes (Pishnamazi et al., 2020). Although high removal was achieved using MOF adsorption, the process was coupled with ultrafiltration. As bovine serum albumin is a large molecule (approximately 66.5

kDa), it may be readily removed by ultrafiltration alone, whereas removal of low

molecular weight DON compounds using coupled MOF-ultrafiltration is yet to be tested.

Cation and anion exchange resins can reportedly remove wastewater effluent

DON. However, removal efficiency varies depending on the resin's functional groups;

ion selectivity; and the electron density, aromaticity, and hydrophobicity of the target

DON compounds (Jorgensen and Weatherley, 2003). Substantial DON removal using

adsorbents or ion exchange resins might be possible by more selectively targeting

different functional groups of DON compounds (e.g., NH_4^+ selective resins may remove

DON compounds with primary amine groups). However, DON would be outcompeted by

NH_4^+ if the water matrix has a high NH_4^+ content (e.g., wastewater influent).

2.4.3. Filtration

There are some reports of effective DON removal using reverse osmosis (RO) or

micro-, ultra-, or nanofiltration (Huang et al., 2021; Zheng et al., 2021). However, as

most wastewater DON is low molecular weight, micro- and ultrafiltration tend to be less

effective compared to RO. Additionally, membrane fouling is one of the major concerns

for any membrane treatment processes, making DON removal very challenging because

the membranes are more prone to fouling in the presence of low molecular weight DON

compounds (Zheng et al., 2021). In addition to membrane fouling, valence of the DON

compounds, which varies as a function of pH due to deprotonation, might play a role in

the effectiveness of membrane treatment for DON removal. For instance, RO generally

offers selective retention of divalent cations compared to monovalent cations (Biesheuvel

et al., 2019). Thus, it is possible that di- or multivalent DON may be retained while the

monovalent forms of DON pass into the permeate depending on the molecular weight

distribution of the DON compounds.

2.4.4. Electrochemical treatment

Emerging technologies like electro-dialysis (ED) and bio-electrochemical cells (BECs) have limited DON removal. In ED and BEC, DIN species outcompete DON due the higher electrostatic interaction between electrodes and the comparatively more electron-dense DIN species (Rabaey et al., 2010; Ward et al., 2018).

Among the various electrochemical cell configurations, DUFC and UNFC remove the most common wastewater DON compound, urea, and the concentrate can be used as urea fertilizer (with co-recovery of energy from the wastewater). In DUFC, electrocatalysis is used to oxidize urea, with nickel serving as the most common catalyst (Sayed et al., 2019). Indirect oxidation of urea by the intermediate $Ni(OH)_2$ or direct oxidation on the electrode can contribute to DON removal (Sayed et al., 2019). A modification for DUFC is a coupled cell UNFC where urea is oxidized in alkaline media and NO_3^- is reduced in acid media. In both DUFC and UNFC, electricity is generated while wastewater N is lost as N_2 in the atmosphere, negating the potential for recovery of wastewater-derived DON. Both DUFC and UNFC are at the early stages of development, and only bench-scale studies using urea have thus far been reported (Nangan et al., 2021). Large-scale implementation of DUFC and UNFC is currently limited by deficiencies in electron transfer caused by loss of activity in the nickel electrodes over time. Alloying electrodes with materials with greater adsorption affinity for urea, including metals (manganese, cobalt, molybdenum, zinc, and chromium), nickel-phosphite nanoparticles, and sulfur-coated nickel hydroxide nanosheets may improve performance (Nangan et al., 2021; Sayed et al., 2019).

2.4.5. Other physicochemical processes

Alum coagulation with a polydiallyldimethyl-ammonium chloride (polyDADMAC) coagulant aid preferentially removed higher molecular weight compounds > 10 kDa (Lee and Westerhoff, 2006). However, given that the major fraction of wastewater DON is low molecular weight (< 1 kDa), coagulation may offer limited opportunity for DON removal.

Among the different options for photocatalysis, use of Pd-In, Pd-Cu, Pd-Sn, or TiO_2 doped with Mg^{2+} and Zn^{2+} can reduce NO_3^- and/or oxidize NH_4^+ and DON (Chaplin et al., 2007; Wang et al., 2021). However, studies of photocatalysis for DON removal used synthetic matrices containing only DON compounds (amino acid solution containing histidine or phenylalanine) (Nitoi et al., 2015). Thus, research is needed to assess feasibility of photocatalysis for wastewater DON removal.

2.4.6. Transformation for enhanced recovery

Among the DON treatment technologies, adsorption-based approaches can be useful for enhanced N recovery by enabling subsequent desorption of DON, ideally in a pure, concentrated form. However, only activated carbon shows effective DON adsorption, and DON recovery efficacy from activated carbon is yet to be explored. One possible route for DON recovery may be first transforming DON to the more readily removable and recoverable DIN species, which can then be further treated using conventional or emerging processes targeting enhanced N removal and recovery. For instance, once transformed to DIN, the N can be recovered using ion exchange and reused as mineral fertilizer or biofuel feedstock (Kim et al., 2020). Successful transformation of non-reactive species to reactive species, e.g., soluble non-reactive phosphorus to soluble reactive phosphorus, has been demonstrated using UV/H_2O_2 and

electrooxidation (Mallick et al., 2021; Sindelar et al., 2016; Venkiteshwaran et al., 2021a). Similarly, transformation of DON to DIN can be achieved via oxidation or hydrolysis.

Currently, there are limited studies of transformation of DON to DIN species. Ahmadi's (2017) thesis reported up to 48% transformation of tertiary effluent DON to DIN with 120-min of ozonation at a dose of 3 mg/L. This study, however, did not explore the transformation mechanism nor optimized conditions for DON to DIN transformation.

Mallick et al. (2021) explored the feasibility of DON to DIN transformation using UV/H_2O_2 compared to electrooxidation (EO). This study (Chapter 4) analyzed four DON compounds representing four types of wastewater DON (protein, amino acid, micropollutant, and urea) in different size categories (less than or greater than1 kDa). Effective DON to DIN transformation was not achieved using UV/H_2O_2, while transformation of urea was $11.7 \pm 0.09\%$ with 30-minutes of EO treatment (under these treatment conditions, $6.41 \pm 1.49\%$ of wastewater effluent DON was transformed to DIN). Greater transformation was achieved using extended treatment times. Notably, EO-based transformation was higher for the low molecular weight DON compounds, which constitute the major fraction of wastewater DON. This study also showed that susceptibility to EO-based transformation depends on the type of bonds in the DON molecule and their susceptibility to cleavage during oxidation. Oxidation was ostensibly achieved through direct electron transfer, rather than via reactive oxidant species.

Although EO-based DON to DIN transformation was more efficient than UV/H_2O_2 in terms of the degree of transformation and energy consumption, large-scale implementation of EO remains challenging due to high capital cost and maintenance,

including electrode replacement over time. Accordingly, transformation of DON to DIN might be more practical as a process byproduct at utilities with existing UV/H_2O_2 advanced oxidation processes targeting trace organic contaminants. For large-scale implementation, future transformation studies should focus on the efficacy of the process, effective treatment conditions, and the susceptibility of different type of DON compounds.

2.5. Conclusions

Release of DON into natural streams has consequences including eutrophication and formation of NDMA or other by-products if the water is subsequently disinfected. Hence, DON discharge into receiving waterbodies should be accounted for when setting treatment targets. Refractory DON can be bio-assimilated over long periods of time or transformed to bioavailable DIN species, eventually causing eutrophication in natural steams. The meta-analysis presented here demonstrates that DON can account for a large fraction of TDN in wastewater effluent as well as environmental waters. Specifically, DON accounted for the majority of dissolved N in nearly half of the 11,803 surface waters evaluated here. Wastewater effluent had higher DON content compared to environmental waters, but the relative DON fraction was often lower (DON accounted for the majority of dissolved N in less than 15% of wastewater effluents, although 90% of effluents contained more than 10% DON). Removal of DON from wastewater can thus help reduce TN discharges while enabling DON recovery.

Conventional wastewater treatment processes target DIN removal to satisfy location-specific DIN and TN regulations. Thus, DON removal is often low, which precludes its subsequent recovery potential. Activated carbon and RO are currently the

only full-scale technologies with effective DON removal capacity. However, further evaluations of the adsorption-desorption mechanisms are needed to support development of effective DON removal and recovery strategies. Several other treatment technologies, e.g., MOF, DUFC, and UNFC, can target DON removal, but have only been tested at the bench-scale using synthetic water matrices. While DUFC and UNFC can be useful for removing DON, they do not offer DON recovery, as these processes release DON as N_2 into the atmosphere.

One strategy to increase DON treatability is transforming DON compounds to the more readily removable and recoverable DIN species using advanced oxidation processes. After transformation to DIN, the N can either be directly reused (e.g., as biofuel feed stock or mineral fertilizer), or further treated with other processes to recover the N (e.g., ion exchange to recover transformed DIN). While EO-based transformation has been demonstrated, evaluations of the efficacy of DON transformation to DIN and the energy required to do so are needed.

Accordingly, assessments of the efficiency and cost effectiveness of treatment processes, with and without advanced pretreatment to transform DON, are needed. Additionally, the susceptibility of DON compounds in different treatment technologies can vary depending on characteristics such as size, functional groups, and polarity. For instance, DON removal during coagulation depends on molecular size, while functional groups influence DON removal using ion exchange. Hence, deeper understanding of the mechanisms and optimum treatment conditions of different DON treatment technologies is needed to inform the development of full-scale technologies that can help advance progress on the grand challenge of N management.

3. LITERATURE REVIEW: REVIEW OF SOLUBLE NON-REACTIVE PHOSPHORUS REMOVAL AND RECOVERY STRATEGIES

3.1. Phosphorus forms and their behavior in aquatic ecosystems and wastewater treatment plants

3.1.1. The importance of phosphorus removal and recovery from wastewater

Phosphorus (P) is critical for sustaining all living beings. However, harmful algal blooms caused by excess P in surface waterbodies can threaten the sustainability of aquatic ecosystems. About 21% of global P release into surface waters is waste-derived (Cordell and White, 2014). Release of P into surface waterbodies therefore needs to be controlled. Hence, treatment technologies targeting enhanced P removal are critical.

Another aspect of P management is to recover P to offset the anthropogenic need for mined P. To meet needs for global food production, the demand for mined P is projected to increase from 18 Mt to 23 – 52 Mt by 2100, a 28 – 189% increase in demand (Helin and Weikard, 2019). Recovery of wastewater-derived P can help meet increasing demand for P fertilizers. A sustainable P management strategy would therefore aim to decrease P discharge into waterbodies and recover waste-derived P to achieve more sustainable P management.

3.1.2. Forms of phosphorus and the importance of the soluble non-reactive fraction

While sustainable P management strategies aim for enhanced P removal and recovery from wastewater, currently available treatment technologies may not effectively treat all forms of P. Aquatic P species can be in both particulate and soluble forms. Moreover, both particulate and soluble P can be in reactive and non-reactive forms. According to the Standard Methods (APHA, 2012), detectable P in a colorimetric test is defined as reactive P while the remaining P is classified as non-reactive P. The non-

reactive P is detectable after complete hydrolysis or digestion. Different forms of P species are shown in Figure 3.1. while different forms of sNRP compounds are shown in Figure 3.2.
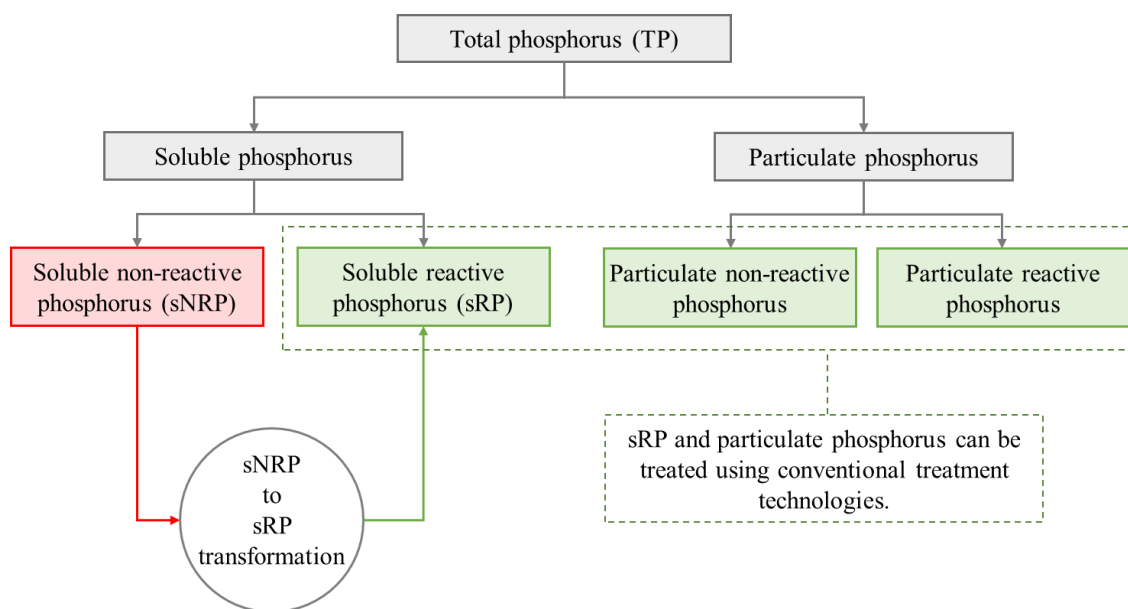
Figure 3.1. Forms of phosphorus (P) in aquatic systems, modified from APHA (2012). Soluble reactive P (sRP) and particulate P (shaded in green) can be effectively treated using conventional methods, while soluble non-reactive P (sNRP, shaded in red) is not effectively treated with current technologies. Treatment technologies targeting transformation of sNRP to more readily removable/recoverable sRP can be employed to enhance P removal and recovery.

In conventional wastewater treatment facilities, particulate P is generally removed during primary settling (Venkiteshwaran et al., 2018a). Among the soluble P species, sRP is effectively removed while the soluble non-reactive P (sNRP) form is generally not well removed owing to its lack of reactivity. Different forms of sNRP compounds include organic P and inorganic polyphosphates (metaphosphate, di-, tri-, tetraphosphates, etc.), as shown in Figure 3.2. Less than 40% sNRP is typically removed during conventional P removal (Gu et al., 2011). Consequently, effluent P may contain 26 – 81% of total P (TP)

in the sNRP form (Qin et al., 2015). Accordingly, treatment technologies targeting sNRP

removal and recovery can offer a more sustainable approach towards P management by

enhancing P removal and recovery.
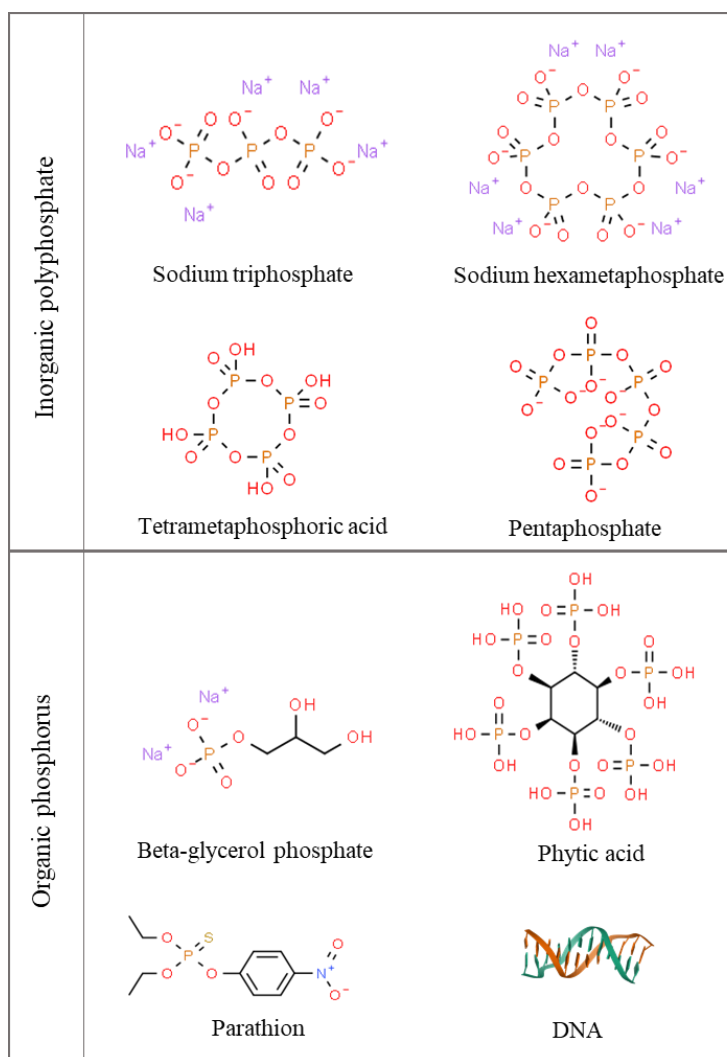
Figure 3.2. Different types of soluble non-reactive phosphorus (sNRP) compounds. Both organic and inorganic phosphorus compounds can be from natural (i.e., plant or microbial) or synthetic sources (anthropogenic). All molecular structures were taken from Chemspider. The image of DNA [PDB ID 1BNA (Drew et al., 1981)] was taken from the RSCB database (Berman et al., 2000).

3.2. Prevalence of non-reactive P in wastewater effluent

An analysis of the occurrence of sNRP in surface waters can be found in Venkiteshwaran et al.'s (2018a) P meta-analysis study. In this current review, the sNRP fraction in wastewater discharge was analyzed. To analyze wastewater-derived non-reactive P discharge into receiving waterbodies, a meta-analysis of P discharge was conducted. Wastewater discharges for 2019 were retrieved from the EPA's Enforcement and Compliance History Online (ECHO) website (https://echo.epa.gov/). Wastewater discharge data includes wastewater P loading from municipal utilities and industrial sources, which is useful in analyzing the total mass of P discharged into waterbodies (concentrations of wastewater P could not be retrieved from the ECHO database). The initial search returned 19,988 P data points. These data were filtered to include only those with geographic/temporally matched total and reactive P measurements, resulting in a total of 571 data points. The ECHO data did not explicitly differentiate between dissolved and particulate species.

The highest TP loading to receiving waterbodies was 9.6 million lb/year, although the highest non-reactive P discharge was 6.8 million lb/year in 2019 (Figure 3.3a). The median loadings were 2,239 and 546 lb/year for TP and non-reactive P, respectively. As shown in Figure 3.3b, up to 100% of TP discharge can be in the non-reactive P form, although the median was 33% (mean = 37.4%, n = 571). The majority of the discharged P was non-reactive in 32.2% of the 571 facilities. Non-reactive P accounted for greater than 90% of the TP discharge in 4% of the facilities (Figure 3.4). The spatial variation of percentage of non-reactive P loading in wastewater discharge across the states is shown in Figure 3.5. Notably, the dataset included points for only 22 states and some states

reported very limited data (<5 points), as shown in the secondary y axis of Figure 3.5. Given the sparsity of data, statistical analyses of differences in spatial loading were not possible.
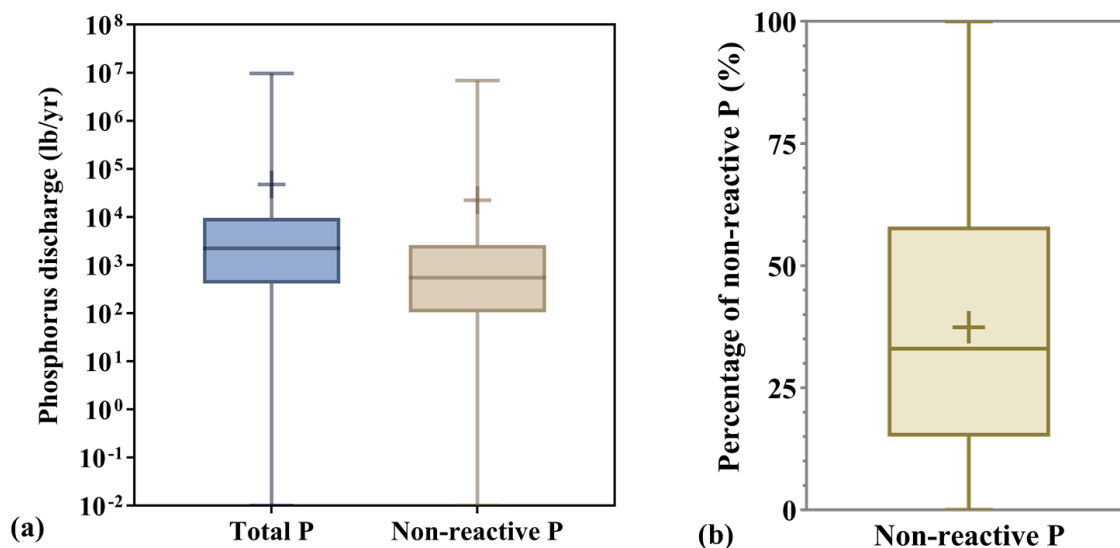
Figure 3.3. Variability of **(a)** total phosphorus (TP) and non-reactive P loading and **(b)** percentage of non-reactive P in wastewater effluent TP discharge. Data for wastewater effluent (n = 571 from 571 sites) was from the Enforcement and Compliance History Online (ECHO) website from the US in 2019. The whiskers represent the minimum and maximum values in the data set, the boxes represent the 25th and 75th percentile values with a median line inside the box, and the mean is shown as a "+" sign.
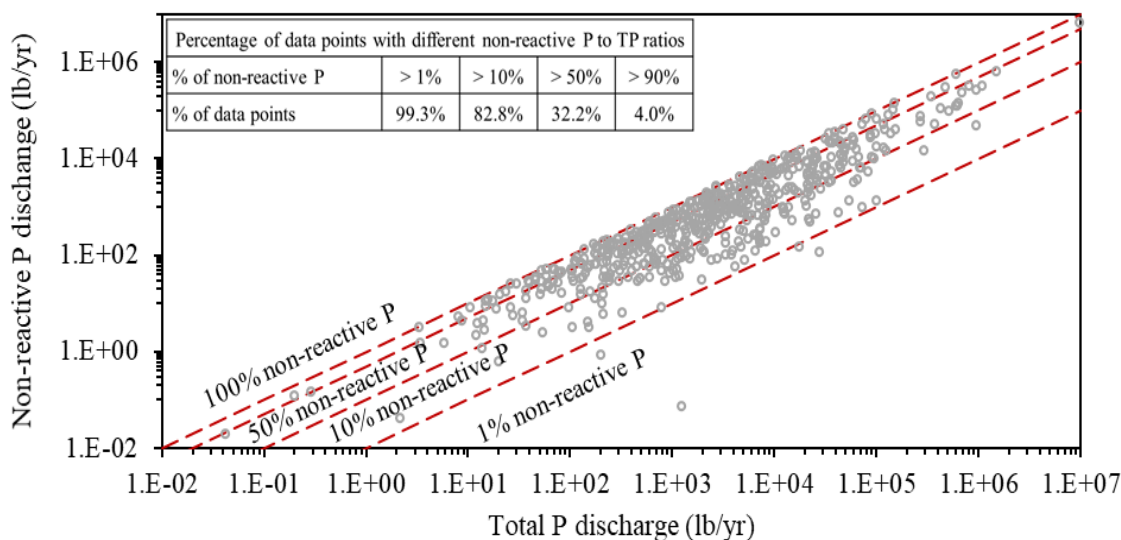
Figure 3.4. Non-reactive phosphorus (P) versus total phosphorus (TP) loading in wastewater effluent. Data includes 571 points from 571 sites across the US in 2019 downloaded from the EPA's Compliance History Online (ECHO) website.

As shown, a substantial fraction of the wastewater effluent TP can be in non-reactive forms. Consequently, receiving environmental waters may contain a substantial amount of non-reactive P. However, reports of non-reactive P in environmental waters are very limited as most studies or databases report sRP and TP fractions. A recent meta-analysis of different P fractions in environmental waters, municipal wastewaters, and manures included particulate P, sRP, and TP data, but the sNRP fraction was not reported (Venkiteshwaran et al., 2018a). Among the limited studies reporting sNRP fractions in environmental waters, Yoshimura et al. (2007) reported that sNRP may comprise 5 – 83% of TP in the North Pacific waters. Another report found that 6 – 40% of total soluble P can be in the sNRP form (Monbet et al., 2009). When released into environmental waters, the non-reactive forms can cause eutrophication either via direct bio-assimilation or after enzymatic transformation to sRP (Qin et al., 2015). Therefore, to decrease TP

discharge and reduce the negative effects of excessive P levels in environmental waters,

wastewater treatment targeting reduction of sNRP as part of TP management is critical.
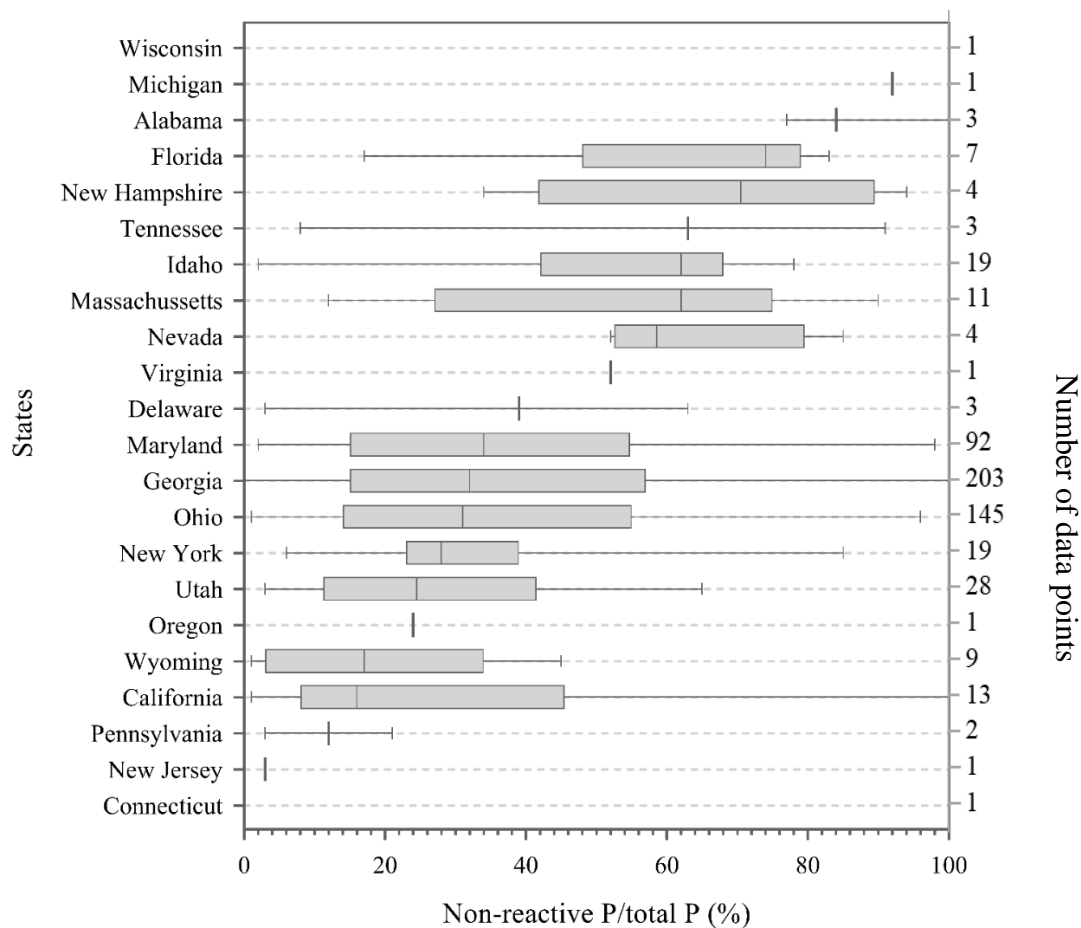
Figure 3.5. Spatial variation of percentage of non-reactive phosphorus (P) across states in the US. A total of 571 data points were found for 22 states. The number of data points reported for each state is as shown in the secondary y axis. The data is from 571 sites across the US in 2019 and was downloaded from the EPA's Compliance History Online (ECHO) website. The ECHO database did not distinguish between particulate and soluble forms. Connecticut and Wisconsin have only one data point each with 0 and 100% non-reactive P loading, respectively.

3.3. Significance of sNRP treatment

Although sRP is generally more bioavailable than sNRP in aquatic ecosystems, studies suggest that some sNRP, e.g., organic P compounds, can also be bioavailable. For instance, many cyanobacteria, i.e., *Trichodesmium,* can utilize organic P compounds for growth by hydrolyzing the P-O-C bonds (Sañudo-Wilhelmy, 2006). There is also evidence of organophosphate and phosphonate uptake by microorganisms (Santos-Beneit et al., 2008). Qin et al. (2015) reported that an algal culture utilized 73 – 75% of sNRP in wastewater effluent within 14 days. Another study of bioavailability of sNRP across 27 estuaries in Midwestern US states reported that more than 95% of the sNRP species were bioavailable in 8 lakes; the median bioavailable sNRP fraction was 78% across the 27 estuaries (Thompson and Cotner, 2018). In addition to direct bio-assimilation, phosphatases, phosphohydrolases, etc. can also transform organic P compounds into more bioavailable reactive P forms, which can further contribute to algal blooms (Zhu et al., 2017). Therefore, sNRP in wastewater discharge should be reduced (beyond solely focusing on sRP). Moreover, as sNRP can account for a substantial fraction of wastewater effluent TP, overall TP discharge can be reduced by targeting sNRP treatment.

Additionally, enhanced P recovery can also be achieved by targeting sNRP recovery. Owing to its lesser extent of reactivity, recoverability of sNRP is also low. Currently available P recovery strategies, e.g., struvite precipitation, generally target sRP. Since sNRP comprises a substantial fraction of wastewater effluent (e.g., median sNRP/TP = 33% according to the meta-analysis conducted in this study), effluent sNRP removal and recovery would greatly contribute to overall P recovery goals.

3.4. sNRP treatment processes

Owing to its recalcitrance, sNRP is typically not removed or recovered effectively with existing water treatment technologies, as discussed in the following sections. Venkiteshwaran et al. (2018a) previously reviewed P removal processes and found that the available wastewater processes are generally effective for removal of particulate P and sRP. That review examined sNRP to sRP transformation processes, but no previous studies have thoroughly reviewed the efficiency of sNRP removal using traditional P removal processes. Here, a summary of available P treatment processes is presented in Table 3.1, along with the effectiveness of each process for sNRP removal. As shown in Table 3.1, sNRP is not typically removed or recovered effectively.

Table 3.1. Currently available phosphorus (P) treatment technologies and susceptibility of soluble non-reactive P (sNRP) to removal/recovery using these technologies.

Technology	sNRP removal/recovery	Current scale of testing	References
Biological processes			
Enhanced biological P removal (EBPR)	< 40% sNRP removal in full-scale EBPR process	Full-scale	(Gu et al., 2011)
Microalgal uptake	Up to 75% uptake of sNRP from wastewater effluent	Full-scale	(Qin et al., 2015)
Constructed wetland	$87.2 \pm 16.6\%$ removal of sNRP compounds	Full-scale	(Liu et al., 2019)
Physical-chemical processes			
Precipitation:			
Precipitation with metal salts, e.g., ferric chloride	Not typically removed	Full-scale	(Bunce et al., 2018)
Struvite precipitation	Not typically removed	Full-scale	(Lorick et al., 2020)

Technology	sNRP removal/recovery	Current scale of testing	References
Adsorption:			
Activated carbon	Up to 14.5 mg/g removal of the sNRP compound triphenyl phosphate	Full-scale	(Wang et al., 2018a)
Hierarchical porous magnesium oxide (Hr-MgO)	Up to 185 mg/g Hr-MgO removal of the sNRP compound chlorpyrifos	Bench	(Sharma and Kakkar, 2017)
Nanomaterials (carbon nanotube)	1.6 mg/g removal of the sNRP compound malathion	Bench	(Campos do Lago et al., 2020)
Resins (XAD4, XAD7hp)	Up to 20.1 mg/g removal of the sNRP compound triphenyl phosphate	Bench	(Wang et al., 2018b)
Lanthanum-aluminum hydroxide	Up to 36.4 mg P/g removal of sNRP compound myo-inositol hexakisphosphate	Bench	(Xu et al., 2020)
Oxidation:			
UV/H_2O_2, Fenton, and photo-Fenton	50 – 70% removal of the sNRP compounds profenofos, diazinon, and fenitrothion at initial concentrations of 50 mg/L	Full-scale	(Badawy et al., 2006)
Laser irradiation	> 90% removal of the sNRP compound diazinon with an initial concentration up to 40 mg/L using 180 mJ of energy	Bench	(Trebše and Franko, 2002)
X-ray irradiation	50% removal of diazinon with an initial concentration of 40 mg/L by applying 160 Gy	Bench	(Trebše and Arčon, 2003)
Sonochemical treatment	Up to 96% degradation of the sNRP compound omethoate	Bench	(Farooq et al., 2003)

Technology	sNRP removal/recovery	Current scale of testing	References
UV/TiO$_2$ (sequential train of ultrafiltration, TiO$_2$ adsorption, and UV/TiO$_2$)	Up to 58% removal of wastewater effluent sNRP where the initial sNRP concentration was 8 µg/L.	Bench	(Gray et al., 2020)

As shown in Table 3.1, and described in further detail in the following sections, existing full-scale P treatment technologies, e.g., enhanced biological P removal (EBPR) generally do not remove sNRP effectively. The other available full-scale biological processes, i.e., microalgal uptake and constructed wetlands, remove sNRP when the system lacks sufficient sRP. As shown in Figure 3.4, only 4% of the wastewaters surveyed had <10% reactive P; accordingly, the ubiquitous presence of reactive P will generally limit sNRP removal by biological processes. Generally, full-scale application of microbial uptake or constructed wetlands do not specify sNRP removal.

Among the different physical-chemical processes, precipitation is an effective process for achieving low P discharge. However, the chemical precipitation mechanism makes it difficult for sNRP removal applications. In aqueous solution, P precipitates by chemically binding with metal oxides or other ligands (e.g., ammonium). Calcium phosphate, ferric phosphate, struvite (ammonium magnesium phosphate), etc. are formed using the orthophosphate form of P. Thus, sNRP compounds are not removed using precipitation processes.

Some adsorption processes offer sNRP removal, but most of these technologies are currently limited to bench-scale testing. Hierarchical porous magnesium oxide (Hr-MgO), carbon nanotube, and XAD resins are reported to remove sNRP compounds in synthetic matrices spiked with only sNRP compounds (Campos do Lago et al., 2020;

Sharma and Kakkar, 2017; Wang et al., 2018b). In addition, hybrid anion exchangers and polymeric hydrogels also offer limited sNRP removal (Mayer et al., 2013). However, to implement these processes in full-scale, the efficacy of sNRP removal in wastewater matrices must be assessed. The only currently implemented full-scale technology for adsorption-based sNRP removal is activated carbon. While activated carbon is not generally installed in full-scale plants to specifically remove sNRP compounds, some sNRP removal might be achieved as a byproduct of the process. In their study of activated carbon for sNRP removal, Wang et al. (2018a) spiked lab-grade sNRP compounds but did not specifically assess wastewater sNRP removal efficacy. Wastewater sNRP removal efficiency using activated carbon will likely be negatively affected by the presence of competing organics.

There are reports of several oxidation processes being assessed for degradation of sNRP compounds. Among the reported processes, UV/H_2O_2 is a full-scale implementable process. Badawy et al. (2006) reported removal of spiked sNRP compounds using UV/H_2O_2. Similarly, emerging technologies like X-ray, laser irradiation, and sonochemical treatment also reported sNRP removal in synthetic water matrices (Farooq et al., 2003; Trebše and Arčon, 2003; Trebše and Franko, 2002). Sequential treatment using ultrafiltration, adsorption on TiO_2, and UV/TiO_2 in sequence was reported to degrade wastewater effluent sNRP (Gray et al., 2020). Gray et al. (2020) indicated that removal of wastewater effluent sNRP was likely facilitated by transformation of sNRP compounds to more readily removable sRP compounds using UV/TiO_2.

The full-scale physical-chemical processes (precipitation processes) either do not remove sNRP, or the processes are not operated to target sNRP removal (oxidation

processes, activated carbon); thus, limited sNRP removal may be observed as a byproduct of operation. Bench-scale studies of adsorptive materials and oxidation processes show some sNRP removal, but more work is needed to support implementation of these processes at full-scale in more realistic wastewater matrices. Specific needs include determining the selectivity of adsorbents for sNRP removal, operating conditions to achieve successful removal of sNRP using adsorbents or oxidation processes, and energy inputs for effective removal.

As discussed in this section, wastewater sNRP removal technologies are currently limited. Similarly, recovery of sNRP compounds is not generally effective using current technologies. The recalcitrant sNRP species can be more easily removed if sNRP is transformed into more readily removable sRP species. Similarly, transformation of sNRP to sRP compounds would also enhance recoverability of P as sRP species are more readily recoverable.

3.5. Transformation of sNRP for enhanced P removal and recovery

Transformation of sNRP compounds to more reactive sRP species can offer a recovery pathway for achieving enhanced P recovery. The transformed sRP species might be recovered using chemical precipitation, such that the precipitate can be reused as fertilizer. Use of ozonation for transformation of recalcitrant N species into more readily removable/recoverable species was reported by Ahmadi (2017). Similarly, sNRP species might be transformed into sRP species to facilitate P recovery.

Currently, there are limited studies reporting sNRP to sRP transformation, including three studies reporting sNRP to sRP transformation using UV/H_2O_2 or UV/TiO_2 (Gray et al., 2020; Sindelar et al., 2016; Venkiteshwaran et al., 2021a). Among

these studies, Gray et al. (2020) did not specifically assess the extent of transformation achieved using UV/TiO_2. In that study, the authors observed removal of sNRP species and concluded that the removal was likely caused by sNRP to sRP transformation. Sindelar et al. (2016) evaluated transformation of the sNRP compound triethyl phosphate using UV/H_2O_2 and reported greater than 90% transformation using 100 mg L^{-1} H_2O_2 and 28.5 J cm^{-2} UV fluence. Venkiteshwaran et al. (2021a) assessed UV/H_2O_2 transformation efficacy of five sNRP compounds, achieving a maximum of 38.1±2.9% transformation of the sNRP compound beta-glycerol phosphate with 34 mg L^{-1} H_2O_2 and 0.43 J cm^{-2} UV fluence. Venkiteshwaran et al. (2021a) also assessed wastewater effluent sNRP transformation efficacy using UV/H_2O_2, but did not achieve any detectable transformation. Since UV/H_2O_2 is not effective in wastewater sNRP transformation, future research is needed to identify alternate approaches to achieve wastewater sNRP transformation.

Electrooxidation (EO) is another possible technology to transform sNRP into sRP. In EO, oxidation can be achieved through multiple pathways, i.e., direct electron transfer on the anode, in-situ generated dissolved or anode-sorbed oxidant species (e.g., HO•, $S_2O_8^{2-}$, $C_2O_6^{2-}$, Cl_2, ClO_4^{-}, SO_4•$^{-}$, Cl•, etc.), or a combination of these pathways (Barazesh et al., 2016; Moreira et al., 2017). Thus, EO can be advantageous over UV/H_2O_2 in achieving more effective transformation. Although EO is being extensively studied for treatment of emerging micropollutants and other recalcitrant compounds, P transformation studies are still not available. Future research is needed to assess the feasibility of EO for sNRP to sRP transformation, especially in realistic wastewater matrices.

3.6. Adsorption and desorption for sNRP removal and recovery

Among the sNRP treatment technologies, adsorption-based processes may be utilized for enhanced P recovery by enabling subsequent desorption of sNRP in a concentrated form. However, the limited sNRP adsorption studies to-date targeted removal of sNRP compounds and did not assess sNRP desorption efficacy.

Highly selective phosphate adsorbents or ion exchangers (e.g., LayneRT[TM] or phosphate-binding protein [PBP] resin) might be useful in removing sNRP compounds with terminal orthophosphate functional groups. For instance, the phosphate-binding protein PstS offers very high affinity towards phosphate and strong selectivity for phosphate even in presence of other oxyanions, e.g., arsenate (Venkiteshwaran et al., 2021b). Immobilized PBP showed higher affinity and faster adsorption of phosphate compared to the phosphate-selective ion exchanger, LayneRT[TM] (Hussein and Mayer, 2022; Venkiteshwaran et al., 2020). Phosphate binds with PBP by forming 12 strong hydrogen bonds between phosphate's 4 oxygen atoms and PBP's amino acid residues (Luecke and Quiocho, 1990). Thus, PBP may also bind with sNRP compounds if accessible phosphate functional groups are present in the molecule. If PBP binds with sNRP compounds, subsequent release of sNRP from PBP might be achieved by adjusting pH (Venkiteshwaran et al., 2020). Released and concentrated sNRP then can be transformed into sRP for enhanced P recovery.

Evaluations of sNRP adsorption and subsequent controlled desorption using promising phosphate-selective adsorbent materials are needed to assess this potential avenue for improved P management.

3.7. Conclusions

The meta-analysis presented here showed that sNRP can comprise a substantial fraction of TP discharge from water resource recovery facilities (WRRFs). The majority of the TP load was in the non-reactive form in 32.2% of the facilities. Although sNRP species are recalcitrant and less bioavailable compared to sRP, they can still cause eutrophication. Therefore, sNRP discharge into receiving waterbodies also needs to be controlled.

A review of currently available P treatment technologies showed that sNRP removal and recovery strategies are limited. Activated carbon and UV/H_2O_2 are full-scale technologies that can be used for sNRP treatment. However, these technologies need to be studied to specifically assess their efficacy for wastewater sNRP treatment. Similarly, emerging adsorbents or other oxidation-based technologies need to be studied further to upgrade their technology readiness to full-scale from the current bench-scale stage.

Owing to its recalcitrance, sNRP is generally not recoverable. Transformation of these recalcitrant species into more readily removable and recoverable sRP species might offer a viable pathway to improve overall P recovery. The transformed sRP species might be further treated with chemical precipitation or ion exchange and reused as fertilizers, biofuel feedstock, etc. Currently, UV-based sNRP to sRP transformation studies are available. However, wastewater sNRP was not transformed using UV/H_2O_2. Hence, alternate transformation processes, e.g., EO, need to be assessed for effective sNRP to sRP transformation, especially in more realistic wastewater matrices.

Another consideration for using advanced oxidation processes to achieve sNRP to sRP transformation is that oxidation processes generally have a high energy demend. To

address this, adsorbents with high affinity for sNRP species might be used to remove

sNRP from water and concentrate it before applying volumetrically energy intensive

oxidation processes for transformation. Ion exchangers or phosphate-selective PBP may

be used to remove sNRP compounds with available orthophosphate functional groups,

but direct tests of their performance for this purpose are needed.

4. OBJECTIVE 1: EVALUATE ELECTROOXIDATION FOR TRANSFORMATION OF DISSOLVED ORGANIC NITROGEN AND SOLUBLE NON-REACTIVE PHOSPHORUS TO MORE READILY REMOVABLE AND RECOVERABLE FORMS

This work was previously published as:

> Mallick, S.P., Ryan, D.R., Venkiteshwaran, K., McNamara, P.J., Mayer, B.K., 2021. Electro-oxidation to convert dissolved organic nitrogen and soluble non-reactive phosphorus to more readily removable and recoverable forms. *Chemosphere*, *279*, 130876.

It is republished here, with minor adjustments, with permission from the journal.

4.1. Introduction

Nitrogen (N) and phosphorus (P) are essential nutrients for all living organisms. They are also the limiting nutrients in many aquatic ecosystems depending on the N:P ratio. Thus, excess release of N and P into surface waterbodies through run-off or discharge of wastewater effluent can lead to eutrophication. This emphasizes the importance of advanced water reclamation processes to meet increasingly stringent nutrient discharge regulations (Mayer et al., 2016). Additionally, sustainable N management can be improved if N is recovered from wastewater, thereby circumventing the expensive and highly energy intensive Haber-Bosch process used to synthesize ammonium from atmospheric N_2 (van der Hoek et al., 2018). Moreover, recovery of wastewater P can be beneficial for food production as intensive P mining to meet increasing demands for fertilizer is depleting non-renewable P resources (Reijnders, 2014; Ma & Rosen, 2021). A sustainable approach is thus needed to remove N and P from wastewater and recover it for use in global food production.

A wide range of wastewater treatment processes is available for N and P removal. Conventional treatment processes, including biological N removal, enhanced biological P

removal, chemical precipitation, coagulation/flocculation/sedimentation, ion exchange, micro- or ultra-filtration, and adsorption generally remove dissolved inorganic N (DIN) and reactive P (Henze, 1991; Venkiteshwaran et al., 2018a). However, dissolved organic N (DON) and soluble non-reactive P (sNRP; fractionation of N and P is shown in Figure B.1 of Appendix B) are generally not effectively removed in conventional treatment processes (Henze, 1991). Consequently, DON often constitutes 65 – 80% of total N in wastewater effluent (Fan et al., 2017). Among the wastewater P fractions, <40% sNRP is typically removed during conventional P removal (Gu et al., 2011), leaving approximately 26 – 81% of effluent P as sNRP (Qin et al., 2015). Once released into the environment, DON and sNRP eventually degrade to bio-available forms of N and P, resulting in eutrophication in the long term (Urgun-Demirtas et al., 2008; Qin et al., 2015). For example, Urgun-Demirtas et al. (2008) reported biomass growth in 14 days using effluent DON. In the same timeframe, Qin et al. (2015) found that 28 – 61% of effluent DON and 73 – 75% of effluent sNRP were utilized by algae. Additionally, the majority of effluent DON (67±24%) is hydrophilic (93%) and of small molecular size (< 1 kDa), which serves as precursors for the disinfection byproduct N-nitrosodimethylamine (NDMA) (Pehlivanoglu-Mantas & Sedlak, 2008). Therefore, it is prudent to develop technologies to effectively remove DON and sNRP.

There are limited studies on DON and sNRP removal. Effective removal of DON using powdered activated carbon and cation exchange has been reported (Parkin & McCarty, 1981; Lee & Westerhoff, 2006). Successful removal or detoxification of organophosphates and other non-reactive P using UV, UV/H_2O_2, UV/TiO_2 (with or without ultrafiltration), Fenton, and photo-Fenton has also been reported (Daneshvar et

al., 2004; Badawy et al., 2006; Gray et al., 2020). However, these studies primarily targeted removal of the parent DON or sNRP compound without assessing transformation to the more readily removable/recoverable DIN and soluble reactive P (sRP) fractions. The DIN species include NH_4^+, NO_3^-, and NO_2^-, while the sRP fraction refers to soluble orthophosphate (APHA 2012). Relative to DON and sNRP, DIN and sRP are more susceptible to removal using conventional treatment processes (Henze, 1991; Venkiteshwaran et al., 2018a). The more bioavailable DIN and sRP fractions are also more easily recoverable for agricultural reuse, e.g., via struvite precipitation, ion exchange, or bioassimilation (Hermassi et al., 2020; Kim et al., 2020; Sun et al., 2020). Accordingly, transformation of DON and sNRP to more readily removable/recoverable forms can be helpful for achieving lower discharge limits and sustainable nutrient management goals.

To our knowledge, Ahmadi's (2017) thesis focused on ozonation is the only published work reporting DON transformation to DIN, achieving up to 13% DON transformation using 30-min ozonation at a dose of 3 mg/L in tertiary wastewater effluent. Sindelar et al. (2016), Gray et al. (2020), and Venkiteshwaran et al. (2021a) published the only identified studies quantifying sNRP transformation to sRP, all using UV-based advanced oxidation processes (AOPs). Sindelar et al. (2016) achieved greater than 90% transformation of the sNRP compound triethyl phosphate (TEP) using 100 mg/L H_2O_2 and 28.5 J/cm^2 UV fluence. Venkiteshwaran et al. (2021a) achieved up to 38.1±2.9% transformation of the sNRP compound beta-glycerol phosphate (BGP) with 34 mg/L H_2O_2 and 0.43 J/cm^2 UV fluence. Gray et al. (2020) reported up to 58% reduction of non-reactive P from wastewater treated with UV/TiO$_2$ photocatalysis.

These reports offer proof-of-concept that AOPs can improve nutrient management at water resource recovery facilities (WRRF). However, AOPs tend to involve relatively high inputs of chemicals and/or energy, particularly when the treatment goal is complete oxidation to stable end products such as nitrate (NO_3^-) and orthophosphate (PO_4^{3-}). For instance, Venkiteshwaran et al. (2021a) reported energy requirements of 9.4×10^2 to 8.2×10^5 kWh/m^3/order for sNRP transformation using UV/H_2O_2. Accordingly, studies focused on assessing the efficacy of AOPs for DON and sNRP transformation are important to further establish the feasibility of this treatment strategy. Electrooxidation (EO) may offer advantages over other AOPs by utilizing anodic oxidation through direct electron transfer and a wide array of oxidizing species (e.g., HO•, $S_2O_8^{2-}$, $C_2O_6^{2-}$, Cl_2, ClO_4^-, SO_4•$^-$, Cl•, and CO_3•$^-$) generated both on the anode surface and in the bulk solution (Barazesh et al., 2016; Moreira et al., 2017). On this basis, we hypothesized that EO would transform DON and sNRP more efficiently, with less energy input, compared to AOPs such as UV/H_2O_2.

The objectives of this study were to: (1) assess EO transformation efficacy of DON and sNRP for variable current density, mixing speed, and water matrices; (2) evaluate the mechanism of DON and sNRP transformation during EO; and (3) compare transformation efficiency using EO to an established UV/H_2O_2 AOP.

4.2. Materials and methods

4.2.1. Water matrices

The majority of the EO tests were performed in well-controlled synthetic water matrices, with a subset performed in secondary-treated wastewater to assess performance in a more realistic matrix. For the synthetic water experiments, DON and sNRP compounds representing a wide range of structures and sizes (Figure 4.1) were

independently spiked at 2 mg N/L or 1 mg P/L in ultrapure water (Elga, High Wycombe,

UK) with a resistivity of 18.2 MΩ-cm at 25 ± 1°C.
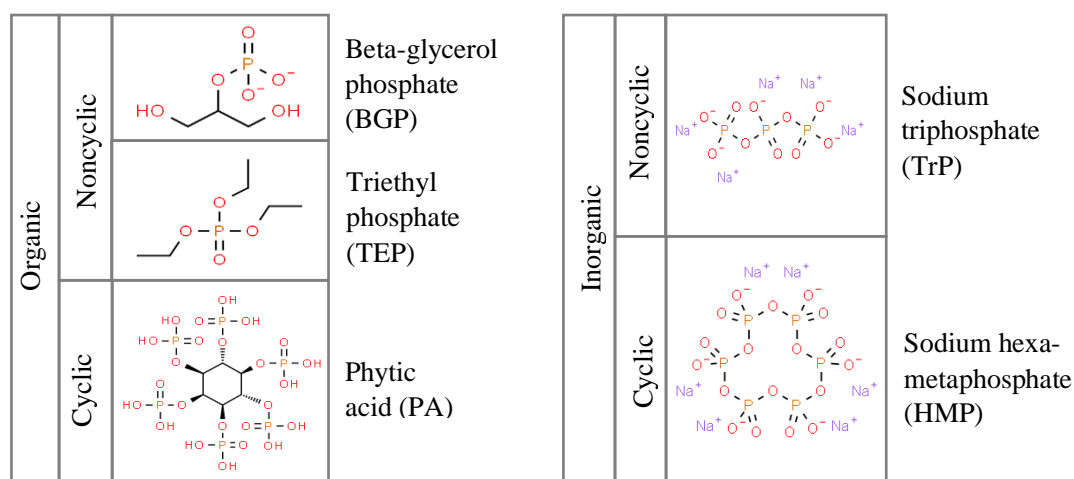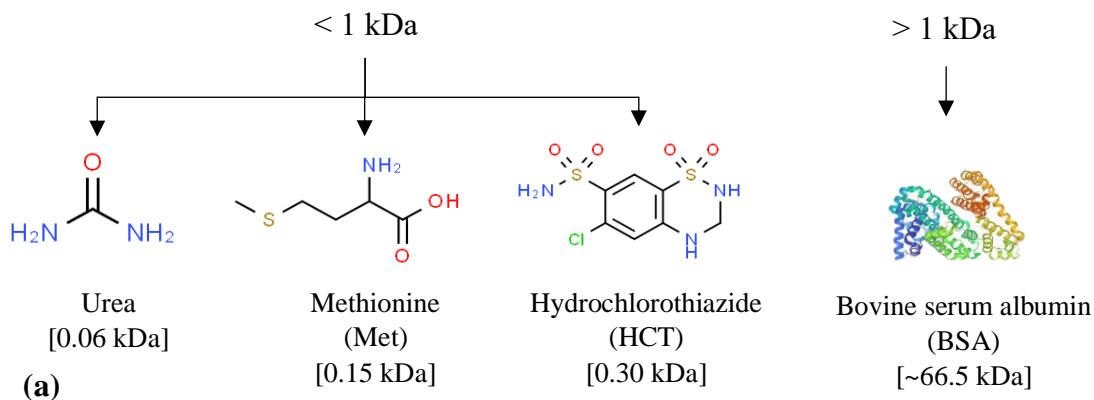
Figure 4.1. **(a)** Dissolved organic nitrogen (DON) and **(b)** soluble non-reactive phosphorus (sNRP) compounds tested in this study. The DON compounds were selected based on size, and they represent a wide range of DON generally present in wastewater effluent such as urea (a common compound), Met (amino acid), HCT (micropollutant), and BSA (protein). The organic and inorganic sNRP compounds selected for this study included a number of different molecular configurations such as P-O-C (organic sNRP) and P-O-P bonds (inorganic sNRP). The image of BSA was taken from Pubmed. All other structures were taken from Chemspider.

Selection of DON compounds representative of wastewater effluent DON species is challenging as most wastewater effluent DON (70%) is unidentifiable (Yu, 2012; Hu et al., 2016). However, it has been reported that most of the unidentifiable wastewater effluent DON is of low molecular weight (67±24% DON is <1 kDa), and small DON compounds are more recalcitrant to conventional treatments and also serve as NDMA precursors (Pehlivanoglu-Mantas & Sedlak, 2008). Hence, size of DON compounds was one of the main factors considered while selecting the four compounds for this study. Three of the selected compounds were less than 1 kDa in size: urea, methionine (Met), and hydrochlorothiazide (HCT). One compound representative of larger DON species was included in the study: bovine serum albumin (BSA).

Five sNRP compounds were used to represent a variety of chemical structures, including both organic and inorganic compounds. The two inorganic sNRP compounds were hexa-meta phosphate (HMP, cyclic structure) and sodium triphosphate (TrP, noncyclic structure). Three organic sNRP compounds were selected for this study: beta-glycerol phosphate (BGP, cyclic structure), phytic acid (PA, noncyclic structure), and triethyl phosphate (TEP, noncyclic structure). The sNRP compounds provided comparisons against the existing reports of AOP- transformation using UV/H_2O_2 (Sindelar et al., 2016; Venkiteshwaran et al., 2021a). All compounds were purchased in 99% pure forms from Sigma Aldrich (St. Louis, MO).

Wastewater experiments were conducted using secondary wastewater effluent (after nitrification) collected from the South Shore Water Reclamation Facility (Oak Creek, WI). Wastewater characteristics, e.g., dissolved organic carbon (DOC), alkalinity, etc. are provided in Table B.1. Effluent DON and sNRP transformation were assessed by

running EO without pH adjustment (pH = 7.07). In a subset of experiments, BGP was spiked into the wastewater to facilitate direct comparison of sNRP transformation in wastewater effluent and ultrapure water matrices.

4.2.2. Electrooxidation

Triplicate EO experiments were conducted by individually spiking one of the DON or sNRP compounds into synthetic water or actual wastewater (or using wastewater directly without spiking). All EO experiments were performed in bench-scale continuously stirred batch reactors consisting of a 250-mL Berzelius beaker (holding 200 mL solution) on a multi-position magnetic stirrer (Bell-ennium, Vineland, NJ). Plastic electrode caps were 3D printed and fitted on top of the reactors to maintain an inter-electrode distance of 1 cm with a submerged electrode surface area of 13.5 cm^2. Boron-doped diamond (BDD) (Fraunhofer, Lansing, MI) was used as the anode and titanium (Performance Titanium Group, San Diego, CA) was used as the cathode. Prior to each experiment, a current density of 3.7 mA/cm^2 was applied for 5 min to clean and polarize the electrode surfaces.

The applied current density was adjusted to 0.74, 1.47, 3.70, or 7.41 mA/cm^2 for EO tests, and mixing speed was maintained at 50 rpm unless otherwise noted. Electrolyte, pH, and wastewater effluent DON and sNRP transformation EO experiments were run at 7.41 mA/cm^2. All EO experiments were run for 30 min except for the kinetic studies, which ranged from 30 min up to 8 h. All kinetic studies were conducted at 0.74 mA/cm^2 based on preliminary experiments run at varying current density for 4 h, which showed that temperature changed over time (Figure B.2), with the least change in solution temperature at 0.74 mA/cm^2. Although faster transformation kinetics could be achieved at higher current densities, such conditions could lead to faster dissipation of the

electrodes and high temperature in the bulk solution, making it challenging for large-scale application.

Since EO generates oxidizing agents in situ, water constituents play an important role in treatment performance. For instance, peroxodisulfate ($S_2O_8^{2-}$) or sulfate radicals ($SO_4\bullet^-$) may be generated if SO_4^{2-} is present in the water matrix (Li et al., 2010; Shin et al., 2019). Similarly, generation of $Cl\bullet$, Cl_2, ClO_4^-, etc. has been reported in matrices with chloride present, and carbonate-based ($CO_3\bullet^-$, $C_2O_6^{2-}$) oxidant species may result when carbonate species are present (Moreira et al., 2017). Hence, EO can be affected by changing water matrix composition depending on the target contaminants and their susceptibility to various oxidants. Four electrolytes -- sodium sulfate (Na_2SO_4), sodium bicarbonate ($NaHCO_3$), sodium chloride ($NaCl$), or sodium perchlorate ($NaClO_4$) -- were used to study the effect of different electrolytes on transformation (each at 650 – 700 µS/cm in the synthetic matrices; molar concentrations are provided in Table B.2). Except for the electrolyte experiments, Na_2SO_4 was used as the electrolyte in all synthetic solution experiments.

The solution pH was adjusted to 7 using NaOH or H_2SO_4 (except for the set of experiments conducted to study the effects of pH, wherein pH ranged from 3 to 9). For NaCl electrolyte experiments, pH was adjusted using HCl to maintain ion consistency. Solution pH following EO treatment was recorded, as shown in Table B.3.

Control EO experiments were conducted using known DIN and sRP concentrations to test if oxidation continued beyond EO exposure or if the oxidants interfered with DIN or sRP measurement. As these tests showed no ongoing oxidation or

analytical interference, oxidant quenchers were not used in subsequent tests. All samples were analyzed for N or P immediately after treatment.

4.2.3. UV/H$_2$O$_2$ experiments

To explore the role of HO• in transformation and provide a point of comparison against conventional AOPs, a set of batch tests was performed using UV/H$_2$O$_2$. For these tests, the same synthetic water matrices used for EO were tested for transformation of the compounds at neutral pH conditions. Tests were performed at varying H$_2$O$_2$ dose (1, 10, 20, or 30 mM) and 0.43 J/cm UV fluence. Control experiments were also performed using no UV or H$_2$O$_2$ (negative control), H$_2$O$_2$ only, and UV only. Sodium sulfate (Na$_2$SO$_4$) was used to quench oxidation after the target exposure time.

For UV/H$_2$O$_2$ tests, a bench-scale UV collimated beam with a low-pressure mercury arc bulb (Model G15T8, USHIO, Cypress, CA) emitting monochromatic light at a peak of 254 nm was used, as described by Venkiteshwaran et al. (2021a). Light intensity at the sample surface was measured using an IL 1700 research radiometer (International Light, Newburyport, MA, USA). The average intensity of light on the sample surface was calculated using Equation 4.1 (Bolton and Linden, 2003):

$$I_{avg} = I_0 * RF * PF * WF * DF \qquad \text{Equation 4.1}$$

where, I_{avg} = average intensity in W/cm^2, I_0 = uncorrected peak intensity reading from the radiometer (W/cm^2), RF = reflection factor, PF = Petri factor, WF = water factor, and DF = divergence factor. The average light intensity was 1.2×10^{-4} W/cm^2 using the correction factors described by Venkiteshwaran et al. (2021a). Fluence was calculated using Equation 4.2.

$$F = I_{avg} * t \hspace{4cm} \text{Equation 4.2}$$

where F is fluence in J/cm^2 and t is time in sec.

4.2.4. Analytical Measurements

Nitrogen measurement

Total nitrogen and ammonium (NH$_4^+$) were measured using Hach (Loveland, CO) TNT 826 and TNT 830 kits, respectively. Nitrate (NO$_3^-$) and nitrite (NO$_2^-$) were measured using ion chromatography (Thermo Scientific™ Dionex ICS 1100, Waltham, MA). The standard curve was generated using Dionex™ combined seven anion standard II. The minimum detection limit (MDL) for NO$_3^-$ was 0.01 mg/L, as determined following the EPA recommended method (EPA, 2016) and concentrations below the MDL were considered as 0.01 mg/L. Effluent DON was calculated by subtracting all DIN species from total dissolved nitrogen (TDN). Among the three DIN species, NH$_4^+$ and NO$_2^-$ concentrations were below detection after EO experiments (0.015 and 0.01 mg/L, respectively), leaving the fully oxidized NO$_3^-$ ion as the sole DIN species in the treated samples (accordingly, DIN = NO$_3^-$ in the treated samples).

Phosphorus measurement

The standard ascorbic acid method was used for total P and sRP (orthophosphate) quantification (APHA 2012). Wastewater samples were filtered through 0.45 µm Whatman™ cellulose membrane filters (GE Healthcare Life Sciences, Chicago, IL) before reactive P measurement to quantify the sRP fraction and sNRP was calculated by subtracting sRP from total soluble P. The MDL for sRP was 0.02 mg/L, as determined following the EPA recommended method (EPA, 2016) and concentrations below the MDL were considered as 0.02 mg/L.

4.2.5. *PCBA degradation to explore the dominant transformation mechanism*

Oxidants generated in the AOPs were assessed in accordance with Barazesh et al. (2016). Synthetic water matrices used for EO or UV/H_2O_2 tests were spiked with 800 µg/L para-chlorobenzoic acid (PCBA) and residual PCBA was measured by liquid chromatography mass spectrometry (LCMS-2020, Shimadzu, Kyoto, Japan) using a method adapted from Vanderford et al. (2007). The kinetic rate of PCBA degradation was used to indicate the dominant mechanism for transformation of DON and sNRP. Specifically, using the rate constant of PCBA degradation by HO• ($k_{PCBA, HO•} = 5 \times 10^9$ L/mol-s) and the residual PCBA concentration, HO• generation was quantified in the UV/H_2O_2 process. For EO, oxidation could occur through direct electron transfer, HO•, and other oxidants generated in situ. Second order PCBA degradation kinetics indicate the dominance of HO• or other oxidants generated in the EO process (Neta et al., 1976). Alternately, zero order PCBA degradation kinetics indicate direct electron transfer as the dominant oxidation mechanism.

4.2.6. Energy consumption calculation

Electrical energy per mass (E_{EM}, Equation 4.3) is used for energy demand estimation when comparing AOPs characterized by zero order reactions (as observed for EO; Figure 4.6 in the Results and Discussion) (Bolton et al., 2001).

$$E_{EM} = \frac{P*t*10^6}{V(C_i-C_f)} \qquad\qquad \text{Equation 4.3}$$

where E_{EM} is the electrical energy (kWh) necessary for unit mass of contaminant removal (kg), P is power (kW), t is time (h), V is volume (L), C_i is initial concentration (mg/L), and C_f is the final concentration (mg/L).

Energy consumption using EO was compared to UV/H$_2$O$_2$ transformation, which is typically characterized by the first order energy efficiency parameter E$_{EO}$ (electrical energy per order, kWh/m^3/order, Equation 4.4) (Bolton et al., 2001). Equation 4.5 was used to relate the two parameters.

$$E_{EO} = \frac{P * t * 10^3}{V \log(C_i/C_f)}$$
<div align="right">Equation 4.4</div>

$$E_{EM} = \frac{10^3 * \log(C_i/C_f)}{(C_i - C_f)} * E_{EO}$$
<div align="right">Equation 4.5</div>

4.2.7. QA/QC

Blanks with ultrapure water were analyzed as negative controls for all N and P experiments. Positive controls consisting of known NO$_3^-$ or PO$_4^{3-}$ concentrations were measured to ensure there was no interference from the ions present in the synthetic water matrices. Triplicate experiments were conducted for all conditions. Statistical analysis was performed using t-test or two-way ANOVA and Tukey post hoc analysis with a significance level of 0.05. GraphPad Prism 9 (La Jolla, CA) was used for all statistical analysis.

4.3. Results and discussion

4.3.1. The impact of EO operating parameters on DON and sNRP transformation efficacy

The influence of the operating parameters current density and mixing speed was assessed in synthetic water matrices. Current density is one of the key controlling parameters in electro-chemical treatment processes as it affects electron transfer rates and HO• generation on the anode surface (Lin et al., 2012; Körbahti et al., 2015). Likewise, mixing conditions can encourage or impede molecular-scale interactions, and impact

mass transfer to the electrode surface. Additionally, EO-based wastewater DON and sNRP transformation was assessed to evaluate the effect of the wastewater constituents on transformation.

Current density

Transformation of urea, PA, and BGP increased with increasing applied current density ($p \leq 0.007$) (Figure 4.2; urea transformation decreased slightly as current density increased from 0.74 to 1.48 mA/cm^2). Transformation of all other compounds was below 5% (Figure 4.2). This trend suggests that the current densities tested here were below the limiting current density, which is the threshold current density depending on the composition of the water matrices, target compounds, reactor configuration, etc. (Dennis & Such, 1993). When the applied current density is below the scenario-specific limiting current density, oxidation is controlled by applied current, resulting in zero order kinetics (Soriano et al., 2017). However, once the limiting currently density is exceeded, oxidation is limited by diffusion, and oxidation kinetics are second order.
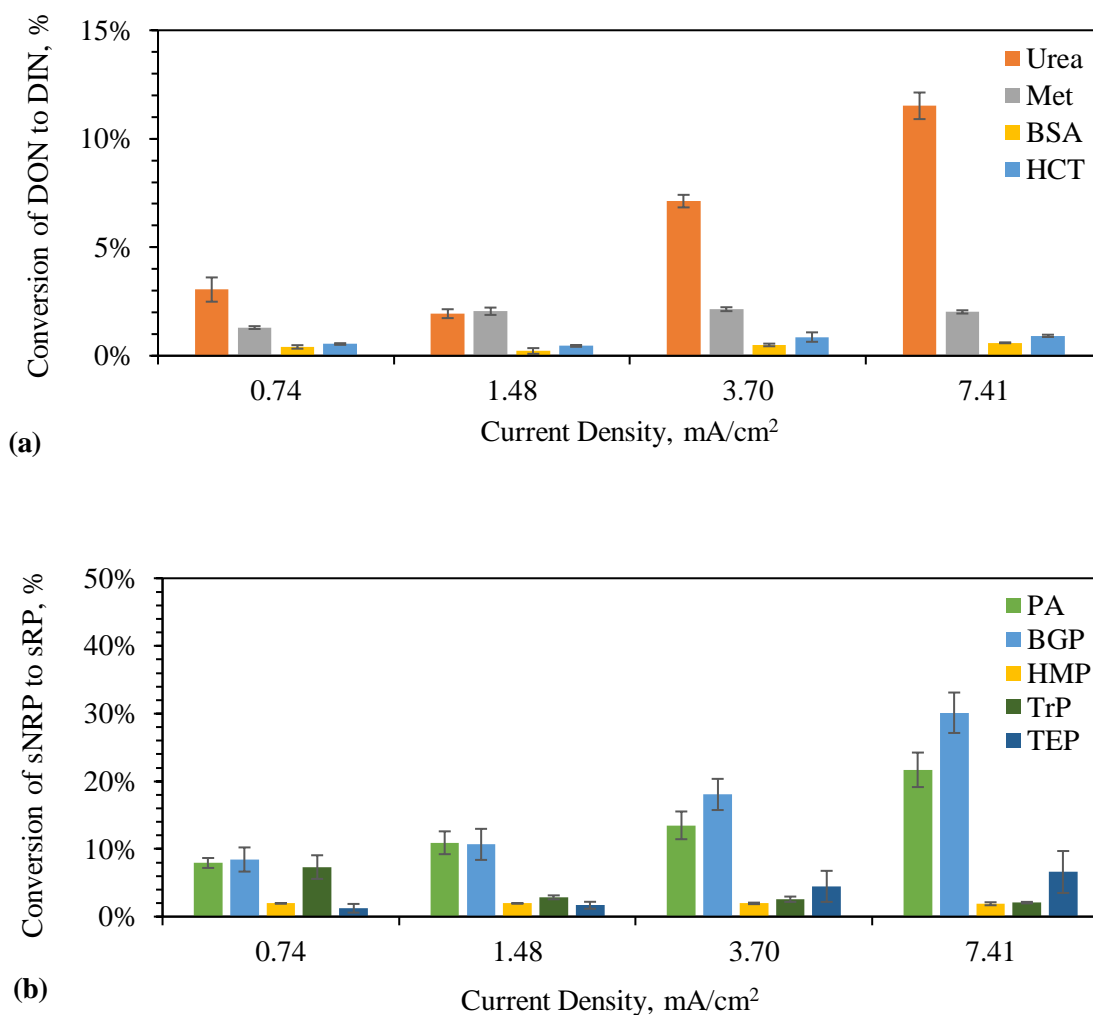
Figure 4.2. Electrooxidation (EO) transformation of **(a)** dissolved organic nitrogen (DON) to dissolved inorganic nitrogen (DIN) and **(b)** soluble non-reactive phosphorus (sNRP) to soluble reactive phosphorus (sRP) at varying current density under the following conditions: pH = 7, time = 30 min, and electrolyte = Na_2SO_4. The bars show the average of triplicate experiments, while the error bars represent ± 1 standard error. (Met = methionine, BSA = bovine serum albumin, HCT = hydrochlorothiazide, PA = phytic acid, BGP = beta-glycerol phosphate, HMP = hexa-meta phosphate, TrP = sodium triphosphate, TEP = triethyl phosphate).

Transformation of DON was less efficient compared to sNRP transformation (Figure 4.2). DON compounds may be more recalcitrant to AOP-based transformation owing to their high bond energy (C-N bond energy = 305 kJ/mol) (Ziegler et al., 1988). Among the DON compounds tested, urea showed the most susceptibility to EO-based transformation. Urea has two primary amines (C-N bond needs to be cleaved for transformation to DIN), whereas Met has one primary amine, and HCT has one primary and two secondary amines (C-N-C bond needs to be cleaved for transformation) (Figure 4.1). Moreover, the two secondary amines in HCT are in the compound's aromatic ring. Hence, transformation of urea may have been more efficient as the two amines are more easily accessible to oxidants, whereas only one amine is accessible for Met transformation, and HCT transformation requires one primary amine cleavage or cleavage of two secondary amines from the aromatic ring. Additionally, the large molecular weight DON compounds in this study showed less susceptibility to EO-based transformation. Successful transformation of the low molecular weight DON compounds is promising as small DON compounds are the most abundant ($67 \pm 24\%$ of wastewater effluent DON are less than 1 kDa in size) and recalcitrant among effluent DON compounds (Pehlivanoglu-Mantas & Sedlak, 2008).

Among the sNRP compounds, organic P compounds were more susceptible to transformation than inorganic P compounds (which had only 5% transformation for all conditions). The orthophosphate groups in the organic and inorganic sNRP compounds are bound with phosphoester (P-O-C) and phosphoanhydride (P-O-P) bonds, respectively (Figure 4.1). The free energy associated with P-O-C bonds is -15 kJ/mol and for P-O-P bonds it is -30 kJ/mol (Müller et al., 2019). Hence, cleavage of P-O-C bonds requires less

energy compared to that needed for P-O-P bonds, resulting in greater oxidation of organic P compounds compared to inorganic P compounds. Transformation of BGP and PA was greater than TEP transformation, possibly due to the availability of orthophosphate groups within the molecular structure. Three P-O-C bonds need to be cleaved to extract one orthophosphate from a TEP molecule, whereas one orthophosphate can be cleaved from both BGP and PA by breaking only one P-O-C bond.

Mixing Speed

EO mixing speed had minimal effect on transformation of the DON and sNRP compounds (Figure 4.3). A single mixing condition for PA yielded a significant response ($7.93 \pm 0.73\%$ at 150 rpm increased to $15.92 \pm 1.99\%$ transformation at 250 rpm, $p = 0.018$), whereas mixing speed had no significant impact on all other compounds ($p > 0.05$). The current density was 0.74 mA/cm^2 in all of the mixing speed experiments, which was likely below the limiting current density, as indicated by the current density experiments. Thus, oxidation was likely controlled by applied current in these experiments rather than being diffusion-limited, at which point mixing speed would influence transformation efficacy (Cañizares et al., 2006).
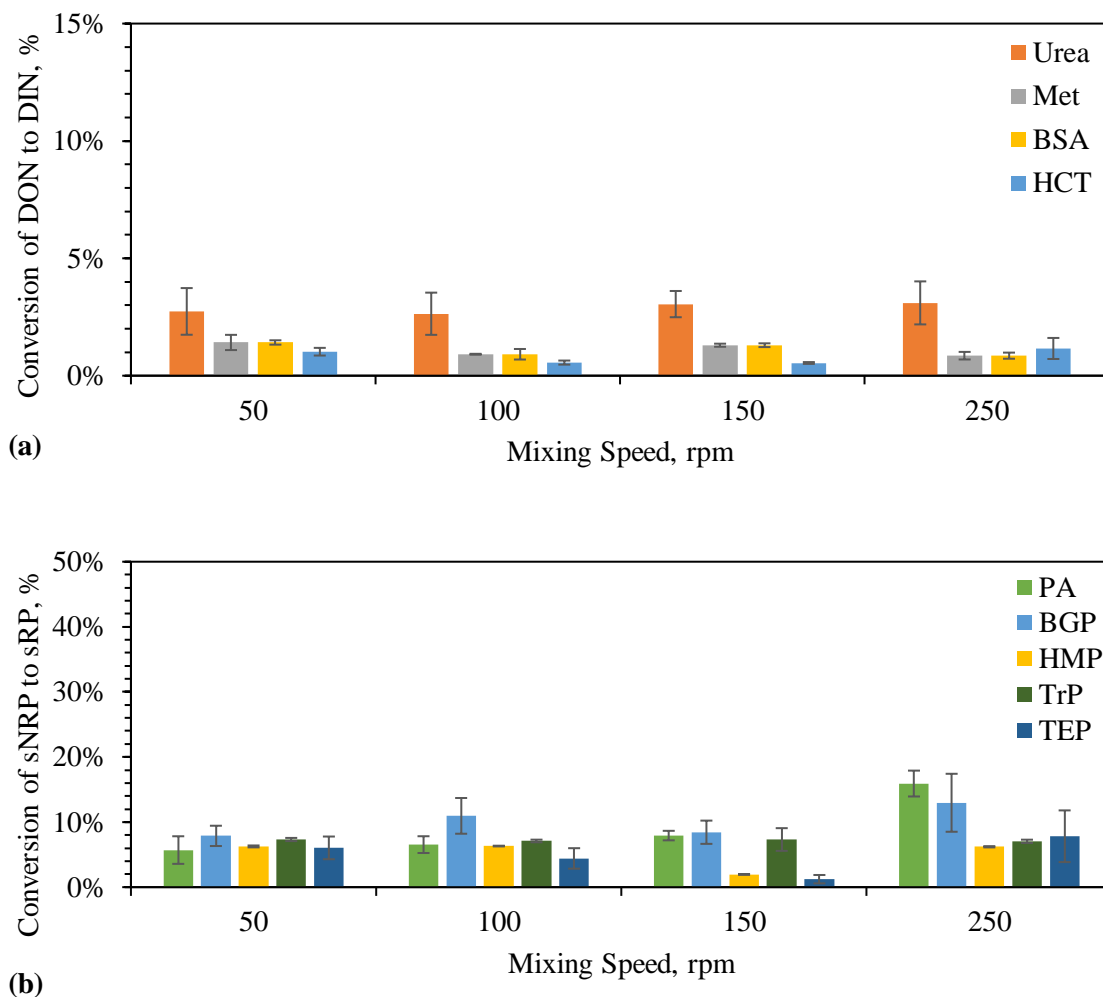
Figure 4.3. Electrooxidation (EO) transformation of **(a)** dissolved organic nitrogen (DON) to dissolved inorganic nitrogen (DIN) and **(b)** soluble non-reactive phosphorus (sNRP) to soluble reactive phosphorus (sRP) at varying mixing speeds under the following conditions: current density = 0.74 mA/cm^2, pH = 7, time = 30 min, and electrolyte = Na$_2$SO$_4$. The bars show the average of triplicate experiments, while the error bars represent ± 1 standard error. (Met = methionine, BSA = bovine serum albumin, HCT = hydrochlorothiazide, PA = phytic acid, BGP = beta-glycerol phosphate, HMP = hexameta phosphate, TrP = sodium triphosphate, TEP = triethyl phosphate).

Wastewater matrices

Wastewater effluent DON and sNRP transformation was either statistically similar or slightly lower than DON and sNRP transformation in synthetic matrices (Table B.4). The effluent DON transformation was slightly lower than urea transformation while

effluent sNRP transformation was comparable to BGP transformation in synthetic water

at the same test conditions (p = 0.642). However, the initial sNRP concentration (0.11 ±

0.01 mg P/L) was 10 times lower in the wastewater effluent compared to the synthetic

water matrices. Thus, for a more direct comparison of P transformation, the effluent was

spiked with BGP to achieve an initial sNRP concentration of 1 mg P/L. In the spiked

effluent, transformation was 3 times less than the synthetic water sNRP transformation.

Although oxidant scavengers in the wastewater effluent (e.g., DOC = 11.5 ± 0.17 mg/L,

32.8 ± 0.98% of which was completely oxidized during treatment) likely undermined

DON and sNRP transformation, similar or less transformation in the synthetic waters

indicated that sNRP compounds present in wastewater were more susceptible to EO-

based transformation than the spiked sNRP compounds. Thus, wastewater effluent DON

and sNRP were likely more amenable to oxidation, possibly owing to partial degradation

during the preceding wastewater treatment processes. Notably, EO transformed less DON

compared to sNRP, indicating that DON was more recalcitrant to EO-based

transformation (and perhaps subject to greater interference from DOC).

4.3.2. Evaluate the mechanism of DON and sNRP transformation during EO

The defining feature of AOPs is HO• production. However, in the case of EO,

multiple oxidation pathways may contribute to transformation of the DON and sNRP

compounds. To probe the mechanism of DON and sNRP transformation during EO,

several sets of tests were performed under variable pH conditions, electrolyte

compositions, and treatment times. The extent of nutrient transformation in response to

changes in each of these parameters provides an indication of the role of HO• in the

transformation process. Additionally, the oxidant probe PCBA was used as an indicator of the dominance of HO•-based oxidation in EO and UV/H_2O_2 AOPs.

pH

Transformation of the DON and sNRP compounds was generally independent of pH (Figure 4.4; $p \geq 0.147$) with the exception of urea (highest transformation at pH 7, $p \leq 0.0001$) and BGP (transformation increasing from $31.07 \pm 0.75\%$ at pH 7 to $37.61 \pm 4.60\%$ at pH 8, $p = 0.046$). Generally, EO-based oxidation is more efficient under acidic conditions, with reduced efficiency under alkaline conditions (Rahmani et al., 2015). Acidic conditions can produce high HO• concentrations on the electrode surfaces, inhibit oxygen evolution, and increase oxygen overpotential, all of which can improve efficiency. However, DON to DIN and sNRP to sRP transformation was not affected by pH at the conditions tested, possibly because HO• oxidation was not the dominant oxidation mechanism in the test configuration. The transformation mechanism was further explored by varying electrolyte composition and treatment time.
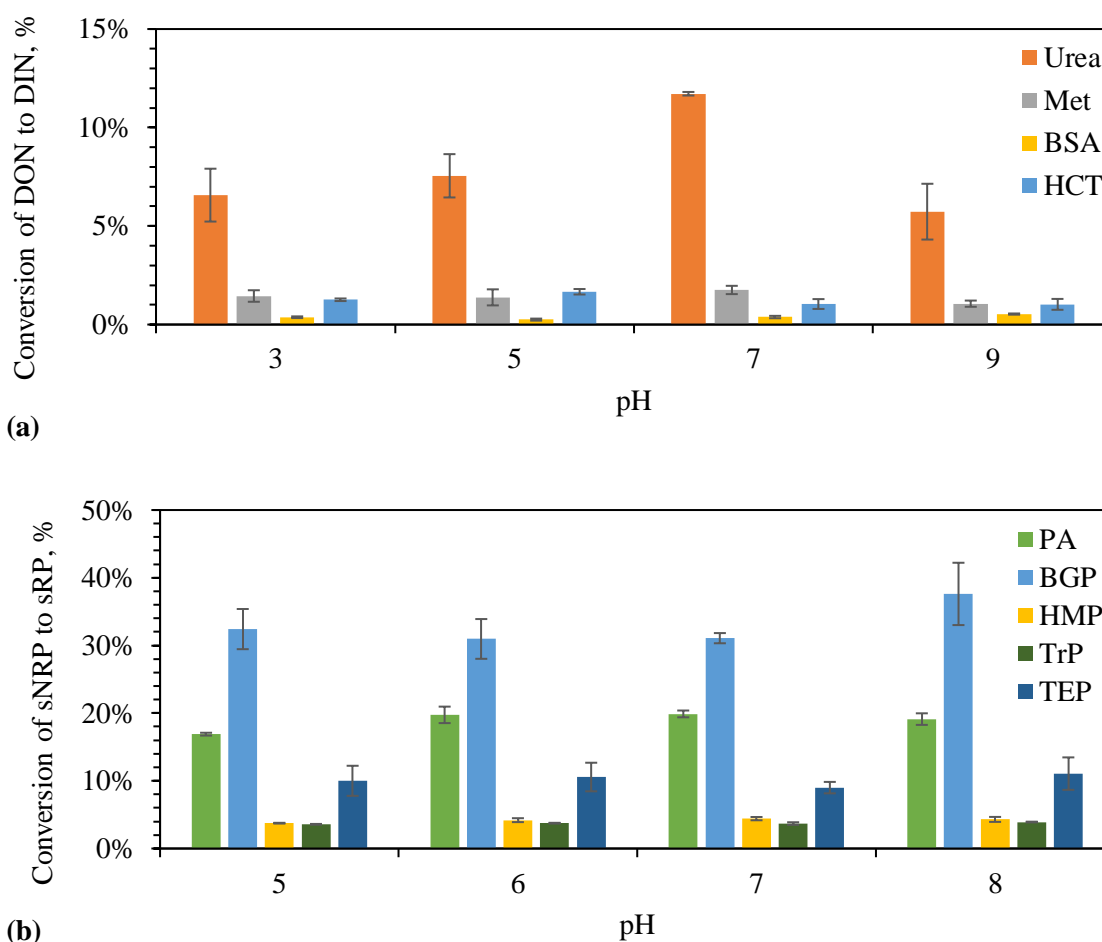
Figure 4.4. Electrooxidation (EO) transformation of **(a)** dissolved organic nitrogen (DON) to dissolved inorganic nitrogen (DIN) and **(b)** soluble non-reactive phosphorus (sNRP) to soluble reactive phosphorus (sRP) at varying initial pH under the following conditions: current density = 7.41 mA/cm^2, time = 30 min, and electrolyte = Na$_2$SO$_4$. The bars show the average of triplicate experiments, while the error bars represent ± 1 standard error. (Met = methionine, BSA = bovine serum albumin, HCT = hydrochlorothiazide, PA = phytic acid, BGP = beta-glycerol phosphate, HMP = hexa-meta phosphate, TrP = sodium triphosphate, TEP = triethyl phosphate).

Electrolyte Composition

Electrolytes provide an electroconductive medium to facilitate charge transfer in EO (Kumar et al., 2020). The electrolyte composition dictates the generation of a range of oxidizers, including highly active radicals both on the anode surface and in the bulk

solution. Thus, electrolyte composition heavily impacts EO performance (Barazesh et al., 2016).

Urea transformation was not affected by the type of electrolyte except for yielding the least transformation in $NaClO_4$ electrolyte solution (Figure 4.5; $p \leq 0.0003$). Transformation of Met and BSA was consistently <5% and was not affected by the type of electrolyte ($p \geq 0.104$). Transformation of HCT was also <5% for both Na_2SO_4 and $NaHCO_3$, but approximately 5 times greater HCT transformation ($p < 0.0001$) was achieved using NaCl as the electrolyte. Among the sNRP compounds, TrP, HMP, and TEP transformation was not affected by electrolytes. Transformation of BGP and PA was the highest with Na_2SO_4 or $NaClO_4$, whereas NaCl solution offered the lowest transformation.
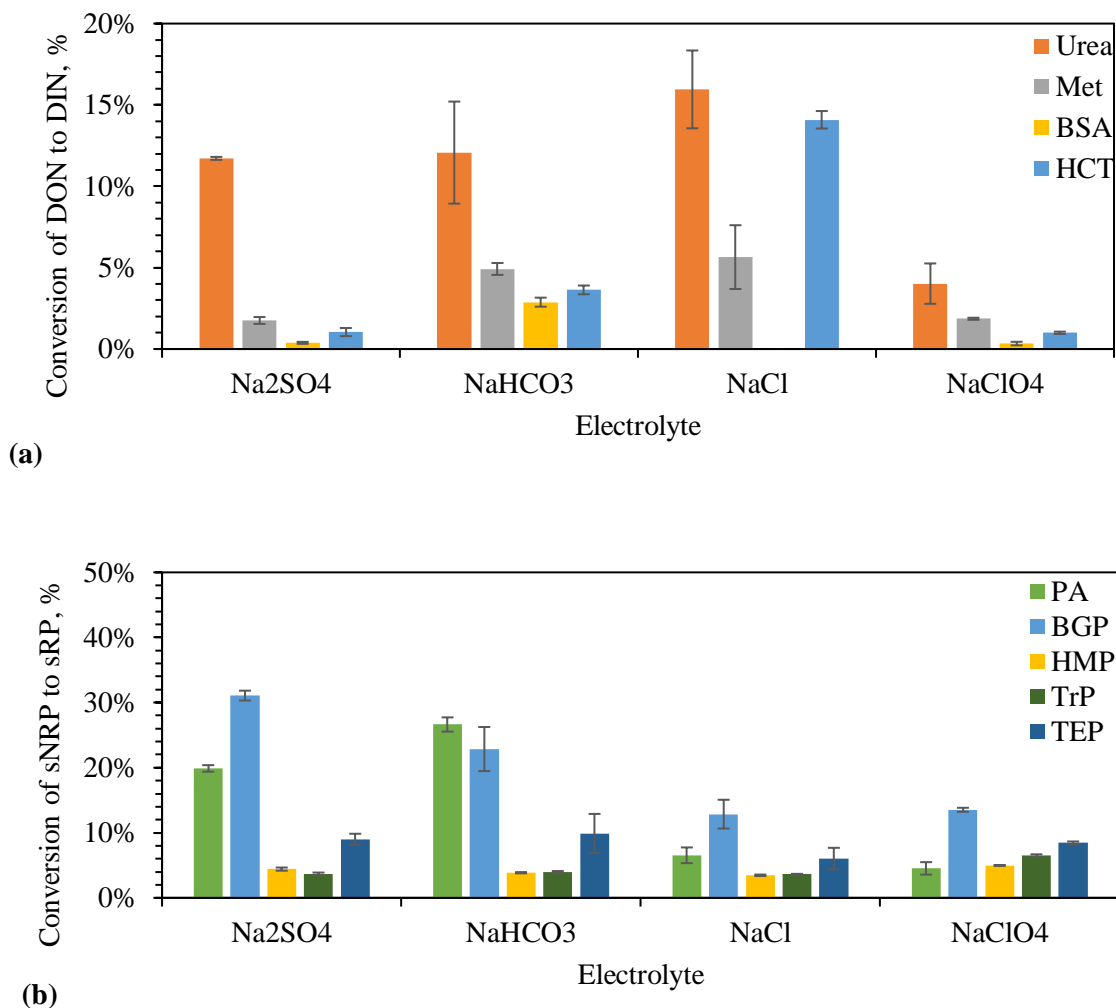
Figure 4.5. Electrooxidation (EO) transformation of **(a)** dissolved organic nitrogen (DON) to dissolved inorganic nitrogen (DIN) and **(b)** soluble non-reactive phosphorus (sNRP) to soluble reactive phosphorus (sRP) in synthetic water matrices with different electrolytes under the following conditions: current density = 7.41 mA/cm^2, time = 30 min, and pH = 7. The bars show the average of triplicate experiments, while the error bars represent ± 1 standard error. (Met = methionine, BSA = bovine serum albumin, HCT = hydrochlorothiazide, PA = phytic acid, BGP = beta-glycerol phosphate, HMP = hexa-meta phosphate, TrP = sodium triphosphate, TEP = triethyl phosphate)

The presence of the fully oxidized sulfate or perchlorate ions can help with direct electron transfer as they may not compete with the target DON or sNRP compounds for oxidation on the anode surface. Additionally, Na$_2$SO$_4$ or NaClO$_4$ electrolytes may have offered higher transformation because sulfate and perchlorate concentrations were low

compared to chloride or bicarbonate levels in NaCl or $NaHCO_3$ solutions (Table B.2), which may have reduced competition on the anode surface. Alternately, chloride and bicarbonate may have competed for electrode sites, thereby inhibiting direct electron transfer and the resulting transformation of DON and sNRP.

Transformation kinetics

Transformation of DON (except for BSA) and organic sNRP compounds increased significantly ($p \leq 0.046$) with increased treatment time; however, BSA and the inorganic sNRP compounds TrP and HMP were not susceptible to EO-based transformation even after 8 h of EO exposure (Figure 4.6). Confirming results from the current density tests, zero order kinetics were observed for the transformation of DON and sNRP compounds (Figure 4.6; kinetic parameters are listed in Table B.5). When HO• oxidation is the dominant mechanism, oxidation follows second order kinetics. Likewise, sulfate-, carbonate-, or chloride-based radicals follow first or second order kinetics (Neta et al., 1976; Hasegawa & Neta, 1977; Canonica et al, 2005). Accordingly, the zero order kinetics observed here indicate that radicals such as HO• were not the dominant oxidation mechanism in EO-based transformation of the recalcitrant DON and sNRP compounds. Instead, direct electron transfer was ostensibly the dominant mechanism.
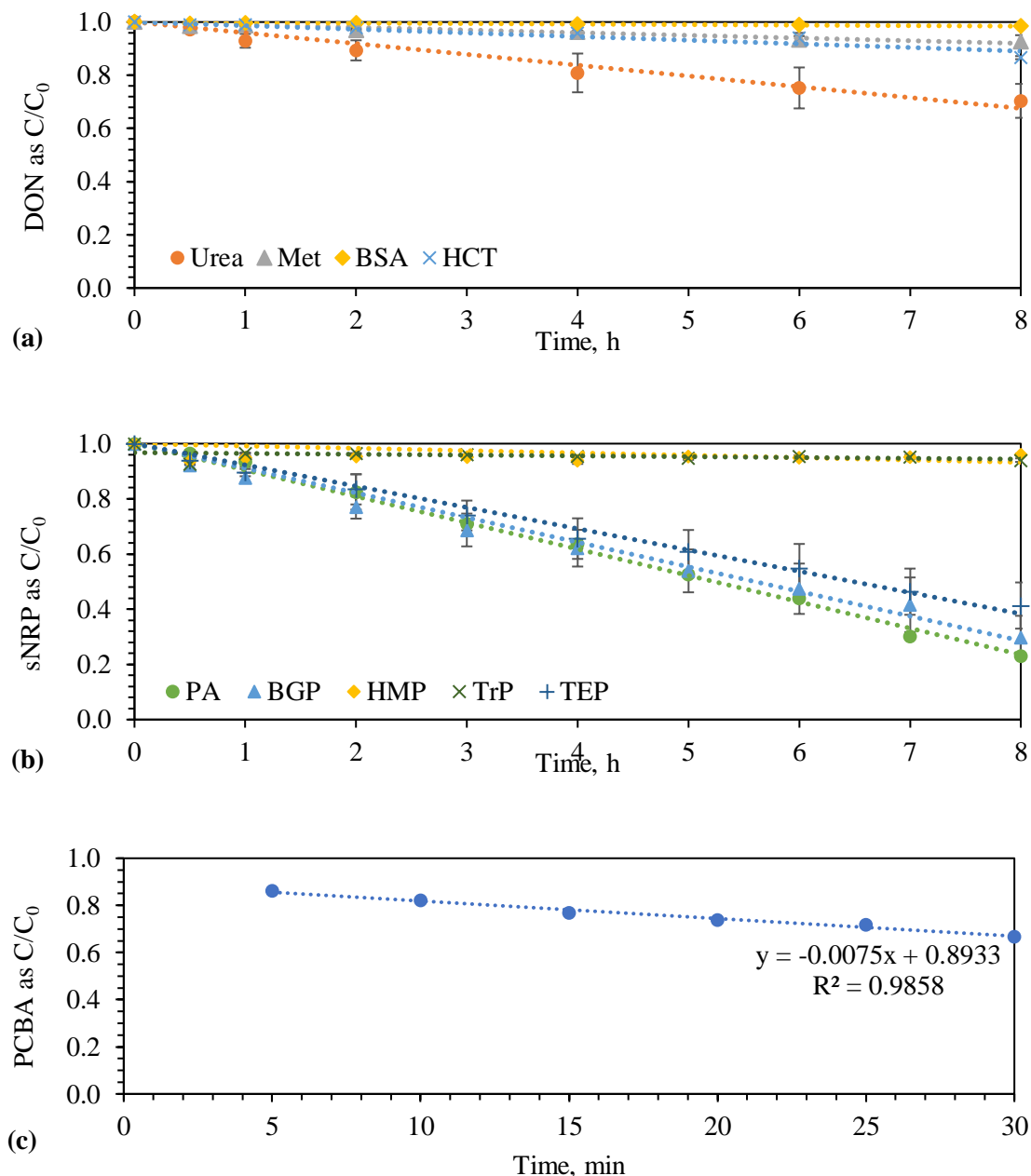
Figure 4.6. (a) Dissolved organic nitrogen (DON) to dissolved inorganic nitrogen (DIN) and **(b)** soluble non-reactive phosphorus (sNRP) to soluble reactive phosphorus (sRP) transformation as a function of electrooxidation (EO) treatment time under the following conditions: current density = 0.74 mA/cm^2, pH = 7, and electrolyte = Na$_2$SO$_4$. The kinetic parameters are shown in Table B.5. **(c)** PCBA degradation under the same EO conditions. The data points in a and b show the average of triplicate experiments (c is the average of duplicate experiments), while the error bars represent ± 1 standard error. Some error bars are too small to be seen. (Met = methionine, BSA = bovine serum albumin, HCT = hydrochlorothiazide, PA = phytic acid, BGP = beta-glycerol phosphate, HMP = hexa-meta phosphate, TrP = sodium triphosphate, TEP = triethyl phosphate).

PCBA oxidant probe

Using PCBA to probe the oxidation mechanism in EO resulted in zero order kinetics (Figure 4.6c), indicating that direct electron transfer was the dominant mechanism for EO-based transformation rather than HO• or sulfate radical oxidation, which would follow second order PCBA kinetics (Neta et al., 1976). Oxidation by HO• involves preferential attack on electron-dense sites (Crittenden et al., 2012). In EO, HO• may attack the electron-rich C bonds, while N and P bonds may be oxidized by direct electron transfer, making it the dominant mechanism for EO-based DON and sNRP transformation.

Alternately, HO• is the dominant oxidant generated by the UV/H_2O_2 AOP. We previously measured a steady state concentration of 1.51×10^{-13} M HO• for the UV/H_2O_2 reactor used here (Venkiteshwaran et al., 2021a). Since HO• was generated in the UV/H_2O_2 system, but negligible DON transformation was observed, the DON compounds appear to be inefficiently oxidized by HO• alone.

4.3.3. EO versus UV/H_2O_2: Process efficiency

Based on EO's multiple oxidation pathways, we hypothesized that EO would provide higher levels of DON and sNRP transformation and be more energy efficient compared to UV/H_2O_2. As shown in Figure 4.7a, EO generally provided higher levels of transformation compared to UV/H_2O_2. Notably, UV/H_2O_2 did not effectively transform DON, whereas EO treatment transformed 11.7% of urea (highest transformation of the DON compounds tested). Using UV/H_2O_2, a maximum of 38.1% transformation of the sNRP compounds was observed, compared to a maximum of 31.0% BGP transformation using EO. With the exception of BGP, transformation of all DON and sNRP compounds

was more energy efficient using EO than using UV/H_2O_2 (Figure 4.7b; E_{EM} values shown in Table B.6).
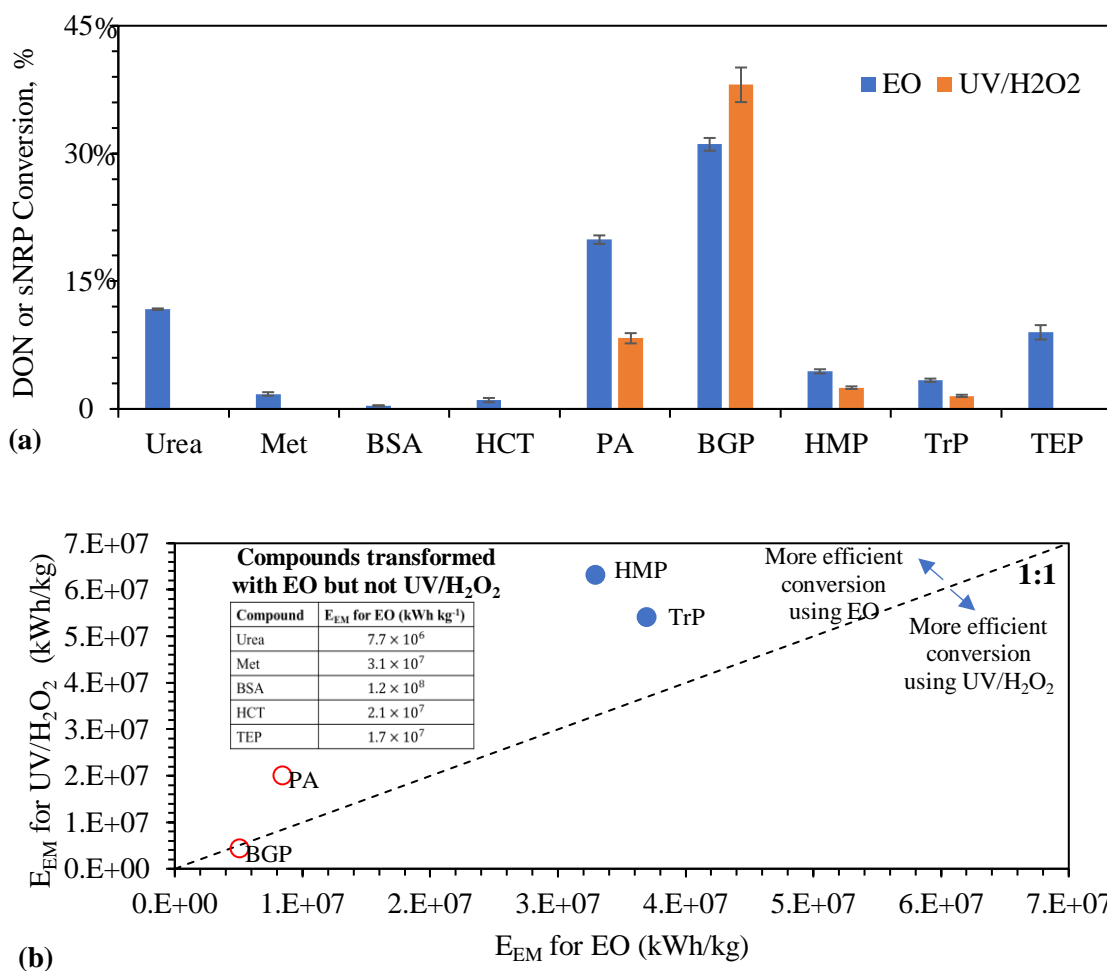
Figure 4.7. (a) Comparison of dissolved organic nitrogen (DON) and soluble non-reactive phosphorus (sNRP) transformation using electrooxidation (EO) and UV/H_2O_2. EO operating conditions: current density = 7.41 mA/cm^2, time = 30 min, pH = 7, and electrolyte = Na_2SO_4. UV/H_2O_2 operating conditions: UV fluence = 0.43 J/cm^2, H_2O_2 dose = 34 mg/L, and pH = 7.5. Values of sNRP transformation using UV/H_2O_2 were reported by Venkiteshwaran et al. (2021a). The bars show the average of triplicate experiments, while the error bars represent ± 1 standard error. **(b)** Comparison of energy consumption for DON and sNRP transformation, where compounds above the 1:1 line were more efficiently transformed using EO. The filled symbols indicate inorganic sNRP, while the open symbols represent organic sNRP. (Met = methionine, BSA = bovine serum albumin, HCT = hydrochlorothiazide, PA = phytic acid, BGP = beta-glycerol phosphate, HMP = hexa-meta phosphate, TrP = sodium triphosphate, TEP = triethyl phosphate).

Although Figure 4.7b shows energy efficiency in terms of E_{EM} (which is used for zero order kinetics, as observed in this study), E_{EO} is commonly used to compare energy efficiency amongst AOPs. Accordingly, to facilitate broader process comparison, the E_{EM} values from this study were transformed to E_{EO}, values of which ranged from 9.29×10^3 to 6.17×10^5 kWh/m/order for EO transformation of DON and sNRP in synthetic matrices (($1.67 \pm 0.16) \times 10^3$ and ($2.81 \pm 1.10) \times 10^3$ kWh/m^3/order for wastewater DON and sNRP, respectively). These values are orders of magnitude greater than typical wastewater treatment E_{EO} values (approximately 0.25 to 150 kWh/m^3/order, Miklos et al. (2018)). However, E_{EO} values for electrochemical treatments are typically higher (up to 10^3 kWh/m^3/order) than conventional AOPs such as UV/H$_2$O$_2$ (Miklos et al., 2018). One possible way to reduce the energy demand for EO-based transformation could be partial oxidation of DON and sNRP, just to the point at which they could be subsequently removed and recovered, thus avoiding the high energy inputs associated with complete oxidation.

4.4. Conclusions

Transformation of recalcitrant DON and sNRP to more readily removable/recoverable DIN and sRP forms could potentially help utilities meet stringent nutrient discharge limits and recover N and P more effectively. EO successfully transformed DON to DIN and sNRP to sRP, with greater transformation of sNRP compared to DON. The resulting DIN (NO$_3^-$) and sRP (orthophosphate) products can then be removed and recovered using approaches such as struvite precipitation, ion exchange, or algal bio-assimilation (Kim et al., 2020; Ribeiro el al., 2020). Using EO, the organic compounds transformed more efficiently compared to the inorganic forms, with

variable results depending on the location of the N and P in the chemical structure. The DON and sNRP naturally present in secondary wastewater effluent may be more amenable to EO transformation compared to spiked recalcitrant compounds due to partial degradation in previous wastewater treatment processes.

Transformation of DON and sNRP was characterized by zero order kinetics, indicating current densities below the limiting current density, and suggesting that direct electron transfer was the dominant pathway for EO-based transformation. Conversely, UV/H_2O_2 transformation stemmed from the presence of HO•, and was less efficient compared to EO. Both DON and sNRP transformation consumed high levels of energy using EO, making it challenging for full-scale application (although if AOP treatment was already in use, e.g., for water reuse, nutrient transformation may be a positive incidental outcome). While complete transformation to nitrate and phosphate may be economically infeasible, partial transformation of DON and sNRP may be achievable using lower EO energy inputs. Thus, future evaluations of the removability and recoverability of partially oxidized DON and sNRP would better inform sustainable nutrient management strategies.

5. **OBJECTIVE 2: ASSESS THE MECHANISM OF ELECTROOXIDATION-BASED TRANSFORMATION OF RECALCITRANT PHOSPHORUS AND RECOVERABILITY OF CENTRATE RECALCITRANT PHOSPHORUS AFTER ELECTROOXIDATION**

5.1. Introduction

Excess release of nutrients, e.g., phosphorus (P), into surface waterbodies can lead to algal blooms or eutrophication, causing hypoxic conditions detrimental to aquatic life. Wastewater P discharge can contribute to increased P loading into surface water bodies. Advanced water reclamation processes can help minimize P discharge. Additionally, P management sustainability can be stimulated by recovering wastewater-derived P as valuable products, e.g., fertilizer, bio-fuel feed stock, etc. Therefore, treatment processes targeting enhanced P removal and recovery can help achieve sustainable P management.

Conventional treatment processes, e.g., enhanced biological P removal, ion exchange, chemical precipitation, filtration, coagulation, sedimentation, flocculation, and adsorption generally remove particulate P and soluble reactive P (sRP), while soluble non-reactive P (sNRP) is generally not treated effectively (Venkiteshwaran et al., 2018a). Approximately 26 – 81% of total P (TP) in wastewater effluent can be present in the sNRP form (Qin et al., 2015). Given sufficient time, discharged sNRP can be transformed into bioavailable forms through microbial processes and cause eutrophication (Qin et al., 2015). Due to the recalcitrance of sNRP species, it also generally cannot be recovered using conventional recovery strategies like precipitation. Removal of sNRP species will decrease overall eutrophication formation potential while its recovery will help achieve enhanced P recovery. Therefore, technologies targeting sNRP removal and recovery are beneficial for achieving enhanced sustainable P management strategies.

Studies using UV/H_2O_2, UV/TiO_2, Fenton, and photo-Fenton have targeted removal or detoxification of sNRP compounds, but recovery has not been assessed (Badawy et al., 2006; Daneshvar et al., 2004; Gray et al., 2020). Transformation of sNRP to sRP can provide a viable pathway for enhanced recovery as sRP is more readily recoverable through ion exchange and struvite precipitation. For example, transformation of sNRP to sRP is possible using electrooxidation (EO), UV/H_2O_2, and ozonation (Ahmadi, 2017; Mallick et al., 2021; Sindelar et al., 2016; Venkiteshwaran et al., 2021a). Mallick et al. (2021) reported that EO-based sNRP to sRP transformation was more effective than conventional advanced oxidation processes (AOPs), e.g., UV/H_2O_2, both in terms of energy efficiency and the degree of transformation (Chapter 4). However, the energy input required for transformation was still very high, making implementation of EO for P transformation purposes challenging (Mallick et al., 2021).

The high energy demand for complete transformation of sNRP compounds may be circumvented if partial transformation of sNRP compounds can improve subsequent recovery using P-selective adsorbents. Partially transformed sNRP compounds might be concentrated using ion exchange and then further treated for enhanced removal and recovery. Therefore, this study evaluated the potential for partial transformation of sNRP using EO to improve the subsequent recoverability of sNRP species using LayneRT[TM] ion exchange media with the hypothesis that recovery of EO-treated sNRP compounds would be higher than untreated sNRP compounds. If LayneRT[TM] can remove more sNRP after EO treatment, then the high energy demand for complete sNRP transformation could be avoided.

The specific study objectives were to: (i) investigate the role of potential EO-based transformation mechanisms (e.g., sorbed oxidants, dissolved oxidants, and direct electron transfer [DET]) and (ii) assess the recoverability of sNRP after EO using ion exchange. The EO-based sNRP to sRP transformation mechanism was studied as the process can be better controlled once the dominant mechanism is identified. For instance, if DET is the dominant mechanism, then an increase in applied current density below the limiting current density would increase transformation. Experiments from the previous chapter indicated that DET was likely the dominant mechanism for EO-based sNRP transformation, but the role of different mechanisms (sorbed vs. dissvoled oxidants, DET) was not extensively studies in Chapter 4. Therefore, the role of sorbed and dissolved oxidants were evaluated and DET was confirmed in this chapter. Lab-grade sNRP compounds were used in the mechanism analysis, whereas municipal wastewater centrate, which contains high levels of P, was used to assess sNRP recoverability after EO treatment. Recoverability of sNRP using ion exchange after EO was first assessed using synthetic water matrices containing phytic acid (PA) or beta-glycerol phosphate (BGP). A real-world wastewater sample, centrate from anaerobic digestor, was then used to assess kinetic and isotherm models of EO-treated sNRP removal using ion exchange.

5.2. Materials and methods

5.2.1. Electrooxidation (EO) reactor

The EO reactor consisted of a 250-mL Berzelius beaker (holding 200 mL solution) with a 3D-printed plastic reactor cap providing 1-cm inter-electrode spacing. Titanium (Performance Titanium Group, San Diego, CA) was used as the cathode while boron-doped diamond (BDD) (Fraunhofer, Lansing, MI) was used as the anode. The electrode surface area was 13.5 cm^2. The reactor contents were continuously stirred at 50

rpm during experiments using a multi-position magnetic stirrer (Bell-ennium, Vineland,

NJ). A current density of 7.41 mA/cm^2 was applied using a Sorensen XPH75-2D DC

Power Supply (AMETEK Inc., Berwyn, PA) for all EO experiments.

5.2.2. Investigation of the role of sorbed and dissolved oxidant mechanisms

Two organic sNRP compounds previously shown to transform during EO

(Mallick et al., 2021 [Chapter 4]), e.g., PA and BGP were selected to explore the role of

sorbed versus dissolved oxidants in quencher experiments. The initial concentrations of

sNRP compounds were 1 mg P/L, consistent with the concentration used in Chapter 4.

Low P concentrations were chosen as P discharge regulations are projected to be

increasingly stringent to prevent eutrophication in receiving waterbodies. In separate

experiments, allyl alcohol was used to quench sorbed oxidants while tertiary butanol was

used to quench dissolved oxidants. The structure of both compounds and quenchers is

shown in Figure C.1 of Appendix C. Due to the interaction between the π-orbital of

unsaturated allyl alcohol and the anode surface, allyl alcohol primarily interacts with

oxidants sorbed on the anode surface (Barazesh et al., 2016). Allylic carbon is highly

reactive with oxidants, and because allyl alcohol interacts very strongly with the anode

surface, highly concentrated allyl alcohol (100 mM) reacts with anode-sorbed oxidants

while the other compounds dissolved in the solution (here, PA or BGP) react with any

dissolved oxidants generated in the system (Celdrán and González-Velasco, 1981; Pastor

et al., 1993).

Tertiary butanol is a saturated alcohol that does not readily interact with the anode

surface, but it does react with dissolved oxidants (Malliaris et al., 1987). Therefore,

tertiary butanol quenches dissolved oxidants and the transformation of PA or BGP in the

presence of tertiary butanol would be attributed to oxidation by sorbed oxidants. High concentrations of quenchers (100 mM) were used to confirm complete quenching of dissolved or sorbed oxidants.

The EO quencher tests were conducted for 30 minutes using 7.41 mA/cm^2 current density. Samples were collected at 1, 2, 5, 10, 20, and 30 minutes to assess the transformation kinetics of PA and BGP in the presence of allyl alcohol or tertiary butanol. All chemicals were purchased as 99% pure forms from Sigma Aldrich (St. Louis, MO).

5.2.3. Investigation of the role of direct electron transfer

Direct electron transfer (DET) on the anode was assessed through chronoamperometry tests using a VersaSTAT 4 potentiostat (Berwyn, PA). These tests were conducted in synthetic water matrices prepared by spiking deionized water with an electrolytic salt: sodium sulfate (Na_2SO_4), sodium bicarbonate ($NaHCO_3$), or sodium chloride (NaCl) were tested independently. Concentrations of the electrolytic salts are shown in Table B.2 in Appendix B. Solutions were spiked with 1 mg P/L BGP, an sNRP compound demonstrating transformation during EO (Mallick et al. 2021 [Chapter 4]). Only BGP was tested in the DET experiment as BGP and PA previously showed similar transformation trends (Mallick et al., 2021 [Chapter 4]). To distinguish between DET of the electrolyte and BGP, control tests were run with the electrolyte alone as well as electrolyte plus BGP. An increase in current after BGP addition would indicate oxidation through DET.

For chronoamperometry experiments, a constant voltage of -1.8 V was applied for 60 s. The applied voltage was set lower than the hydroxyl radical (HO•) generation

overpotential to avoid producing HO• to specifically test DET potential for sNRP to sRP transformation.

5.2.4. Centrate characterization and treatment

After exploring the mechanisms of EO-based sNRP transformation in synthetic matrices, transformation was tested in actual wastewater matrices with high P content, i.e., centrate. Centrate was collected from the South Shore Water Reclamation Facility (Oak Creek, WI) where solids from anaerobic digestor are conditioned with Mannich polymer (Clarifloc C-321) and then thickened using a gravity belt thickener. Centrate was characterized by measuring total solids (TS), total suspended solids (TSS), volatile solids (VS), volatile suspended solids (VSS), total chemical oxygen demand (TCOD), soluble chemical oxygen demand (sCOD), dissolved organic carbon (DOC), P speciation (total P, total soluble P, total reactive P, sRP), and UV absorbance.

The solids tests were conducted following the protocols described in 2540 B, D, and E of standard methods (APHA, 2012). The COD tests were conducted using a chemical-reaction digestion method (U.S. EPA approved Hach Method 8000, Loveland, CO). After filtering samples through a 0.45 µm PTFE syringe filter (Agela Technologies, Wilmington, DE) and acidifying them with HCl, DOC was measured using a Shimadzu TOC VCSN analyzer (Kyoto, Japan), in accordance with U.S. EPA Method 415.3. These results are compiled in Table C.3 of Appendix C.

Centrate samples were treated with 7.41 mA/cm^2 current density EO for 2, 4, or 6 hours to achieve varying degrees of P transformation. Mineralization of organics was determined by measuring DOC after EO treatment. Transformation of organics was further evaluated by analyzing UV absorbance after EO treatment. A UV-VIS spectroscopy scan was conducted from 200 to 400 nm using a Genesys 50 UV-VIS

Spectrophotometer (Fisher Scientific, Waltham MA) for both untreated and treated

centrate samples. UV absorbance at 254 nm was recorded to assess the extent of organic

transformation during EO treatment and $SUVA_{254}$ was calculated by normalizing DOC to

UV_{254} absorbance.

5.2.5. Ion exchange tests

LayneRT[TM] ion exchange resin (Layne Christensen Company, The Woodlands,

TX) was used to assess the recoverability of partially transformed sNRP compounds after

EO treatment. After the ion exchange experiments, total soluble P and sRP analyses were

conducted (as described in Section 5.2.6) to determine the removal of EO-treated sNRP

using ion exchange.

5.2.5.1. Testing sNRP removal using ion exchange after EO treatment in synthetic matrices

Synthetic water matrices were prepared by spiking an electrolytic solution

(Na_2SO_4 dissolved into deionized water) with the sNRP compound PA or BGP (15 mg

P/L) in separate experiments. These synthetic water matrices were then treated with EO

for 2, 4, or 6 hr. Batch ion exchange experiments were conducted by dosing 10 mL

untreated or EO-treated sNRP solutions with 250 mg LayneRT[TM] in accordance with

Tong et al. (2017)'s protocol for P removal using LayneRT[TM]. Samples were mixed on a

Multi-Purpose Tube Rotator at 20 rpm for 5 days (Thermo Fisher Scientific, Waltham,

MA).

5.2.5.2. Kinetics of centrate sNRP removal using ion exchange

Removal of centrate sNRP using LayneRT[TM] was evaluated after 0, 2, 4, or 6 hr

EO treatment. The kinetics of sNRP removal using ion exchange were tested by dosing

10 mL of EO-treated centrate with 250 mg LayneRT[TM] in independent sorption tests for

0.5, 1, 2, 3, 5, 24.5, or 48 hours with constant mixing at 20 rpm on a Multi-Purpose Tube

Rotator. For kinetic modeling, data points were evaluated for pseudo-first order and

pseudo-second order kinetics. The linear form of pseudo-first order kinetics is shown in

Equation 5.1, while the linear form of pseudo-second order kinetics is shown in Equation

5.2.

$$\ln(q_e - q_t) = \ln q_e - K_{PFO}\, t \qquad\qquad \text{Equation 5.1}$$

$$\frac{t}{q_t} = \frac{1}{K_{PSO}\, q_e^2} + \frac{1}{q_e} t \qquad\qquad \text{Equation 5.2}$$

where, q_e = adsorption of sNRP at equilibrium (mg P/ g LayneRT^{TM}),

q_t = adsorption capacity of sNRP at time t in hr (mg P/ g LayneRT^{TM}),

K_{PFO} = pseudo-first order rate constant (1/hr), and

K_{PSO} = pseudo-second order rate constant (g LayneRT^{TM} /mg P-hr).

Using the best linear model fit, nonlinear modeling was performed, as shown in

Equations 5.3 and 5.4 for pseudo-first and pseudo-second order kinetic modeling,

respectively:

$$q_t = q_e(1 - e^{-K_{PFO}\, t}) \qquad\qquad \text{Equation 5.3}$$

$$q_t = \frac{q_e^2\, K_{PSO}\, t}{q_e\, K_{PSO}\, t + 1} \qquad\qquad \text{Equation 5.4}$$

5.2.5.3. Isotherms of centrate sNRP removal using ion exchange

For adsorption isotherm modeling, sNRP removal using LayneRT^{TM} ion exchange

resin was tested by dosing 10 mL of centrate with 25, 50, 100, 150, 200, or 250 mg

LayneRT^{TM}. The kinetic tests of sNRP removal using LayneRT^{TM} indicated that the

change in sNRP concentration was less than 5% after 4 days. Thus, isotherm experiments

were conducted for 5 days with 20 rpm mixing in a Multi-Purpose Tube Rotator. The Langmuir (Equation 5.5) and Freundlich (Equation 5.6) linear models were evaluated using the data.

$$\frac{C_e}{q_e} = \frac{1}{K_L \, q_{max}} + \frac{C_e}{q_{max}}$$
Equation 5.5

$$\log q_e = \log K_F + \frac{1}{n}\log C_e$$
Equation 5.6

where, C_e = concentration of sNRP in equilibrium (mg P/L),

q_{max} = maximum sNRP adsorption capacity (mg P/ g LayneRT^{TM}),

K_L = Langmuir constant (1/mg P),

K_F = Freundlich constant ([mg P/ g LayneRT^{TM}]*[L/mg P]$^{1/n}$), and

n = unitless empirical constant in the Freundlich isotherm model.

Using the best linear model fit, nonlinear modeling was performed using the Langmuir (Equation 5.7) or Freundlich (Equation 5.8) nonlinear isotherm models:

$$q_e = \frac{q_{max} \, K_L \, C_e}{1 + K_L \, C_e}$$
Equation 5.7

$$q_e = K_F \, C_e^{1/n}$$
Equation 5.8

5.2.6. P analyses

Total P (TP) and reactive P measurements (after persulfate digestion, Method 4500 P B 5) were conducted using the ascorbic acid method (4500 P E) according to standard methods (APHA, 2012). Filtered samples (0.45 μm Whatman™ cellulose membrane filter, GE Healthcare Life Sciences, Chicago, IL) were used to measure dissolved species. The concentration of sNRP was calculated by subtracting sRP from

total soluble P. The minimum detection level (MDL) of the ascorbic acid method was

0.02 mg/L, calculated in accordance with the EPA recommended method (EPA, 2016).

5.2.7. Precipitate analysis

After EO, solid white precipitate was observed on the cathode surface (Figure

C.3). This solid was analyzed using energy dispersive x-ray (EDX) analysis. The EDX

analysis was conducted with a JEOL JSM 6510 LV SEM (Jeol USA Inc., Peabody, MA)

at 20 kV using backscatter electron imaging in the low vacuum mode. The solid

precipitate was dissolved into 5 mL 50% HCl and then analyzed using ICP-MS (7700

Series, Agilent Technologies, Santa Clara, CA) as well as via the ascorbic acid method to

determine its reactive P content.

5.2.8. QA/QC and statistical analysis

All centrate characterization analyses were run in triplicate. All quenching

experiments for investigating sorbed and dissolved oxidant impacts on transformation as

well as the ion exchange experiments were run in triplicate, with results representing the

average of three different centrate samples. Statistical analyses were performed using

one-way ANOVA and Tukey post hoc analysis with a significance level of $\alpha = 0.05$ in

GraphPad Prism 9.3.1 (La Jolla, CA).

5.3. Results and discussion

5.3.1. The role of sorbed and dissolved oxidants in electrooxidation (EO)-based phosphorus transformation

Transformation of the sNRP compounds PA and BGP in the presence of allyl

alcohol and tertiary butanol was significantly less compared to transformation without

any quencher ($p < 0.0001$), indicating that neither sorbed nor dissolved oxidants played a

critical role in the transformation of sNRP compounds (Figure 5.1a). While DET

transformation of PA or BGP should still occur in the presence of either of the quenchers, the low levels of transformation observed are believed to be a result of the relatively high concentration of quenchers used (100 mM) compared to the orders of magnitude lower concentrations of PA (5.4 µM PA or 1 mg P/L) and BGP (32.3 µM or 1 mg P/L) in solution. The highly concentrated quenchers likely outcompeted PA or BGP for DET, resulting in low sNRP transformation.

Transformation of PA and BGP followed zero order kinetics in the presence of the quenchers (Figure 5.1b), consistent to PA and BGP transformation without quenching, as reported in Mallick et al.'s (2021) study (Chapter 4). Zero order kinetics are expected to prevail when DET is the dominant mechanism in the electrochemical reactor (Almomani et al., 2020). The rate constants corresponding to PA and BGP transformation with quenchers were statistically similar ($p \geq 0.1572$) and are listed in Table C.1.
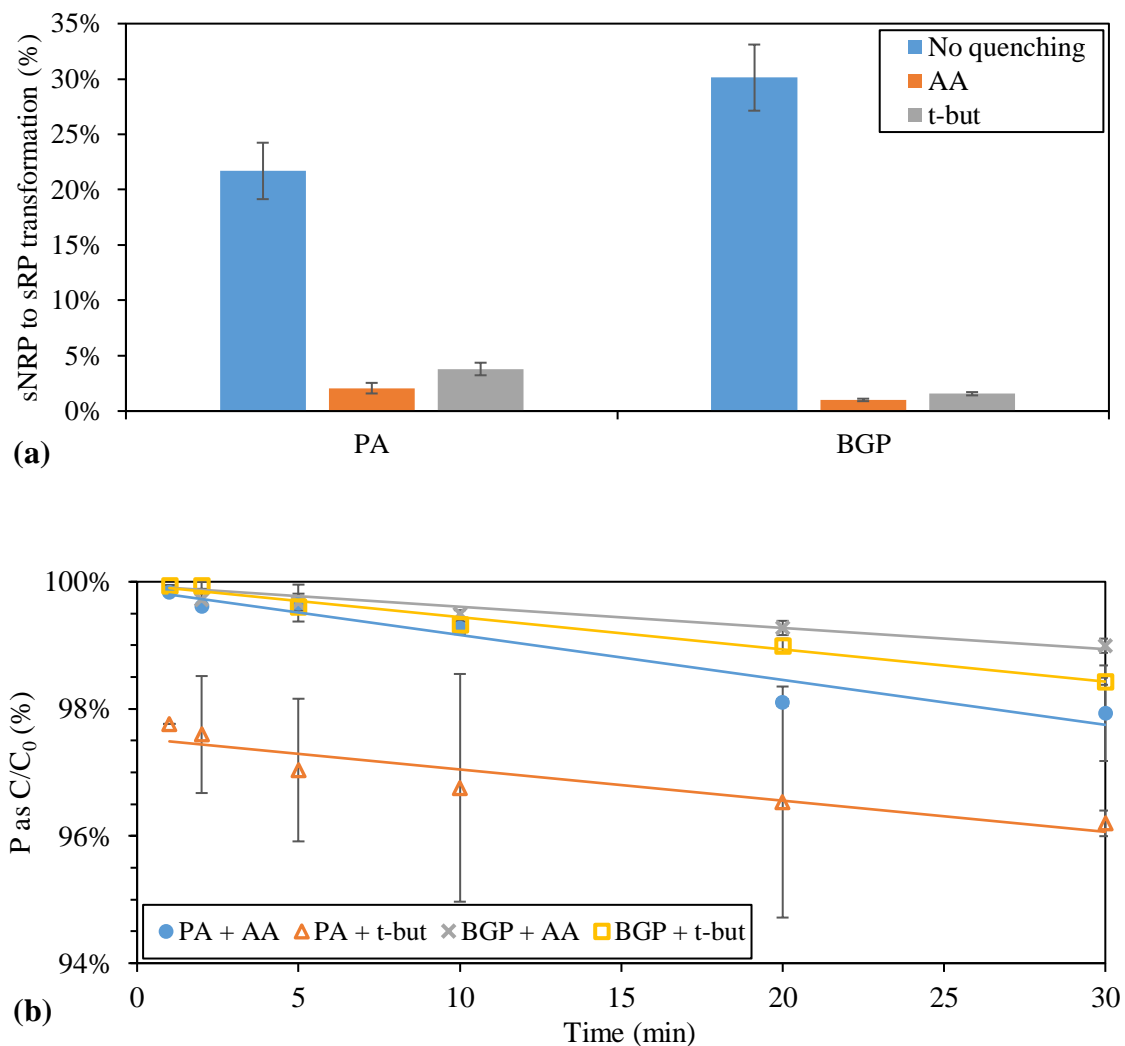
Figure 5.1. (a) Electrooxidation (EO)-based transformation of phytic acid (PA) and beta-glycerol phosphate (BGP) in 600 mg/L Na_2SO_4 electrolyte with and without the addition of 100 mM allyl-alcohol (AA) or tertiary butanol (t-but) quenchers under neutral pH condition after 30 minutes of EO treatment conducted at 7.41 mA/cm^2 current density and 50 rpm mixing speed. **(b)** Transformation kinetics for PA and BGP transformation in the presence of AA and t-but quenchers under the same EO treatment conditions. Data points show the average of triplicate experiments, and the error bars represent ±1 standard error. Note that the scale of the y axes is different to enhance readability.

5.3.2. Confirmation of direct electron transfer (DET) for phosphorus transformation

As discussed in the previous section, EO-based sNRP to sRP transformation was

likely achieved due to DET. However, the quencher experiments did not directly assess

DET of sNRP compounds. Therefore, chronoamperometry experiments were conducted

using BGP to assess DET. Compared to the control tests run with the electrolyte alone,

addition of the sNRP compound BGP increased current in the chronoamperometry tests

(Figure 5.2), indicating that BGP caused additional electron transfer, or DET, in the

system. Similar results were observed for the other electrolytes, $NaHCO_3$ and $NaCl$

(Figure C.2).

The cumulative evidence of low transformation in the presence of oxidant

quenchers, zero order kinetics, and chronoamperometry experiments indicated that DET

was the dominant mechanism in EO-based sNRP transformation. This information is

important to inform process control. For instance, since DET is the dominant mechanism

in EO-based transformation, higher transformation can be achieved by applying higher

current density.
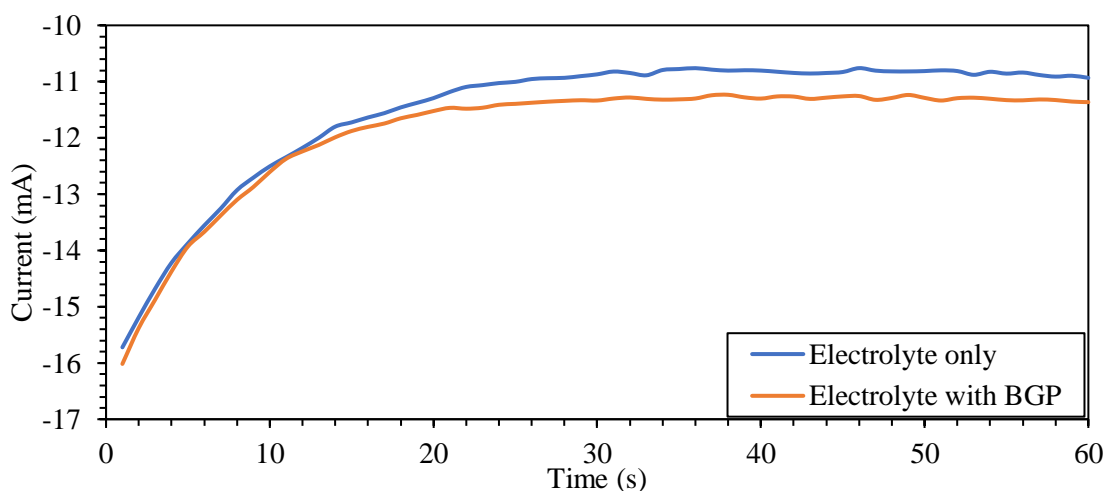
Figure 5.2. Direct electron transfer tests using chronoamperometry in synthetic water matrices using 600 mg/L Na_2SO_4 as electrolyte. One set of experiments was conducted using only the electrolyte and another set of experiments was conducted using the electrolyte spiked with 1 mg P/L beta-glycerol phosphate (BGP). An increase in current indicates that BGP underwent direct electron transfer in the electrooxidation reactor.

5.3.3. Removal of sNRP after EO treatment using ion exchange: Synthetic water matrices

After EO treatment, sNRP removal using ion exchange in synthetic water matrices containing PA or BGP improved significantly with each incremental increase in EO treatment ($p < 0.0001$, Figure 5.3). Increased sNRP adsorption to LayneRT^{TM} after EO treatment indicates that partially transformed sNRP compounds were better removed using ion exchange. Compared to untreated synthetic matrices, the 6 hr EO-treated centrate sample increased sNRP removal using ion exchange by 11%.
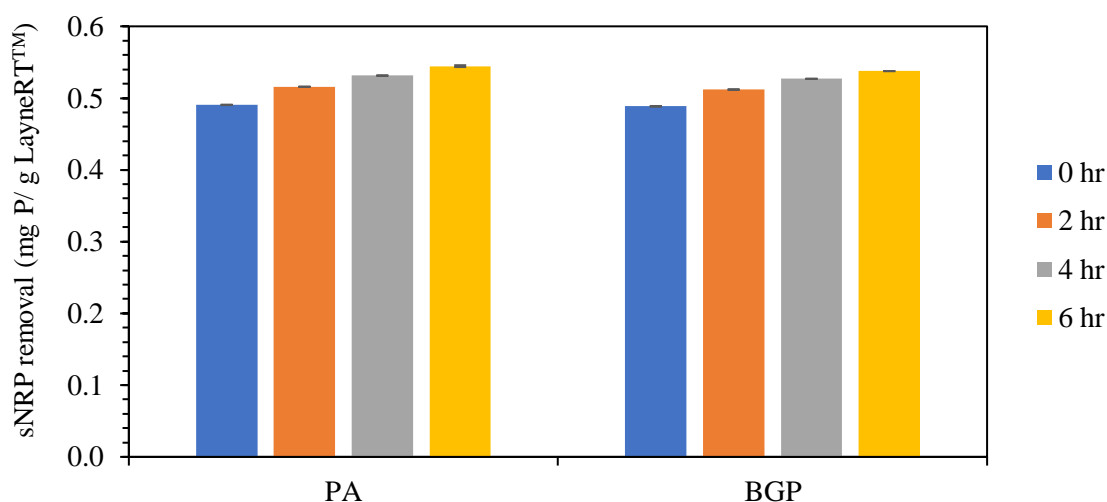
Figure 5.3. Removal of soluble non-reactive (sNRP) using LayneRT^{TM} after EO treatment in electrolytic (600 mg/L Na$_2$SO$_4$) synthetic water matrices containing either phytic acid (PA) or beta-glycerol phosphate (BGP). Electrooxidation was performed using 7.41 mA/cm^2 current density and 50 rpm mixing speed for 0, 2, 4, or 6 hr. The ion exchange experiments were conducted for 5 days in batch experiments at 20 rpm mixing speed dosing 10 mL of synthetic water matrices (15 mg P/L) with 250 mg LayneRT^{TM}. The bars in the figure represent averages of triplicate analyses while the error bars represent ±1 standard error.

5.3.4. Shifts in centrate phosphorus (P) speciation after electrooxidation (EO)

In realistic water matrices, the presence of organics and other constituents could compete with sNRP removal. Therefore, removal of EO-treated sNRP in centrate using ion exchange was tested. To assess centrate sNRP removal using ion exchange after EO treatment, centrate was first treated with EO for 2, 4, or 6 hr. Complete transformation of wastewater centrate sNRP (as indicated by an increase in reactive P species) was not observed after EO treatment (Figure 5.4). However, TP and total reactive P decreased significantly ($p \leq 0.0058$) after 2 hr of EO treatment, with no further decreases after 4 and 6 hr of EO treatment ($p \geq 0.5584$). Given that there was no significant change in total soluble P, sRP, or sNRP before and after treatment ($p \geq 0.147$), the decrease in TP and total reactive P was attributed to transformation to particulate reactive P, which partitioned out of solution, as observed by the deposition of white precipitates (Figure C.3) on the titanium cathode surface after EO treatment.
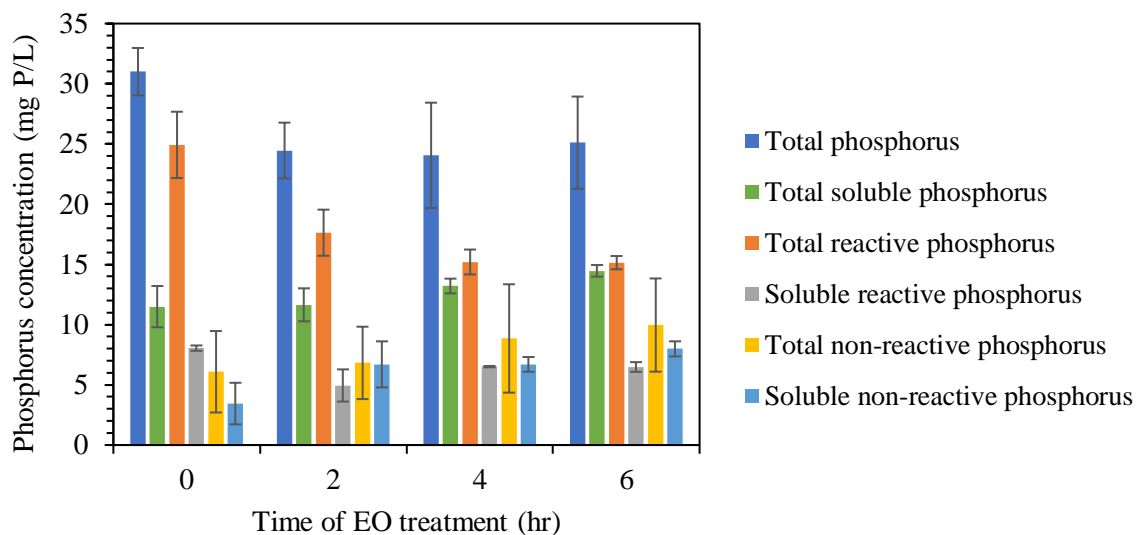
Figure 5.4. Phosphorus (P) speciation in municipal wastewater centrate before and after electrooxidation (EO). EO was performed using 7.41 mA/cm^2 current density and 50 rpm mixing speed. The bars in the figure represent averages of triplicate analyses while the error bars represent ±1 standard error. Soluble non-reactive

The composition of the solids was further analyzed using EDX, which showed

peaks for magnesium, calcium, phosphorus, oxygen, and carbon (Figure C.4) indicating

that the precipitate might contain phosphates of magnesium and calcium. The precipitate

was dissolved in 50% HCl for reactive P and ICP-MS analyses. The precipitate contained

1.2 mg or 38 µmol P. The summation of reactive P in the precipitate and bulk solution

was statistically similar to the bulk solution reactive P content in the untreated centrate

(Figure C.5, $p = 0.7730$). ICP-MS analysis showed that the precipitate contained 1.5 mg

(62 µmol) magnesium and 5.2 mg (131 µmol) calcium, indicating that the precipitate

could be a mix of calcium and magnesium phosphates. The bulk solution pH (8.2 – 8.4)

did not change with EO treatment; this slightly alkaline pH is generally not suitable for

magnesium or calcium phosphate precipitation (Diaz et al., 1994). However, the local pH

at the titanium cathodes can be much higher (9.9 – 14.5) facilitating precipitation on the electrode surface (Lei et al., 2017).

Although no transformation to sRP was achieved, mineralization of organic carbon was observed during EO treatment (Figure 5.5a). Organic carbon mineralization was $17.8 \pm 3.2\%$, $12.7 \pm 2.9\%$, and $30.4 \pm 3.7\%$ after 2, 4, and 6 hr of EO treatment, respectively. Organic carbon mineralization after 2 and 4 hr of EO treatment was statistically similar ($p = 0.1295$) but significantly higher mineralization ($p = 0.0001$) was achieved after 6 hr of EO treatment. The centrate $SUVA_{254}$ (Figure 5.5b) was statistically similar between the untreated centrate and 2 hr EO treatment ($p = 0.2402$). After 4 hr of EO treatment, a significant decrease ($p = 0.0009$) in $SUVA_{254}$ was achieved, but no further decrease was achieved with 6 hr EO treatment ($p = 0.7822$). The complete UV spectrum from 200 nm to 400 nm for centrate treated with EO for 0, 2, 4, and 6 hr is provided in Figure C.6. Overall, EO was able fully oxidize a fraction of the organics present (reduction in DOC) and partially oxidize others (shift in $SUVA_{254}$, indicating less relative aromaticity in centrate organics after EO treatment), although sNRP transformation to sRP was not achieved.
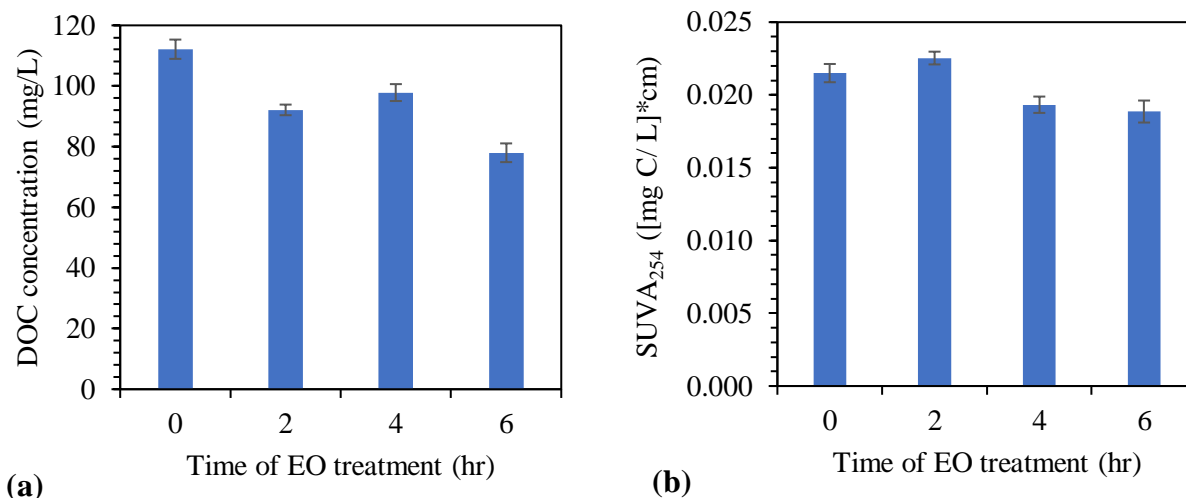
Figure 5.5. **(a)** Change in municipal wastewater centrate dissolved organic carbon (DOC) and **(b)** specific UV absorbance (SUVA$_{254}$) after electrooxidation (EO) treatment. EO was operated at 7.41 mA/cm^2 current density and 50 rpm mixing speed. The bars in the figure represent averages of triplicate analyses while the errors bars represent ±1 standard error

5.3.5. Removal of EO-treated centrate P using ion exchange: Kinetics and isotherms

A major objective of this study was to assess if EO treatment could increase the recoverability of centrate sNRP such that improved removal of partially transformed sNRP after EO would circumvent the high energy demand of complete transformation to sRP (the P form most amenable to removal and recovery). As shown by the kinetic (Figure 5.6) and isotherm (Figure 5.7) modeling using LayneRT^{TM} ion exchange resin, EO treatment improved removal of centrate sNRP species without the need for complete transformation to sRP.

Both pseudo-first order and pseudo-second order kinetic models of sNRP removal using LayneRT^{TM} offered strong fits (R^2 > 0.95, linear models shown in Figure C.7). However, the pseudo-second order nonlinear model (with the exception of 4 hr EO-treated centrate) offered a better fit (Figure 5.6), indicating that sNRP removal using

LayneRT^{TM} depended on the diffusion of sNRP to the ion exchange sites (Plazinski et al., 2013).

There was a significant increase in sNRP removal capacity (q_e) between the untreated centrate sample (t = 0) and after 2 hr of EO treatment (p = 0.0061) (Figure 5.6). Subsequent incremental increases in EO treatment time did not significantly improve adsorption capacity (p $\geq$ 0.0920). This demonstrates that even though EO did not completely transform sNRP compounds (Figure 5.4), the compounds were still more easily removable and recoverable using ion exchange after EO.

(a)

(b)
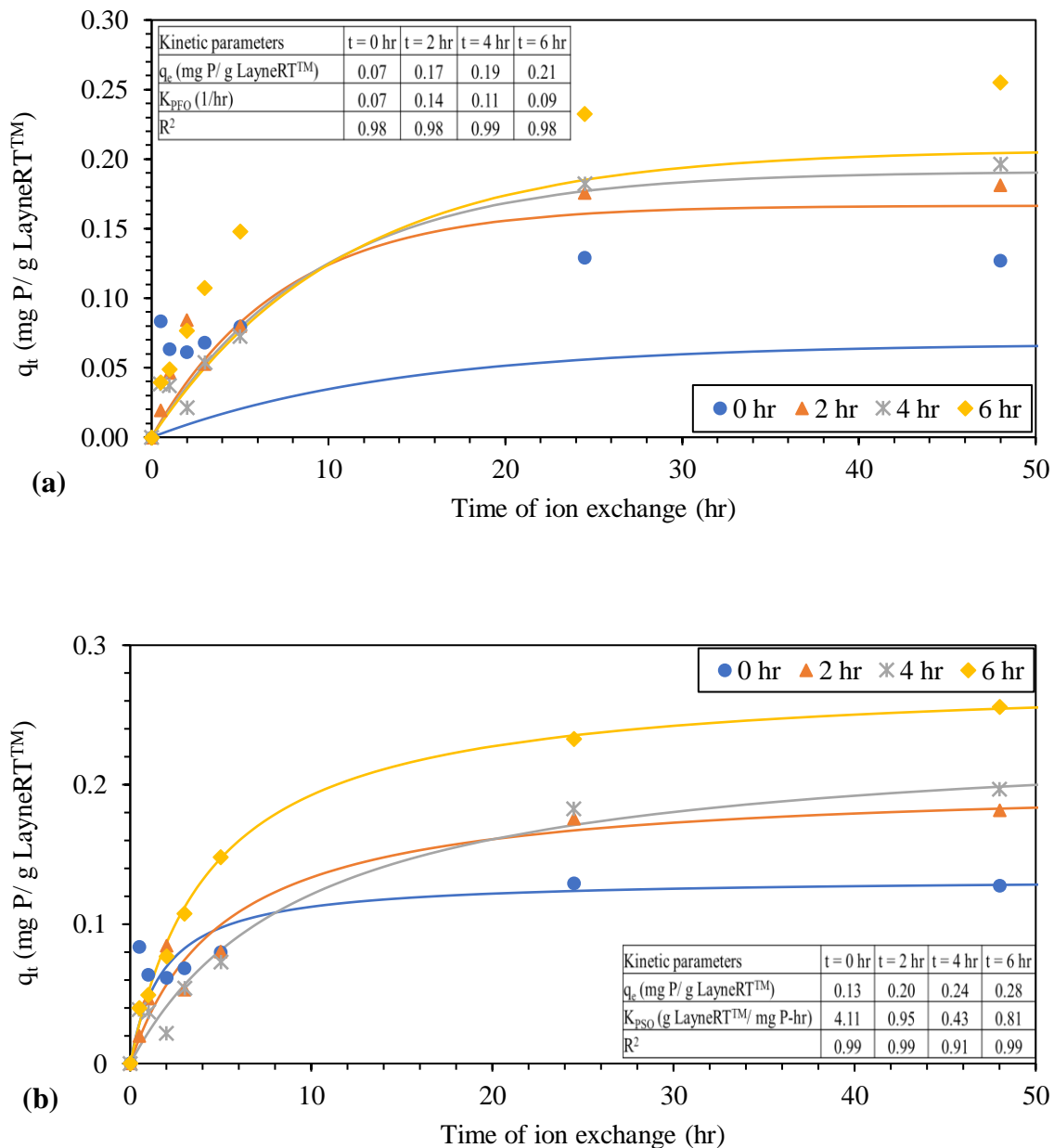
Figure 5.6. (a) Pseudo-first order and **(b)** pseudo-second order kinetic models of soluble non-reactive P (sNRP) removal from wastewater centrate using LayneRT^{TM} ion exchange resin after electrooxidation (EO) treatment for 0, 2, 4, or 6 hr. EO was operated at 7.41 mA/cm^2 current density and 50 rpm mixing speed. The ion exchange kinetics were conducted in batch experiments at 20 rpm mixing speed dosing 10 mL of centrate with 250 mg LayneRT^{TM}. The R^2 values listed in the tables represent R^2 associated linear fitting of the respective models.

The linear Langmuir model provided a better fit ($R^2 \geq 0.85$) for sNRP removal using LayneRT^{TM} than the Freundlich model ($R^2 \leq 0.11$) (Figure C.8). The nonlinear Langmuir model is thus shown in Figure 5.7. The maximum sNRP removal capacity (q_{max}) increased significantly after 2 hr of EO treatment ($p = 0.0141$). However, further improvement in q_{max} was not achieved after 4 and 6 hr of EO treatment ($p \geq 0.7146$). LayneRT^{TM}'s affinity for sNRP adsorption, represented by the Langmuir constant (K_L), did not change significantly after EO treatment ($p \geq 0.8069$). Given that complete sNRP transformation was not observed (Figure 5.4) and that partial transformation of sNRP would be anticipated to improve sorption capacity (Figure 5.3), this lack of change in affinity suggests that negligible sNRP transformation occurred. However, the wastewater organic analysis showed that after EO treatment, there were fewer organics (particularly aromatic organics, as represented by $SUVA_{254}$), such that sNRP had less competition for the ion exchange sites (Tong et al., 2017).
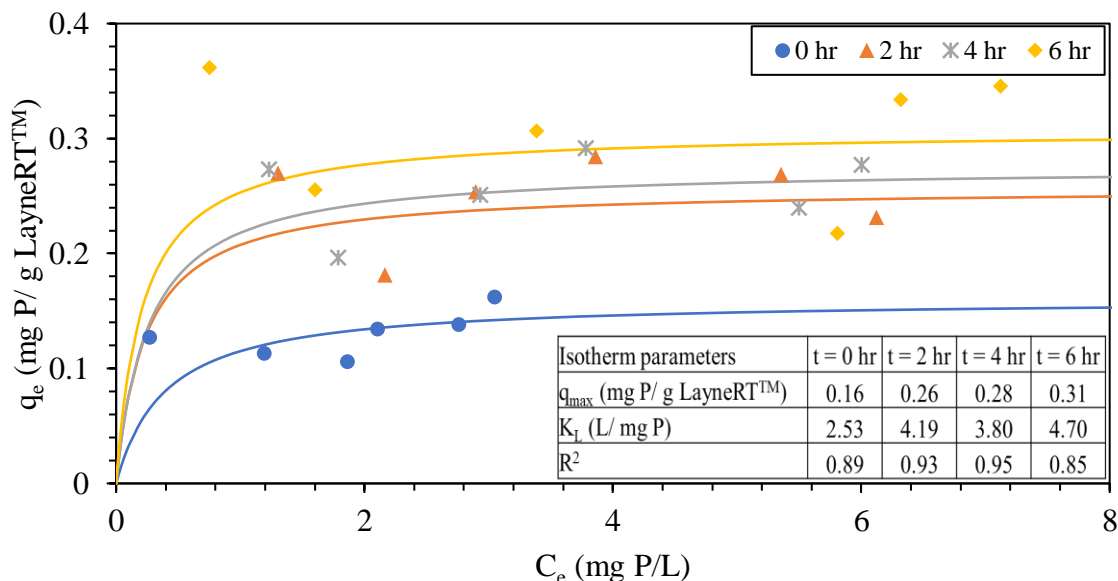
Figure 5.7. Langmuir isotherm of soluble non-reactive phosphorus (sNRP) removal using LayneRT^{TM} ion exchange material after electrooxidation (EO) treatment for 2, 4, or 6 hr. EO was operated at 7.41 mA/cm^2 current density and 50 rpm mixing speed. Isotherms were conducted in batch experiments at 20 rpm mixing speed for 5 days, which was sufficient to achieve equilibrium. The R^2 values listed in the tables represent R^2 associated linear fitting of the respective models.

5.4. Conclusions

Transformation of sNRP using EO can offer a viable pathway for non-reactive P recovery as shown in Mallick et al's (2021) study (Chapter 4). In this chapter, the EO-based sNRP to sRP transformation mechanism was investigated and the recoverability of centrate sNRP after EO treatment was evaluated. Transformation of sNRP appears to be due to DET on the anode.

Removal of sNRP compounds in synthetic water matrices using ion exchange improved significantly after EO treatment. To assess performance in a more realistic water matrix, centrate was treated with EO and sNRP removal using ion exchange was evaluated. Complete transformation of centrate sNRP was not achieved using EO, although reactive P from the bulk solution precipitated as particulate P (ostensibly

magnesium and calcium phosphates) on the cathode surface. Electrochemical

precipitation can thus offer a P recovery pathway if the precipitate is separated for reuse

applications, e.g., as fertilizer. Even though centrate sNRP did not completely transform,

recoverability of the EO-treated centrate sNRP increased. Since the affinity for sNRP

removal using LayneRT^{TM} was virtually the same after EO treatment, increased removal

of sNRP after EO treatment can likely be attributed to less competition from organics in

the EO-treated centrate samples. However, increasing recoverability of centrate sNRP

using EO might not be a practical choice due to the low increase in recoverability in

response to the high energy input. Alternate pathways, e.g., selective adsorption, may

offer a more efficient means of improved sNRP removal and recovery from wastewater.

6. OBJECTIVE 3: EVALUATE ADSORPTION OF RECALCITRANT PHOSPHORUS COMPOUNDS USING THE PHOSPHATE-SELECTIVE BINDING-PROTEIN PSTS

This work was previously published as:

> Mallick, S.P., Hussein, F.B., Husted, S., Mayer, B.K., 2022. Adsorption of Recalcitrant Phosphorus Compounds using the Phosphate-Selective Binding-Protein PstS. *Chemosphere*, *304*, 135311.

It is republished here, with minor adjustments, with permission from the journal.

6.1. Introduction

Phosphorus (P) is the limiting nutrient in most freshwater ecosystems, such that excess P in surface waters can cause harmful algal blooms or eutrophication (Carpenter, 2008). Major sources of P release into surface waterbodies can include stormwater run-off of agricultural P products or wastewater-derived P discharge (Drolc and Zagorc Koncan, 2002). Reducing P discharges into surface waterbodies is therefore critical. Water resource recovery facilities (WRRFs) may need to consider advanced treatment to reduce P discharge as much as possible (Mayer et al., 2016). Beyond P removal, recovery of wastewater-derived P can enhance P sustainability as non-renewable mineral P resources are depleted to meet increasing fertilizer demands (Reijnders, 2014). Recovery of waste-derived P for reuse as fertilizer is therefore important to meet both environmental protection goals and sustain high levels of global food production.

Conventional biological and physical-chemical wastewater treatment processes used for P treatment include enhanced biological P removal, adsorption, ion exchange, chemical precipitation, micro- or ultra-filtration, and coagulation/flocculation/sedimentation (Morse et al., 1998). However, only particulate P and the reactive form of P (primarily consisting of orthophosphate) are generally

removed using these conventional treatment processes (Venkiteshwaran et al., 2018a).

Reactive P is defined as being detectable in a colorimetric test, whereas the remaining P,

classified as non-reactive P, must undergo hydrolysis or oxidation to make it detectable

(APHA, 2012). Gu et al. (2011) showed that conventional P treatment typically removes

less than 40% of soluble non-reactive P (sNRP). Consequently, approximately 26 – 81%

of wastewater effluent P can be in the more recalcitrant sNRP form (Qin et al., 2015).

Following effluent discharge to environmental waters, sNRP can be transformed through

enzymatic processes or photolysis, or directly utilized by microbes in a reactive-P-limited

aquatic environment (Qin et al., 2015). For example, Qin et al. (2015) demonstrated

approximately 75% utilization of effluent sNRP for algal biomass growth. Therefore,

developing technologies to effectively remove sNRP from wastewater is critical to reduce

P discharge and the associated negative effects.

Currently, sNRP removal studies are limited, and focus primarily on advanced

oxidation processes (AOPs). Removal, detoxification, or transformation of sNRP

compounds using AOPs such as UV/H_2O_2, UV/TiO_2, Fenton, photo-Fenton, and

electrooxidation has been reported (Badawy et al., 2006; Daneshvar et al., 2004; Gray et

al., 2020; Mallick et al., 2021; Sindelar et al., 2016; Venkiteshwaran et al., 2021a).

Adsorption offers another route to achieve effective sNRP removal without direct

energy inputs, but there are currently limited reports of sNRP adsorption/desorption

efficiency. Long contact times were needed to remove sNRP using hierarchical porous

magnesium oxide (Hr-MgO), granular activated carbon (GAC), powdered activated

carbon (PAC), carbon nanotubes, XAD resin, and lanthanum (La)-based adsorbents

(Campos do Lago et al., 2020; Xu et al., 2020; Sharma and Kakkar, 2017; Wang et al.,

2018a, 2018b). Most of these studies reported that the time to reach adsorption equilibrium ranged from hours to longer than a day (although adsorption of triphenyl phosphate on PAC was faster, at approximately 15 minutes). An additional consideration is that these materials are non-selective for sNRP or other P species. This may negatively impact adsorption efficiency and limits the potential to recover pure P products.

Resins with selectivity for orthophosphate, or reactive phosphorus (P_i), (e.g., LayneRT^{TM} or phosphate-binding protein resin) may offer a means to adsorb sNRP compounds, particularly those compounds with phosphate functional groups, while minimizing non-target adsorption. However, evaluations of the adsorption potential of sNRP compounds on P-selective materials is lacking. In this study, we assessed the adsorption/desorption potential of sNRP using a promising protein-based phosphate-selective adsorbent featuring immobilized PstS phosphate-binding proteins (PBP).

The P-selective PBP PstS is an integral part of the high-affinity phosphate-specific transporter system expressed naturally by many microorganisms when P_i concentrations are low. The protein's ability to adsorb monobasic ($H_2PO_4^-$) and dibasic (HPO_4^{2-}) P_i (Wang et al., 1994) even at low levels makes it attractive for use in systems targeting ultra-low effluent P concentrations. The PBP sequesters P_i in a deep cleft using 12 strong hydrogen bonds formed between the phosphate molecule's 4 oxygen atoms and the protein's amino acid residues (Luecke and Quiocho, 1990). These interactions yield PBP's exquisite P_i-specificity (Luecke and Quiocho, 1990), which has been harnessed to remove and recover P_i using both proteins in microbial cells and extracted proteins immobilized on resins suitable for flow-through filter operation (Hussein and Mayer, 2022; Venkiteshwaran et al., 2021b; Venkiteshwaran et al., 2018b; Yang et al., 2016;

Choi et al., 2013; Li et al., 2009; Kuroda et al., 2000). Notably, immobilized PBP adsorbents offer faster adsorption and greater P_i selectivity compared to metal-oxide P_i-selective materials, including LayneRT P_i-selective ion exchange material (Hussein and Mayer, 2022; Venkiteshwaran et al. 2020), but have yet to be tested for sNRP removal/recovery. Recalcitrant sNRP compounds with accessible phosphate functional groups may be able to bind to PBP's active site, facilitating removal, followed by pH adjustment to stimulate sNRP release, facilitating recovery (Venkiteshwaran et al., 2020). Since orthophosphate binds with PBP using hydrogen bonds between the oxygen atoms of phosphate molecules and amino acid residues of PBP, it was hypothesized that PBP would adsorb sNRP compounds with terminal orthophosphate functional groups. Therefore, the objectives of this study were to: (1) assess sNRP adsorption efficiency using immobilized PBP, including testing sNRP binding affinity, kinetics, adsorption isotherms, thermodynamics, and competition between P_i and sNRP; and (2) evaluate the recoverability of adsorbed sNRP compounds through desorption experiments.

6.2. Materials and methods

6.2.1. sNRP compounds

Four sNRP compounds were selected to represent different types of wastewater sNRP (e.g., organic and inorganic compounds with cyclic or simple structure): beta-glycerol phosphate (BGP), phytic acid (PA), sodium triphosphate (TrP), and sodium hexametaphosphate (HMP) (Figure 6.1). BGP is a simple organic compound whereas PA is a cyclic organic compound. Among the inorganic sNRP compounds tested, TrP has a simple structure while HMP has a complex cyclic structure. All compounds were 99% pure, and purchased from Sigma Aldrich (St. Louis, MO). All sNRP solutions were made by spiking Tris buffer (10 mM Tris-HCl, 1 mM $MgCl_2$, pH 7) with sNRP at an initial

concentration of 0.36 ± 0.02 mg P/L. During the adsorption isotherm experiments, a range of sNRP concentrations were tested: 0.075, 0.1, 0.2, 0.25, 0.3, and 0.35 mg P/L. Low concentrations were used to assess the adsorption capacity of PBP resin targeting removal of total phosphorus (TP) from initially low levels to ultra-low levels (i.e., tertiary treatment to satisfy ultra-low discharge regulations).
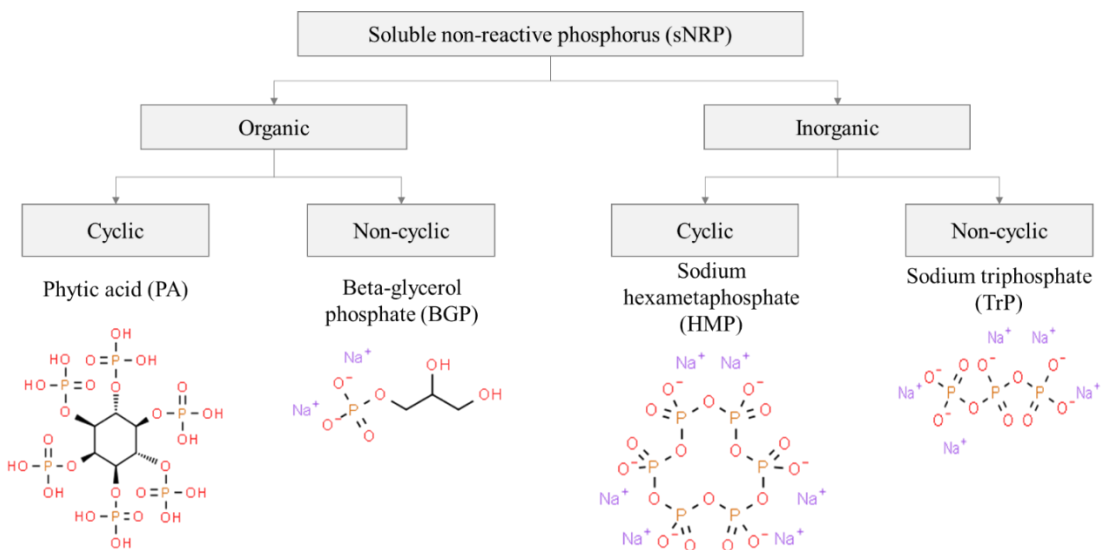
Figure 6.1. Selected soluble non-reactive phosphorus (sNRP) compounds tested in this study. Different types of compounds (organic, inorganic, cyclic, non-cyclic) were tested to represent a range of wastewater sNRP compounds. All chemical structure images were taken from Chemspider.

6.2.2. PBP resin preparation

The adsorption and desorption experiments were conducted using immobilized PBP (PBP resin) as immobilized PBP is better suited for wastewater treatment applications. The PBP resin was prepared by expressing, purifying, and immobilizing PBP on NHS-activated Sepharose beads, in accordance with protocols described by Venkiteshwaran et al. (2018b). Briefly, His-tagged PBP was over-expressed into *E. coli* BL21 (DE3) cells (Thermo Fisher Scientific, Waltham, MA) grown in Luria broth (LB)

using isopropyl β-D-1-thiogalactopyranoside (IPTG). After 4-hours at 35 ⁰C, cells were centrifuged and the cell pellets were collected and stored at 4 ⁰C. Over-expression of PBP was confirmed using SDS-PAGE. Cell pellets were resuspended in a binding buffer (50 mM NaH_2PO_4, 500 mM NaCl, 10 mM imidazole, pH 6) and lysed via sonication at 45% amplitude and a pulse rate of 15 s on and 45 s off (Q500 sonicator, QSonica L.L.C., Newtown, CT). The solution was then centrifuged (1000 rpm, 6700 xg) to remove cellular debris. The supernatant containing PBP was added to a Ni^{2+} column (Ni Sepharose[TM] 6 Fast Flow, Cytiva, Marlborough, MA) containing the binding buffer and gently mixed for 1 hour. The Ni^{2+} column was then rinsed 5 times using an elution buffer at pH 8. The elution buffer consisted of 137.5 mL of purification buffer (50 mM NaH_2PO_4, 500 mM NaCl) and 12.5 mL of 3 M imidazole. An SDS-PAGE gel was used to confirm the presence of purified PBP. Purified PBP was then dialyzed in a dialysis buffer (0.2 M $NaHCO_3$, 0.5 M NaCl, pH 8) for 4.5 hours and stored in 70% glycerol at -80 ⁰C (volumetric ratio of PBP to glycerol was 4 to 1). The purified PBP concentration was 9.4 ± 0.3 mg/mL, as measured using a Pierce[TM] BCA Protein Assay Kit (Thermo Fisher Scientific, Waltham, MA).

To immobilize PBP on the NHS-activated Sepharose 4 Fast Flow beads (Cytiva, Marlborough, MA), purified PBP was first dialyzed for 4.5 hours in the dialysis buffer using a Spectra/Por 2 dialysis membrane (MWCO 12 – 14 kDa, Spectrum Laboratories Inc., Rancho Dominguez, CA) to remove the glycerol storage solution. The NHS beads were prepared following the manufacturer's protocol (71-5000-14AAD, Cytiva, Marlborough, MA). Dialyzed PBP was added to the NHS beads and gently mixed for 4 hr. After 4 hr, the solution was drained and the PBP resin was washed 3 times using acid

(0.1 M Na-acetate, 0.5 M NaCl, pH 4.5) and base (0.1 M Tris-HCl, pH 8) solutions. The

PBP resin was stored in storage buffer (10 mM Tris-HCl, 1 mM $MgCl_2$, pH 7) at 4 ℃ for

up to 48 hr prior to experimentation. Before experiments, PBP resin was washed in

storage buffer at pH 7 and pH 12. The alkaline buffer solution removed residual P from

the PBP resin. The PBP resin was then resuspended in an equal bed volume of storage

buffer at pH 7. The concentration of PBP was measured using a Pierce™ BCA Protein

Assay Kit before and after attachment to determine attachment efficiency on the NHS

beads. The PBP concentration on the NHS beads ranged from 15.6 to 16.5 nmol/mL.

Ultrapure water (resistivity of 18.2 MΩ*cm at 25 ± 1°C, Elga, High Wycombe, UK) was

used to prepare all solutions and buffers.

6.2.3. PBP binding affinity for sNRP compared to P_i

The PBP's affinity for different sNRP compounds was evaluated using isothermal

titration calorimetry (ITC) (performed by Charles River Laboratories, Essex, UK).

Briefly, refolded PBP was dialyzed in size exclusion chromatography (SEC) buffer (20

mM Na-HEPES, 150 mM NaCl, pH 7.4). In individual experiments, 0.5 – 5 mM of each

P compound (PA, BGP, HMP, TrP, or P_i) was titrated with 50 µM PBP in SEC buffer at

25 ˚C. Changes in heat, or enthalpy (ΔH, kJ/mol), were measured using a VP-ITC

MicroCalorimeter (MicroCal Incorporated, Commerce, CA). A plot of ΔH versus molar

ratio was used to calculate the dissociation constant, K_D, and change in entropy (ΔS,

kJ/mol-K). For protein-ligand binding, the lower the K_D value, the higher the protein's

affinity to bind with the ligand. The thermodynamic feasibility of binding (change in

Gibb's free energy, $\Delta G = \Delta H – T\Delta S$, where T = temperature in K and ΔG is quantified in

kJ/mol) was calculated using the ΔH and ΔS values to provide an indicator of

thermodynamic feasibility of the binding reaction (signified by negative ΔG).

6.2.4. Adsorption (kinetics, isotherms, competition) and desorption experiments

Kinetic experiments were conducted using 15.6 – 17.3 nmol PBP (1.3 mL of PBP resin suspension) together with 10.5 mL of sNRP solution (pH 7) containing 0.36 ± 0.02 mg P/L mixed on a Multi-Purpose Tube Rotator at 20 rpm (Thermo Fisher Scientific, Waltham, MA). To determine how quickly sNRP compounds adsorbed, independent batch experiments were run for 0.5, 1, 2, 5, 10, and 20 minutes.

Isotherm experiments were conducted using 16.6 nmol PBP (1.3 mL PBP resin suspension) together with 10.5 mL of sNRP solution (pH 7) containing different P concentrations: 0.071, 0.106, 0.204, 0.242, 0.301, and 0.363 mg P/L. These experiments were conducted for 10 minutes (sufficient to achieve equilibrium, as indicated by the kinetic experiments).

To assess for competition between P_i and the sNRP compounds, a pH 7 buffer containing varying ratios of sNRP to P_i (20%, 60%, 70%, or 100% TP as sNRP) was exposed to 21 nmol PBP for 10 minutes.

Phosphorus desorption experiments were conducted by first adsorbing sNRP onto 21 nmol PBP resin for 10 minutes at pH 7. After 10 minutes, the solution was decanted and the saturated PBP resin was resuspended into a Tris buffer (10 mM Tris-HCl, 1 mM $MgCl_2$) at pH 8, 10, or 12 for 10 minutes. All experiments were conducted at 25 ˚C.

6.2.5. Kinetic modeling

Adsorption kinetics generally follow pseudo-first order (PFO) or pseudo-second order (PSO) models (Revellame et al., 2020). The fit of both models was evaluated for the adsorption data in this study. The nonlinear forms of the PFO and PSO models are shown in Equations 6.1 and 6.2, respectively (the linear forms are shown in Appendix 0):

$$q_t = q_e(1 - e^{-K_{PFO} t})$$ Equation 6.1

$$q_t = \frac{q_e^2 K_{PSO} t}{q_e K_{PSO} t + 1}$$ Equation 6.2

where, q_e = adsorption of sNRP at equilibrium (nmol P/ nmol PBP),

q_t = adsorption capacity of sNRP at time t in min (nmol P/ nmol PBP),

K_{PFO} = pseudo-first order rate constant (1/min), and

K_{PSO} = pseudo-second order rate constant (nmol PBP/ nmol P-min).

6.2.6. Isotherm modeling

Adsorption data were fit to the Langmuir and Freundlich isotherm models, the nonlinear forms of which are shown in Equations 6.3 and 6.4, respectively (the linear forms are shown in Appendix 0).

$$q_e = \frac{q_{max} K_L C_e}{1 + K_L C_e}$$ Equation 6.3

$$q_e = K_F C_e^{1/n}$$ Equation 6.4

where, C_e = concentration of sNRP in equilibrium (µM P),

q_{max} = maximum sNRP adsorption capacity (nmol P/nmol PBP),

K_L = Langmuir constant (1/µM P),

K_F = Freundlich constant ([nmol P/nmol PBP]*[L/µmol P]$^{1/n}$), and

n = unitless empirical constant in the Freundlich isotherm model.

6.2.7. Analytical methods and QA/QC

The concentrations of P_i and sNRP were measured immediately after adsorption or desorption experiments in accordance with APHA (2012) standard methods for ascorbic acid P_i (4500-P E) and TP (4500-P B) analyses by means of absorbance at 880

nm (Agilent Technologies, Santa Clara, CA, USA). The minimum detection limit (MDL)

for the P_i and TP tests was 0.017 and 0.015 mg P/L, respectively, as determined

following the EPA method (EPA, 2016). Phosphorus-free storage buffer blanks (10 mM

Tris-HCl, 1 mM $MgCl_2$, pH 7) were used for all P_i and TP analyses. All experiments

were run in triplicate. Statistical analysis was performed using two-way ANOVA and

Tukey post hoc tests ($\alpha = 0.05$) using GraphPad Prism 9.3.1 (GraphPad Software Inc., La

Jolla, CA).

6.3. Results and Discussion

6.3.1. PBP binding affinity and thermodynamic feasibility for sNRP compared to P_i

The ITC K_D values indicated that, unsurprisingly, PBP (*phosphate*-binding

protein) had the greatest affinity for P_i (Table 6.1). However, PBP was also able to bind

sNRP, albeit with lesser affinity. Among the sNRP compounds, PBP exhibited the

greatest affinity for PA (K_D similar to P_i) followed by BGP, HMP, and TrP.

The change in Gibb's free energy (ΔG) for each ligand pairing calculated using

ΔS from the ITC results indicated thermodynamic feasibility of sNRP binding to PBP,

although P_i binding was most favorable (Table 6.1).

Table 6.1. Thermodynamic properties of binding between phosphate-binding proteins (PBP) and soluble reactive phosphorus (sRP) or soluble non-reactive phosphorus (sNRP). The dissociation constant (K_D), change in enthalpy (ΔH), change in entropy (ΔS), and change in Gibb's free energy (ΔG) were assessed using isothermal titration calorimetry (ITC).

Classification	Compounds	K_D (μM P)	ΔH (kJ/ mol)	ΔS (kJ/mol -K)	ΔG (kJ/ mol)
sRP	Orthophosphate (P_i)	0.030	-14.5	8×10^{-3}	-16.9
sNRP	Phytic acid (PA)	0.031	-2.9	1×10^{-3}	-5.9
	Sodium triphosphate (TrP)	1.80	-1.6	8×10^{-3}	-4.0
	Sodium hexametaphosphate (HMP)	0.167	-0.6	9×10^{-3}	-3.4
	Beta-glycerol phosphate (BGP)	0.106	-2.6	1×10^{-3}	-5.7

Previously reported K_D values for PBP-P_i binding (Wang et al., 1997) coincide with our findings. However, previously reported ΔG values for PBP-P_i binding indicated greater thermodynamic favorability for PBP-P_i binding (-41.3 kJ/mol) (Venkiteshwaran et al., 2020). Differences in approaches between the two studies may account for the variability. For example, Venkiteshwaran et al. (2020) calculated ΔG from experimental isotherm parameters, whereas calorimetric determination of the thermodynamics of binding was performed here using ITC measurements. Moreover, the ITC experiments performed here were conducted with suspended PBP, whereas immobilized PBP was used previously (Venkiteshwaran et al., 2020). Finally, the PBP tested in the two studies may have differed in the proportion of initially available active sites as the suspended PBP used for ITC was unfolded to remove residual P_i while a pH 12 wash was used to remove residual P_i in the immobilized PBP tests.

6.3.2. Rates of sNRP adsorption on PBP resin

Given that the ITC results showed that sNRP binding on PBP was thermodynamically feasible, experiments were performed to test sNRP adsorption using PBP resin. The rate of adsorption is an important parameter in system design as more rapid adsorption kinetics allow for smaller process volume or lower hydraulic retention times.

The PSO model provided a better fit for sNRP adsorption onto PBP resin ($R^2 \geq 0.98$) compared to the PFO model ($R^2 \leq 0.69$). The non-linear PSO model is shown in Figure 6.2a (the linear PFO and PSO models and associated R^2 values are shown in Figure D.1 in Appendix 0). Similarly, Venkiteshwaran et al. (2020) showed that P_i adsorption on PBP resin followed PSO kinetics.

The relative rate of adsorption was HMP > PA > TrP > BGP. Adsorption of sNRP onto PBP was rapid (time for 95% adsorption, $t_{95\%}$, < 4 min), whereas $t_{95\%}$ was approximately an order of magnitude higher, generally exceeding 30 min, for sNRP adsorption using activated carbon, carbon nanotubes, XAD resins, or La-based adsorbents (Figure 6.2b) (Campos do Lago et al., 2020; Xu et al., 2020; Wang et al., 2018a, 2018b). However, with the exception of HMP, PBP-sNRP binding was slower than PBP-P_i binding, which achieved 95% adsorption in less than 1 minute (Venkiteshwaran et al., 2020).

Kinetic properties	PA	TrP	BGP	HMP
q_e (nmol P/ nmol PBP)	2.22	1.69	1.25	1.04
K_{PSO} (nmol PBP/ nmol P $-$ min)	10.3	2.89	8.08	71.3
$t_{95\%}$ (min)	0.83	3.89	1.88	0.26
R^2	0.99	0.99	0.98	0.99

(a)

(b)
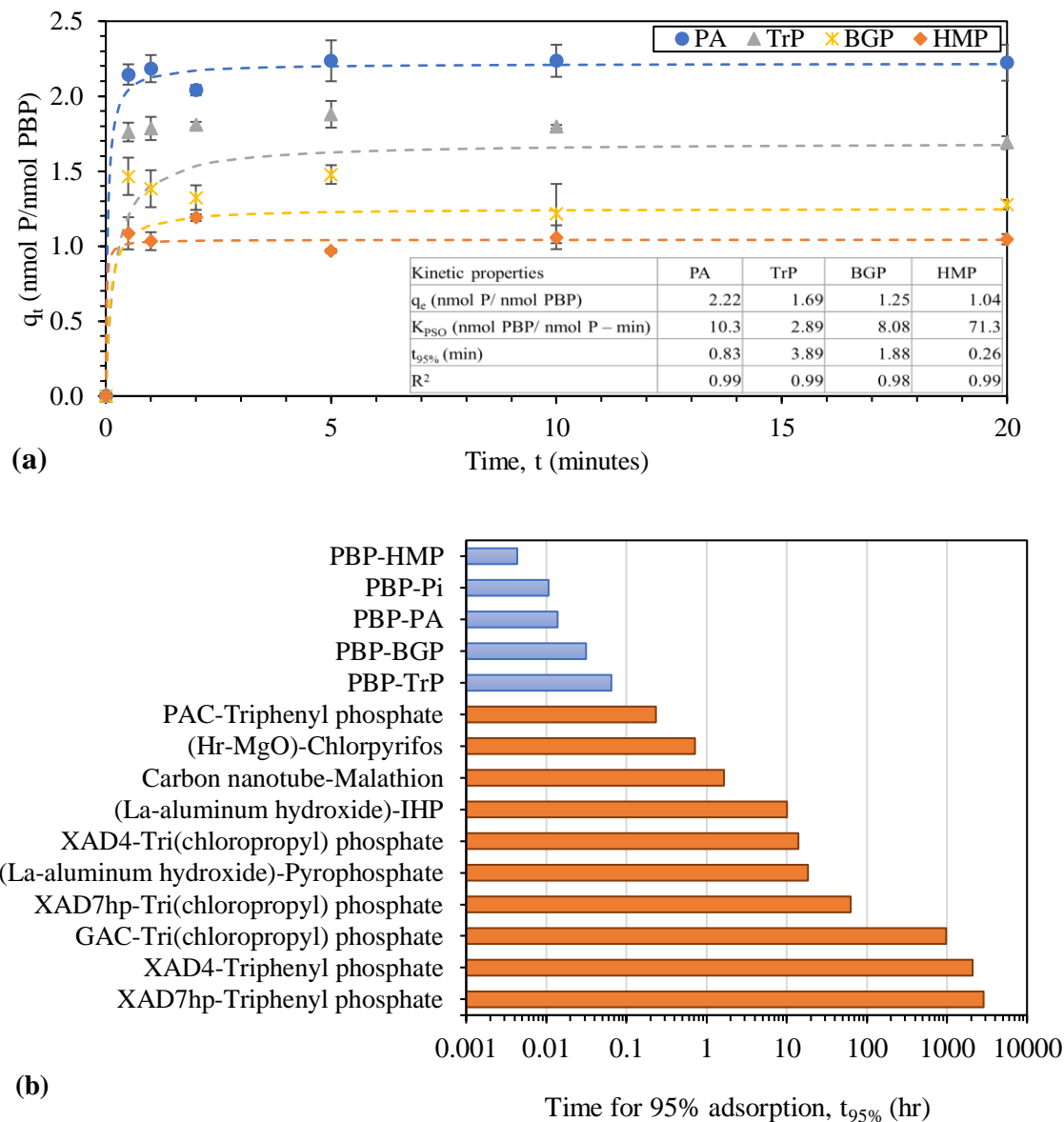
Figure 6.2. (a) Pseudo-second order (PSO) kinetic model for adsorption of phytic acid (PA), sodium triphosphate (TrP), beta-glycerol phosphate (BGP), and sodium hexametaphosphate (HMP) on phosphate-binding protein (PBP) resin. Tests were run at 25 °C under neutral pH conditions. Error bars represent ±1 standard error of triplicate experiments. **(b)** Comparison of the time required to achieve 95% adsorption of P using different adsorbates (written as adsorbent-adsorbate). The blue bars show results using PBP resin to adsorb soluble non-reactive phosphorus (sNRP, this study) as well as reactive phosphorus (P_i) (Venkiteshwaran et al., 2020). The orange bars show results of other adsorbent-sNRP pairings reported in the literature (Campos do Lago et al., 2020; Xu et al., 2020; Sharma and Kakkar, 2017; Wang et al., 2018a, 2018b), all of which take longer than PBP resin to achieve the same extent of sNRP adsorption. The sNRP compound (IHP) removed in the La-aluminum hydroxide study was myo-inositol hexakisphosphate.

6.3.3. Isotherm modeling to determine capacity of PBP resin for sNRP adsorption

The Langmuir isotherm model (nonlinear model shown in Figure 6.3a; linear model, $R^2 \geq 0.96$, shown in Figure D.2a) provided a better fit to the experimental data compared to the Freundlich isotherm model ($R^2 \leq 0.80$, Figure D.2b). The Langmuir isotherm model is used for adsorbents with homogeneous, identical, and energetically equivalent active adsorption sites, for which the adsorbate does not interact with other sites, and once a molecule is bound to an active site, no further binding is possible (Saadi et al., 2015). Accordingly, the strong Langmuir model fit indicates that the active protein-binding site on each PBP molecule binds one available phosphate group (either P_i or an available phosphate group in an sNRP molecule). As shown in Figure 6.3b, PBP offers higher affinity for sNRP compared to sNRP affinity using XAD resins, activated carbon, carbon nanotubes, Hr-MgO, and La-based adsorbents. Notably, among the other adsorbents compared here, PAC had high affinity for triphenyl phosphate (similar order of magnitude to PBP resin, Figure 6.3b), and also provided the most rapid sNRP adsorption after PBP resin (Figure 6.2b).

Langmuir isotherm properties	PA	TrP	BGP	HMP
q_{max} (nmol P/ nmol PBP)	2.37	1.78	1.28	1.04
K_L (L/μmol P)	4.79	2.82	1.71	0.90
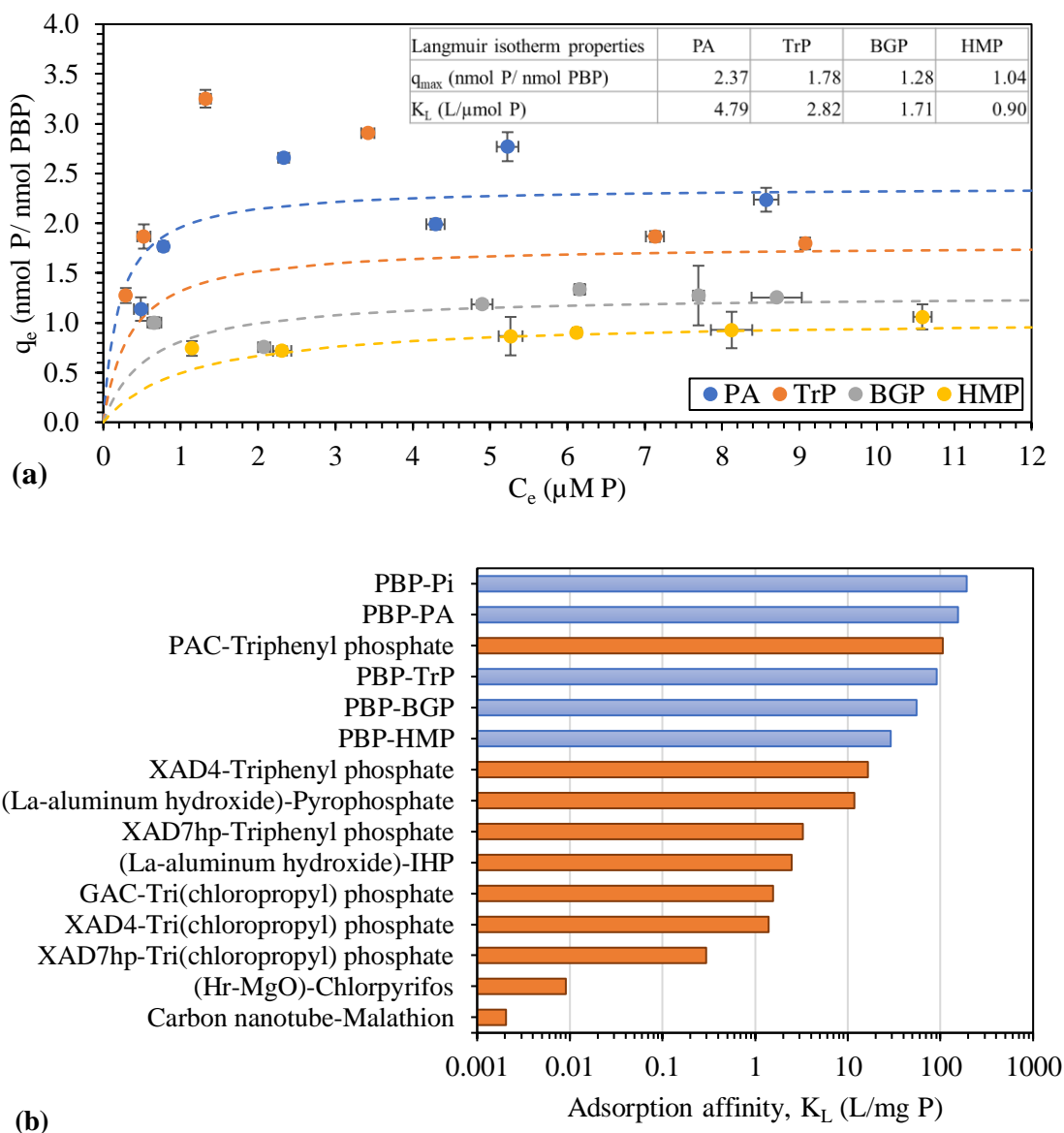
Figure 6.3. (a) Langmuir isotherm model for adsorption of phytic acid (PA), sodium triphosphate (TrP), beta-glycerol phosphate (BGP), and sodium hexametaphosphate (HMP) on phosphate-binding protein (PBP) resin. Tests were run at 25 ⁰C for 10 minutes under neutral pH conditions. Error bars represent ±1 standard error of triplicate experiments. **(b)** Comparison of adsorption affinity, represented as the Langmuir constant (K_L), for adsorption of different adsorbates (written as adsorbent-adsorbate). The blue bars show results using PBP resin to adsorb soluble non-reactive phosphorus (sNRP, this study) as well as reactive phosphorus (P_i) (Venkiteshwaran et al., 2020). The orange bars show results of other adsorbent-sNRP pairings reported in the literature (Campos do Lago et al., 2020; Xu et al., 2020; Sharma and Kakkar, 2017; Wang et al., 2018a, 2018b), many of which have lower sNRP binding affinity compared to PBP resin. The sNRP compound (IHP) removed in the La-aluminum hydroxide study was myo-inositol hexakisphosphate.

The q_{max} values for the sNRP compounds were generally higher compared to the maximum adsorption capacity for P_i on PBP resin (0.90 nmol P_i/ nmol PBP) reported by Venkiteshwaran et al. (2020). This is likely because one terminal phosphate group in an sNRP compound attached to the phosphate-binding site, but total P removal from the solution was higher given that the captured sNRP compounds contained more than one P atom. Adsorption of the sNRP compound HMP (6 P atoms) did not, however, align with this finding. Binding of HMP on the phosphate-binding site might be negatively affected by the lack of two available oxygen atoms in the terminal phosphate group, which would reduce the number of hydrogen bonds formed, and ostensibly needed for effective attachment in the protein cleft (Wang et al., 1997).

The relative order of sNRP adsorption capacity on PBP resin was PA > TrP > BGP > HMP. For comparison, suspended PBP's relative order of binding affinity was PA > BGP > HMP > TrP. This variation highlights the potential for differences in binding and removal coefficients determined using ITC (K_D, calculated from molecular binding energy) versus adsorption isotherm experiments (K_L, calculated from P removal). Although K_D and K_L can be calculated from one another, they reflect differences in determination based on objective. For example, while PBP has one to one molar capacity for P_i binding, higher molar ratios of sNRP removal can be achieved due to higher P content in sNRP molecules. Moreover, as discussed previously, the experimental approach using ITC and adsorption experiments differed (mobilized versus immobilized PBP and unfolding versus alkaline wash to release residual P_i from the purified proteins). Accordingly, the PBP-sNRP binding energy and the actual removal capacity of sNRP

using PBP resin (more representative of wastewater treatment applications) are not necessarily directly proportional.

6.3.4. Competition between P_i and sNRP for adsorption onto PBP resin

PBP exhibits extraordinary affinity for P_i, even relative to very similarly structured oxyanions such as arsenate (Venkiteshwaran et al., 2021b). The ITC results in this study also demonstrated that PBP has stronger affinity for P_i compared to sNRP. However, immobilized PBP's ability to adsorb sNRP even in the presence of P_i, a likely scenario in wastewater matrices, has yet to be tested. Thus, mixtures of sNRP (PA) and P_i were used to assess competitive binding on the PBP resin (Figure 6.4). For solutions containing a mixture of P_i and sNRP, no significant change in P_i binding was observed regardless of the relative ratio of the compounds ($p \geq 0.2437$). This result aligns well with Poole and Hancock's (1984) finding that P_i binding using suspended PBP was not inhibited by organophosphates, even when sNRP was present at 1000-fold higher levels than P_i. However, significantly less sNRP removal resulted as the fraction of sNRP decreased from 100% to 70% and 70% to 60% ($p \leq 0.0002$). No further reduction in sNRP removal was observed when sNRP decreased from 60% to 20% ($p = 0.9711$).
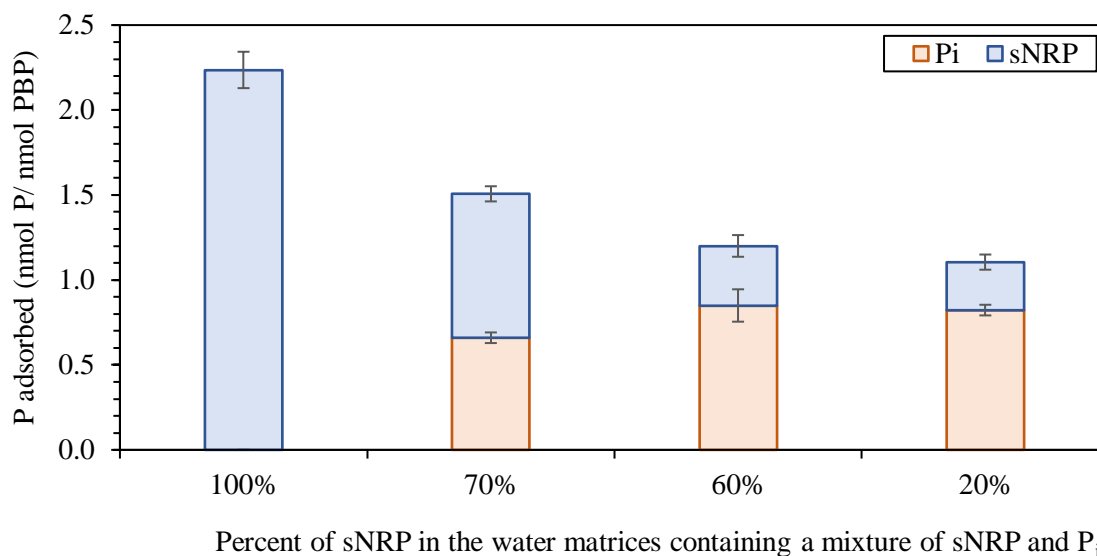
Figure 6.4. Adsorption of orthophosphate (P_i) and sNRP (phytic acid [PA] was used in this test) on phosphate-binding protein (PBP) resin for solutions with varying ratios of P_i to sNRP. The total phosphorus (TP) concentration was 0.35 mg P/L in all tests. Tests were run at 25 ºC for 10 minutes under neutral pH conditions. The error bars represent ±1 standard error of triplicate experiments.

As shown in Figure 6.4, TP removal decreased significantly (p = 0.0068) when P_i was present in the bulk solution. This likely reflects preferential P_i binding, which reduces the number of sites available for sNRP; since each molecule of sNRP contains more P than a molecule of P_i, this results in less TP removal.

6.3.5. Release of sNRP from PBP

Desorption experiments were conducted to assess the recoverability of the sNRP compounds after adsorption on the PBP resin. Venkiteshwaran et al. (2018b) previously showed that PBP released P_i as pH increased; thus, desorption of sNRP was assessed at pH 8, 10, and 12. Desorption of PA and HMP did not increase significantly from pH 8 to 10 (Figure 6.5, $p \geq 0.8920$), but significantly greater desorption occurred when pH increased from 10 to 12 ($p \leq 0.0189$). Desorption of TrP and BGP did not increase significantly from pH 8 to pH 10, nor from pH 10 to pH 12 ($p \geq 0.0670$); however,

desorption at pH 12 was significantly better than pH 8 ($p \leq 0.0269$). Therefore, sNRP adsorption can be performed at circumneutral pH, while desorption can be achieved at pH 12, consistent with recommendations for P_i removal and recovery (Venkiteshwaran et al., 2018b). This result further supports that the sNRP bound to the protein's phosphate-binding site (as opposed to adsorbing on the surface of PBP), which is most active at pH 5.6 to pH 7 and loses its binding activity at pH > 9 (Luecke and Quiocho, 1990; Wang et al., 1994). Via this desorption step, the sNRP can be concentrated into a smaller volume, and subsequently transformed, e.g., using electrooxidation (Mallick et al., 2021 [Chapter 4]) into more readily recoverable forms for enhanced recovery of P products such as struvite.
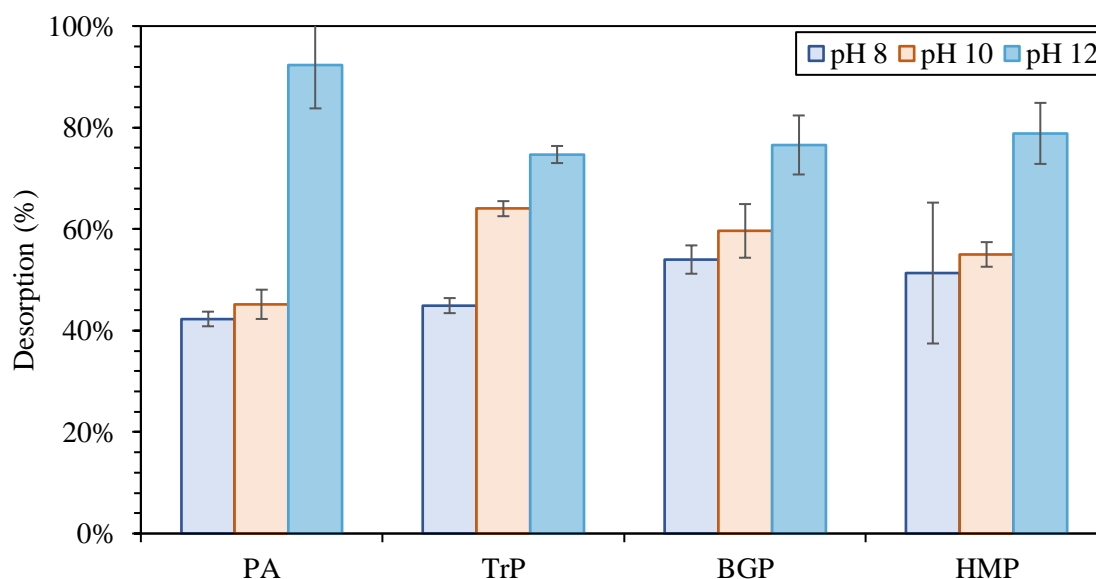
Figure 6.5. Desorption of sNRP – phytic acid (PA), sodium triphosphate (TrP), beta-glycerol phosphate (BGP), and sodium hexametaphosphate (HMP) – after adsorption on phosphate-binding protein (PBP) resin. Tests were run at 25 ⁰C for 10 minutes. The test compounds were first adsorbed on PBP for 10 minutes under neutral pH conditions, then desorbed using pH 8, 10, or 12 buffers. The bars show averages and error bars represent ±1 standard error of triplicate experiments.

6.3.6. Adsorption mechanism for sNRP binding with PBP

As shown in the previous sections, PBP-sNRP binding demonstrated similarity with PBP-P_i binding in terms of rapid binding kinetics, strong Langmuir isotherm model fit, and release of adsorbed sNRP under alkaline condition. This cumulative evidence suggests that sNRP likely bound to PBP's phosphate-binding site using the phosphate functional groups of the sNRP compounds.

When PBP binds P_i, it relies on the formation of 12 hydrogen bonds between the protein's amino acid residues and the oxygen atoms in monobasic or dibasic P_i molecules (Figure 6.6). Although bacteria rely on phosphate-specific transporters (wherein PBP performs the critical initial attachment step) to uptake P_i, when P_i is not available, cells are also capable of using organophosphates (P_i esters, e.g., the organic sNRP species tested here, PA and BGP), inorganic phosphite, and phosphonates. Some organophosphates and phosphonates can enter the cell intact (Santos-Benoit et al., 2008). For example, the binding-protein-dependent Ugp transporter uptakes *sn*-glycerol-3-phosphate (G-3-P) and glycerophosphoryl diesters (whereas Pst or Pit transporters are responsible for P_i uptake) (Wanner 1993). However, since most organophosphates are not transportable, the P_i is typically freed from the organic molecule prior to uptake, e.g., via enzymatic hydrolysis (Ohtake et al., 1998). While the phosphate-specific transport system (Pst) does not transport sNRP into cells, we hypothesize that the binding protein was able to bind accessible phosphate groups on the sNRP molecules that we tested, albeit at lower efficiency compared to P_i due to the presence of the other molecular constituents. For example, BGP's phosphate group may form hydrogen bonds between the three available oxygens and PBP residues, identically to P_i, as shown in Figure 6.6, while the remaining O attached to the $C_3H_7O_2$ does not bind to the active site. Related,

the availability of only a single oxygen atom in HMP may impede its PBP binding

efficiency (thus yielding less P removal even though it has six phosphate functional

groups). Future crystallography assessments of this binding mechanism and the structural

and chemical properties of the ligand interactions are needed to further test this

hypothesis.

Phosphate atom	Hydrogen bond partner residue
O1	Thr 10
	Thr 10
	Arg 135
O2	Arg 135
	Ser 139
	Thr 141
	Thr 141
O3	Ser 38
	Ser 38
	Gly 140
O4	Phe 11
O4-H	Asp 56
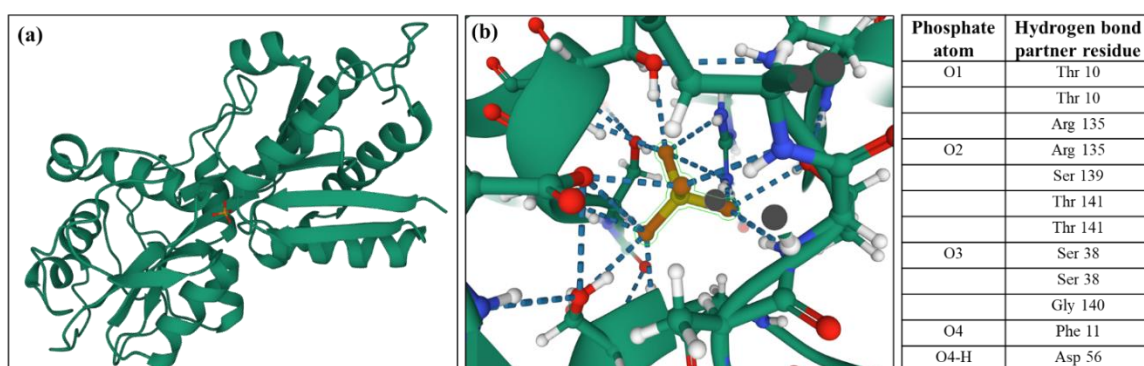
Figure 6.6. (a) Phosphate-binding protein (green) complexed with phosphate (red). (b) Detailed view of the ligand interaction. The phosphate molecule is bound by 12 hydrogen bonds, as specified in the table (Leucke and Quiocho, 1990). Panels a and b were created using PDB ID 1IXH as input to Mol* at www.rcb.org (Sehnal et al., 2021).

Accordingly, sNRP structure and the availability of oxygens to bind at PBP's

active site are likely to strongly influence TP removal and recovery. A combination of

other ambient water quality parameters has also been shown to influence P binding using

immobilized PBP, particularly pH and temperature (Venkiteshwaran et al., 2020).

6.4. Conclusions

Currently available P treatment technologies do not effectively remove or recover

sNRP (Venkiteshwaran et al., 2018a). Previous adsorption studies targeting sNRP

removal report long contact times for adsorption and low adsorption/desorption affinities

(Campos do Lago et al., 2020; Xu et al., 2020; Sharma and Kakkar, 2017; Wang et al.,

2018a, 2018b). The phosphate-selective PBP resin tested in this study previously demonstrated effective adsorption and desorption for P_i removal and recovery, and here we showed for the first time that the PBP resin also effectively adsorbs sNRP. While PBP has stronger affinity for P_i, adsorption of all sNRP compounds tested, including organic (phosphoester bonds), inorganic (phosphoanhydride bonds), cyclic, and noncyclic molecules, was thermodynamically feasible using PBP, with 95% of maximum adsorption occurring within 4 min.

Adsorption of the sNRP compounds followed the Langmuir isotherm model, indicating 1:1 adsorption of a phosphate group on PBP's single active site. As the PBP likely binds sNRP molecules using a single terminal phosphate, "bonus" P removal can be achieved without direct binding since some sNRP compounds contain more than one phosphate group. However, poorer removal of HMP suggests that when multiple oxygen atoms in the phosphate group are bound to other atoms, it reduces their ability to bind to the protein, and negatively affects sNRP adsorption. Compared to other adsorbents, PBP adsorbed sNRP at a higher rate with greater affinity. However, as noted by Venkiteshwaran et al. (2020) for P_i adsorption using PBP resin, the material's overall sNRP capacity was low compared to other adsorbents due to the protein's high molecular weight relative to other commonly used P-binding chemical functional groups. Future work focused on increasing the adsorption capacity of immobilized PBP materials is needed.

After adsorption on the PBP resin, controlled desorption of sNRP was achieved under high pH conditions (pH 12), demonstrating effective recoverability of the sNRP compounds. The PBP resin can thus be used to concentrate sNRP compounds for further

treatment. For instance, concentrated PBP can be transformed to sRP using processes such as electrooxidation. Thus, PBP resin can contribute to sustainable P management strategies by facilitating enhanced sNRP removal and recovery.

7. CONCLUSIONS

Removal and recovery of recalcitrant nutrients, e.g., dissolved organic nitrogen (DON) and soluble non-reactive phosphorus (sNRP), will help decrease overall nutrient discharge and advance the national goal of improved nutrient recovery. Owing to the lesser extent of reactivity, DON and sNRP are not typically treated effectively. Transformation of these nutrient species into more readily removable/recoverable species and adsorption on a selective adsorbent will facilitate improved nutrient management.

7.1. Key Findings

The first objective of this research was to evaluate EO for DON and sNRP transformation into more readily removable/recoverable DIN and sRP species. Successful transformation of DON and sNRP compounds was achieved using EO. Up to 77% sNRP transformation was achieved by applying 0.74 mA/cm^2 for 8 hrs. Transformation was limited by applied current density and followed zero order kinetics. Transformation of DON was lower compared to sNRP transformation using EO. Compared to UV/H$_2$O$_2$, EO-based DON and sNRP transformation was higher and more energy efficient, as hypothesized in this objective.

The second objective was to determine the mechanisms of EO-based nutrient transformation and assess recoverability of EO-treated sNRP using ion exchange. Neither sorbed nor dissolved oxidants played a role in EO-based transformation of sNRP. Chronoamperometry experiments confirmed DET of sNRP compounds. Improved recoverability of EO-treated sNRP, with 1.6 times more sNRP recovery using ion exchange after EO treatment, was achieved using ion exchange, as hypothesized in

Objective 2. However, centrate sNRP recoverability likely improved due to a lack of competing organics after EO treatment as opposed to partial transformation of sNRP.

The third objective was to evaluate the efficacy of a phosphate-binding protein (PBP) for sNRP adsorption. Adsorption of sNRP on immobilized PBP was rapid, with 95% of maximum adsorption taking place within 4 minutes. Adsorption of sNRP on PBP followed a Langmuir isotherm, which is characteristic of monolayer adsorption on energetically homogenous binding sites. Controlled release of adsorbed sNRP was achieved at pH 12. Binding of sNRP compounds likely took place at the phosphate-binding site of PBP as sNRP adsorption was similar to phosphate adsorption on PBP. Compared to other sNRP adsorption studies using different adsorbent materials, PBP provided higher affinity and faster adsorption of sNRP compounds. These results supported the hypothesis that PBP can adsorb sNRP compounds. The adsorbed sNRP compounds can be concentrated through desorption at pH 12 and then transformed using EO for enhanced sNRP recovery.

7.2. Recommendations for Future Research

Overall, this research showed that EO-based transformation can be advantageous over a more conventional AOP, UV/H_2O_2, in terms of greater transformation with relatively less energy consumption. However, energy consumption for EO-based nutrient transformation was still high. The results in this research suggested that DET was likely the dominant mechanism in EO-based transformation of nutrients. Since DET is an anode surface-mediated oxidation mechanism, electrode surface area and material impact the degree of oxidation. Moreover, depending on the electrode material, generation of in-situ oxidants might also be affected. Thus, in a different EO reactor configuration, in-situ

generated oxidants rather than DET might dominate EO-based nutrient transformation. Process controlling parameters largely depend on the oxidation pathways, e.g., the process is controlled by applied potential when DET dominates while diffusion controls oxidation when in-situ generated oxidants dominate oxidation. Future research in EO reactor configuration (electrode materials, surface area of electrode, etc.) is needed to develop better understanding of EO-based nutrient transformation process efficiency.

Additionally, EO-based nutrient transformation was highly energy demanding. In an EO process, energy can be lost through the hydrogen evolution reaction, oxygen evolution reactions, intermediate formation, resistance of the system due to double layer capacitance on the anode surface, etc. Assessing each of these aspects will help in identifying the lost energy to improve energy efficiency of EO-based nutrient transformation.

The reactive nutrient species, e.g., NH_4^+, NO_3^-, NO_2^-, soluble reactive phosphorus, were measured to quantify transformation of DON and sNRP compounds. However, intermediates are likely to form during oxidation. Consequently, the intermediate species formed during EO-based transformation need to be evaluated to ensure that no harmful byproducts or more recalcitrant compounds are generated.

Assessment of sNRP adsorption on PBP was conducted using un-transformed sNRP compounds. Assessment of the intermediates formed during EO-based sNRP transformation will help understand if those intermediates have terminal orthophosphate functional groups. Since sNRP compounds likely bind at the phosphate-binding site of PBP through terminal orthophosphate functional groups, EO-transformed intermediates with accessible phosphate functional groups might be better removed using PBP.

The PBP was immobilized on NHS beads to make immobilized PBP resin. Since sNRP compounds bind at the phosphate-binding site of PBP, the overall removal capacity of the immobilized PBP depends on the attachment capacity of PBP on the NHS beads. Other surfaces (e.g., nanoparticles) need to be evaluated for PBP immobilization to increase PBP attachment capacity, which would result in higher sNRP removal.

Additionally, removal of compounds with high P content was higher using PBP, but the polyphosphates tested in this study contained a maximum of six phosphate groups in the molecules. Compounds with long polyphosphate chains might negatively affect binding at the small phosphate-binding cleft of PBP. Therefore, a range of wastewater sNRP compounds with varying degree of polymerization need to be evaluated for adsorption on PBP.

BIBLIOGRAPHY

Abdollahbeigi, M., Asgari, M., 2020. Investigation of nitrogen removal in municipal wastewater treatment plants. Journal of Chemical Reviews 2, 257–273. https://dx.doi.org/10.22034/jcr.2020.246588.1082

Ahmadi, K., 2017. Treatability of dissolved organic nitrogen in Truckee meadows water reclamation facility using coagulation or ozone treatment. Thesis, University of Nevada, Reno (UNR), Reno, Nevada. http://dx.doi.org/10.13140/rg.2.2.13537.61280

Almomani, F., Bhosale, R., Khraisheh, M., Kumar, A., Tawalbeh, M., 2020. Electrochemical oxidation of ammonia on nickel oxide nanoparticles. International Journal of Hydrogen Energy 45, 10398–10408. https://doi.org/10.1016/j.ijhydene.2019.11.071

Andrade, S.L.A., Dickmanns, A., Ficner, R., Einsle, O., 2005. Crystal structure of the archaeal ammonium transporter Amt-1 from *Archaeoglobus fulgidus*. Proceedings of the National Academy of Sciences of the United States of America 102, 14994–14999. https://doi.org/10.1073/pnas.0506254102

APHA, 2012. Standard methods for the examination of water and wastewater, 22nd edition edited by E. W. Rice, R. B. Baird, A. D. Eaton and L. S. Clesceri. American Public Health Association (APHA), American Water Works Association (AWWA) and Water Environment Federation (WEF), Washington, D.C., USA.

Arnaldos, M., Pagilla, K., 2010. Effluent dissolved organic nitrogen and dissolved phosphorus removal by enhanced coagulation and microfiltration. Water Research 44, 5306–5315. https://doi.org/10.1016/j.watres.2010.06.066

Arredondo, M.R., Kuntke, P., Jeremiasse, A.W., Sleutels, T.H.J.A., Buisman, C.J.N., ter Heijne, A., 2015. Bioelectrochemical systems for nitrogen removal and recovery from wastewater. Environmental Science: Water Research & Technology 1, 22–33. https://doi.org/10.1039/c4ew00066h

Badawy, M.I., Ghaly, M.Y., Gad-Allah, T.A., 2006. Advanced oxidation processes for the removal of organophosphorus pesticides from wastewater. Desalination 194, 166–175. https://doi.org/10.1016/j.desal.2005.09.027

Barazesh, J.M., Prasse, C., Sedlak, D.L., 2016. Electrochemical transformation of trace organic contaminants in the presence of halide and carbonate ions. Environmental Science and Technology 50, 10143–10152. https://doi.org/10.1021/acs.est.6b02232

Beaulieu, J.J., DelSontro, T., Downing, J.A., 2019. Eutrophication will increase methane emissions from lakes and impoundments during the 21st century. Nature Communications 10, 1–5. https://doi.org/10.1038/s41467-019-09100-5

Beckinghausen, A., Odlare, M., Thorin, E., Schwede, S., 2020. From removal to recovery: An evaluation of nitrogen recovery techniques from wastewater. Applied Energy 263, 114616. https://doi.org/10.1016/J.APENERGY.2020.114616

Bentley, G., Dodson, E., Dodson, G., Hodgkin, D., Mercola, D., 1976. Structure of insulin in 4-zinc insulin. Nature 261, 166–168. https://doi.org/10.1038/261166A0

Berman, H.M., Westbrook, J., Feng, Z., Gilliland, G., Bhat, T.N., Weissig,H., Shindyalov, I.N., Bourne, P.E., 2000. The protein data bank nucleic acids research 28, 235-242. https://doi.org/10.1093/nar/28.1.235

Berman, T., Deborah, A.B., 2003. Dissolved organic nitrogen: A dynamic participant in aquatic ecosystems. Aquatic Microbial Ecology 31, 279–305. https://doi.org/doi:10.3354/ame031279

Biesheuvel, P.M., Zhang, L., Gasquet, P., Blankert, B., Elimelech, M., van der Meer, W.G.J., 2019. Ion selectivity in brackish water desalination by reverse osmosis: Theory, measurements, and implications. Environmental Science & Technology Letters 7, 42–47. https://doi.org/10.1021/ACS.ESTLETT.9B00686

Bolton, J.R., Bircher, K.G., Tumas, W., Tolman, C.A., 2001. Figures-of-merit for the technical development and application of advanced oxidation technologies for both electric-and solar-driven systems (IUPAC Technical Report). In Pure and Applied Chemistry 73, 622-637. https://doi.org/10.1351/pac200173040627

Bradley, P.B., Sanderson, M.P., Frischer, M.E., Brofft, J., Booth, M.G., Kerkhof, L.J., Bronk, D.A., 2010. Inorganic and organic nitrogen uptake by phytoplankton and heterotrophic bacteria in the stratified Mid-Atlantic Bight. Estuarine, Coastal and Shelf Science 88, 429–441. https://doi.org/10.1016/j.ecss.2010.02.001

Bunce, J.T., Ndam, E., Ofiteru, I.D., Moore, A., Graham, D.W., 2018. A review of phosphorus removal technologies and their applicability to small-scale domestic wastewater treatment systems. Frontiers in Environmental Science 6, 8. https://doi.org/10.3389/FENVS.2018.00008/BIBTEX

Campos do Lago, A., da Silva Cavalcanti, M.H., Rosa, M.A., Silveira, A.T., Teixeira Tarley, C.R., Figueiredo, E.C., 2020. Magnetic restricted-access carbon nanotubes for dispersive solid phase extraction of organophosphates pesticides from bovine milk samples. Analytica Chimica Acta 1102, 11–23. https://doi.org/10.1016/J.ACA.2019.12.039

Cañizares, P., García-Gómez, J., de Marcos, I.F., Rodrigo, M.A., Lobato, J., 2006. Measurement of mass-transfer coefficients by an electrochemical technique. The Chemical Educator 83, 1204–1207. https://doi.org/10.1007/s00897020579a

Canonica, S., Kohn, T., Mac, M., Real, F.J., Wirz, J., von Gunten, U., 2005. Photosensitizer method to determine rate constants for the reaction of carbonate

radical with organic compounds. Environmental Science & Technology 39, 9182-9188. https://doi.org/10.1021/es051236b

Carpenter, S.R., 2008. Phosphorus control is critical to mitigating eutrophication. Proceedings of the National Academy of Sciences 105, 11039–11040. https://doi.org/10.1073/pnas.0806112105

Celdrán, R., González-Velasco, J.J., 1981. Oxidation mechanism of allyl alcohol on an Au-electrode in basic solutions. Electrochimica Acta 26, 525–533. https://doi.org/10.1016/0013-4686(81)87033-8

Chaplin, B.P., Shapley, J.R., Werth, C.J., 2007. Regeneration of sulfur-fouled bimetallic pd-based catalysts. Environmental Science & Technology 41, 5491–5497. https://doi.org/10.1021/es0704333

Chen, B., Kim, Y., Westerhoff, P., 2011. Occurrence and treatment of wastewater-derived organic nitrogen. Water Research 45, 4641–4650. https://doi.org/10.1016/j.watres.2011.06.018

Choi, S.S., Lee, H.M., Ha, J.H., Kang, D.G., Kim, C.S., Seo, J.H., Cha, H.J., 2013. Biological removal of phosphate at low concentrations using recombinant *Escherichia coli* expressing phosphate-binding protein in periplasmic space. Applied Biochemistry and Biotechnology 171, 1170–1177. https://doi.org/10.1007/s12010-013-0187-1

Clough, T.J., Condron, L.M., Kammann, C., Müller, C., 2013. A review of biochar and soil nitrogen dynamics. Agronomy 3, 275-293. https://doi.org/10.3390/agronomy3020275

Conley, D.J., 1999. Biogeochemical nutrient cycles and nutrient management strategies. Hydrobiologia 410, 87–96. https://doi.org/10.1023/A:1003784504005

Conley, D.J., Paerl, H.W., Howarth, R.W., Boesch, D.F., Seitzinger, S.P., Havens, K.E., Lancelot, C., Likens. Gene E., 2009. Controlling eutrophication: Nitrogen and phosphorus. Science 323, 1014–1015. https://doi.org/10.1126/science.1167755

Cordell, D., White, S., 2014. Life's bottleneck: Sustaining the world's phosphorus for a food secure future. Annual Review of Environment and Resources 39, 161–188. https://doi.org/10.1146/annurev-environ-010213-113300

Crittenden, J.C., Trussell, R.R., Hand, D.W., Howe, K.J., Tchobanoglous, G., 2012. MWH's Water Treatment: Principles and Design (3rd ed.). Hoboken, New Jersey: John Wiley & Sons, Inc.

Czerwionka, K., Makinia, J., 2014. Dissolved and colloidal organic nitrogen removal from wastewater treatment plants effluents and reject waters using physical–chemical processes. 6Water Science and Technology 70, 561–568. https://doi.org/10.2166/wst.2014.267

Daneshvar, N., Hejazi, M.J., Rangarangy, B., Khataee, A.R., 2004. Photocatalytic degradation of an organophosphorus pesticide phosalone in aqueous suspensions of titanium dioxide. Journal of Environmental Science and Health - Part B Pesticides, Food Contaminants, and Agricultural Wastes 39, 285–296. https://doi.org/10.1081/PFC-120030242

de Melo da Silva, L., Gozzi, F., Sirés, I., Brillas, E., de Oliviera, S., Machulek, A., 2018. Degradation of 4-aminoantipyrine by electro-oxidation with a boron-doped diamond anode: Optimization by central composite design, oxidation products and toxicity. Science of the Total Environment. 631-632, 1079-1088. https://doi.org/10.1016/j.scitotenv.2018.03.092.

Dennis, J.K., Such, T.E., 1993. High-speed plating in nickel and chromium plating (Third Edition), In Woodhead Publishing Series in Metals and Surface Engineering, 423 – 441. Woodhead Publishing, Cambridge, UK. https://doi.org/10.1533/9781845698638.423

Diaz, O.A., Reddy, K.R., Moore, P.A., 1994. Solubility of inorganic phosphorus in stream water as influenced by pH and calcium concentration. Water Research 28, 1755–1763. https://doi.org/10.1016/0043-1354(94)90248-8

Díez-Montero, R., Belohlav, V., Ortiz, A., Uggetti, E., García-Galán, M.J., García, J., 2020. Evaluation of daily and seasonal variations in a semi-closed photobioreactor for microalgae-based bioremediation of agricultural runoff at full-scale. Algal Research 47, 101859. https://doi.org/10.1016/J.ALGAL.2020.101859

Drew, H.R., Wing, R.M., Takano, T., Broka, C., Tanaka, S., Itakura, K., Dickerson, R.E., 1981. Structure of a B-DNA dodecamer: Conformation and dynamics. Proceedings of the National Academy of Sciences 78, 2179–2183. https://doi.org/10.1073/pnas.78.4.2179

Drolc, A., Zagorc Koncan, J., 2002. Estimation of sources of total phosphorus in a river basin and assessment of alternatives for river pollution reduction. Environment International 28, 393–400. https://doi.org/10.1016/S0160-4120(02)00062-4

Durand, P., Breuer, L., Johnes, P.J., Billen, G., Butturini, A., Pinay, G., van Grinsven, H., Garnier, J., Rivett, M., Reay, D.S., Curtis, C., Siemens, J., Maberly, S., Kaste, O., Humborg, C., Loeb, R., de Klein, J., Hejzlar, J., Skoulikidis, N.,…Wright, R., 2011. Nitrogen processes in aquatic ecosystems, in: Sutton, M.A., Howard, C.M., Erisman, J.W., Billen, G., Bleeker, A., Grennfelt, P., van Grinsven, H., Grizzetti, B. (Eds.), The European Nitrogen Assessment. Cambridge University Press, Cambridge, pp. 126–146.

Eom, H., Park, C., 2021. Investigation of characteristics of effluent DON derived from conventional activated sludge (CAS) and predenitrification biological removal (BNR): In terms of proteins and humic substances. Environmental Research 196, 110912. https://doi.org/10.1016/j.envres.2021.110912

EPA, 2013. Total nitrogen. Washington, D.C.

EPA, 2016. Definition and procedure for the determination of the method detection limit, Revision 2. https://www.epa.gov/cwa-methods

Fan, L., Brett, M.T., Jiang, W., Li, B., 2017. Dissolved organic nitrogen recalcitrance and bioavailable nitrogen quantification for effluents from advanced nitrogen removal wastewater treatment facilities. Environmental Pollution 229, 255–263. https://doi.org/10.1016/j.envpol.2017.05.093

Farooq, R., Lin, F., Shaukat, S.F., Huang, J., 2003. Sonochemical degradation of organophosphorus pesticide in dilute aqueous solutions - IOS Press. Journal of Environmental Sciences 15, 710–714.

Feng, J., Zhang, X., Zhang, G., Li, J., Song, W., Xu, Z., 2021. Improved photocatalytic conversion of high−concentration ammonia in water by low−cost Cu/TiO_2 and its mechanism study. Chemosphere 274, 129689. https://doi.org/10.1016/j.chemosphere.2021.129689

Feng, W., Liu, S., Li, C., Li, X., Song, F., Wang, B., Chen, H., Wu, F., 2019. Algal uptake of hydrophilic and hydrophobic dissolved organic nitrogen in the eutrophic lakes. Chemosphere 214, 295–302. https://doi.org/10.1016/j.chemosphere.2018.09.070

Gray, H.E., Powell, T., Choi, S., Smith, D.S., Parker, W.J., 2020. Organic phosphorus removal using an integrated advanced oxidation-ultrafiltration process. Water Research 182, 115968. https://doi.org/10.1016/j.watres.2020.115968

Gu, A.Z., Liu, L., Neethling, J.B., Stensel, H.D., Murthy, S., 2011. Treatability and fate of various phosphorus fractions in different wastewater treatment processes. Water Science and Technology 63, 804–810. https://doi.org/10.2166/wst.2011.312

Gunes, Y., Barut, F., Kaykioglu, G., Dincer, A.R., 2020. Comparison of ozonation, adsorption, and air stripping process for ammonia nitrogen removal from real textile wastewater. Sigma Journal of Engineering and Natural Sciences 38, 1179–1189.

Han, B., Butterly, C., Zhang, W., He, J. zheng, Chen, D., 2021. Adsorbent materials for ammonium and ammonia removal: A review. Journal of Cleaner Production 283, 124611. https://doi.org/10.1016/j.jclepro.2020.124611

Hasegawa, K., Neta, P., 1977. Rate constants and mechanisms of reaction of Cl_2^- radicals. The Journal of Physical Chemistry 82, 854 – 857. https://doi.org/10.1021/j100497a003

Helin, J., Weikard, H.P., 2019. A model for estimating phosphorus requirements of world food production. Agricultural Systems 176, 102666. https://doi.org/10.1016/j.agsy.2019.102666

Henze, M., 1991. Capabilities of biological nitrogen removal processes from wastewater. Water Science & Technology 23, 669–679. https://doi.org/10.2166/wst.1991.0517

Hermassi, M., Valderrama, C., Font, O., Moreno, N., Querol, X., Batis, N.H., Cortina, J.L., 2020. Phosphate recovery from aqueous solution by K-zeolite synthesized from fly ash for subsequent valorisation as slow release fertilizer. Science of the Total Environment 731, 139002. https://doi.org/10.1016/j.scitotenv.2020.139002.

Hu, H., Ding, L., Geng, J., Huang, H., Xu, K., Ren, H., 2016. Effect of coagulation on dissolved organic nitrogen (DON) bioavailability in municipal wastewater effluents. Journal of Environmental Chemical Engineering 4, 2536–2544. https://doi.org/10.1016/j.jece.2016.04.036

Hu, Q., Liu, H., Zhang, Z., Xie, Y., 2020. Nitrate removal from aqueous solution using polyaniline modified activated carbon: Optimization and characterization. Journal of Molecular Liquids 309, 113057. https://doi.org/10.1016/j.molliq.2020.113057

Huang, Y., Shang, C., Li, L., 2021. Novel N-doped graphene enhanced ultrafiltration nano-porous polyvinylidene fluoride membrane with high permeability and stability for water treatment. Separation and Purification Technology 267, 118622. https://doi.org/10.1016/j.seppur.2021.118622

Hussein, F.B., Mayer, B.K., 2022. Fixed-bed column study of phosphate adsorption using immobilized phosphate-binding protein. Chemosphere 295. https://doi.org/10.1016/j.chemosphere.2022.133908

International Fertilizer Association, 2019. Fertilizer consumption - historical trend by country or region: In the world [WWW Document]. URL https://www.ifastat.org/databases/graph/1_1 (accessed 12.28.21).

Jickells, T.D., Buitenhuis, E., Altieri, K., Baker, A.R., Capone, D., Duce, R.A., Dentener, F., Fennel, K., Kanakidou, M., LaRoche, J., Lee, K., Liss, P., Middelburg, J.J., Moore, J.K., Okin, G., Oschlies, A., Sarin, M., Seitzinger, S., Sharples, J., Singh, A., Suntharalingam, P., Uematsu, M., Zamora, L.M., 2017. A reevaluation of the magnitude and impacts of anthropogenic atmospheric nitrogen inputs on the ocean. Global Biogeochemical Cycles 31, 289–305. https://doi.org/10.1002/2016gb005586

Jørgensen, N.O.G., 2009. Organic nitrogen, in: Likens, G.E. (Ed.), Encyclopedia of Inland Waters. Academic Press, pp. 832–851. https://doi.org/10.1016/b978-012370626-3.00119-8

Jorgensen, T.C., Weatherley, L.R., 2003. Ammonia removal from wastewater by ion exchange in the presence of organic contaminants. Water Research 37, 1723–1728. https://doi.org/10.1016/S0043-1354(02)00571-7

Joye, S.B., Anderson, I.C., 2008. Nitrogen cycling in coastal sediments, in: Nitrogen in the Marine Environment. Elsevier Inc., pp. 867–915. https://doi.org/10.1016/B978-0-12-372522-6.00019-0

Kim, D.I., Gonzales, R.R., Dorji, P., Gwak, G., Phuntsho, S., Hong, S., Shon, H., 2020. Efficient recovery of nitrate from municipal wastewater via MCDI using anion-exchange polymer coated electrode embedded with nitrate selective resin. Desalination, 484, 114425. https://doi.org/10.1016/j.desal.2020.114425.

Körbahti, B.K., Taşyürek, S., Körbahti, B.K., Taşyürek, S., 2015. Electrochemical oxidation of ampicillin antibiotic at boron-doped diamond electrodes and process optimization using response surface methodology. Environmental Science and Pollution Research, 22, 3265–3278. https://doi.org/10.1007/s11356-014-3101-7

Krasner, S.W., Chinn, R., Guo, Y.C., Hwang, C.J., Pastor, S.J., Sclimenti, M.J., Westerhoff, P., Chen, B., Chowdhury, Z.K., Sinha, S., Rittmann, B., 2005. Contribution of wastewater to DBP formation, in: AWWA 124th Annual Conference and Exposition: The World's Water Event, ACE 2005. AWWA, San Francisco.

Kumar, A., Shrivastava, S., Verma, N., Hsueh, C.C., Chang, C.T., Chen, B.Y., 2020. Electrolyte-free electro-oxidation of aqueous glyphosate: CuPc-ACF electrode and optimization of operating parameters. Process Safety and Environmental Protection 142, 260–271. https://doi.org/10.1016/j.psep.2020.06.022

Kuroda, A., Kunimoto, H., Morohoshi, T., Ikeda, T., Kato, J., Takiguchi, N., Miya, A., Ohtake, H., 2000. Evaluation of phosphate removal from water by immobilized phosphate-binding protein PstS. Journal of Bioscience and Bioengineering 90, 688-90. https://doi.org/10.1263/jbb.90.688

Lazaratou, C.V., Vayenas, D.V., Papoulis, D., 2020. The role of clays, clay minerals and clay-based materials for nitrate removal from water systems: A review. Applied Clay Science 185, 105377. https://doi.org/10.1016/j.clay.2019.105377

Lee, W., Westerhoff, P., 2006. Dissolved organic nitrogen removal during water treatment by aluminum sulfate and cationic polymer coagulation. Water Research 40, 3767–3774. https://doi.org/10.1016/j.watres.2006.08.008

Lei, Y., Song, B., van der Weijden, R.D., Saakes, M., Buisman, C.J.N., 2017. Electrochemical induced calcium phosphate precipitation: Importance of local pH. Environmental Science and Technology 51, 11156–11164. https://doi.org/10.1021/acs.est.7b03909

Li, H., Zhu, X., Ni, J., 2010. Inactivation of *Escherichia coli* in Na_2SO_4 electrolyte using boron-doped diamond anode. Electrochimica Acta, 56, 448–453. https://doi.org/10.1016/j.electacta.2010.08.055

Li, Q., Li, X., Sun, J., Song, H., Wu, J., Wang, G., Li, A., 2020. Removal of organic and inorganic matters from secondary effluent using resin adsorption and reuse of desorption eluate using ozone oxidation. Chemosphere 251, 126442. https://doi.org/10.1016/j.chemosphere.2020.126442

Li, Q., Yu, Z., Shao, X., He, J., Li, L., 2009. Improved phosphate biosorption by bacterial surface display of phosphate-binding protein utilizing ice nucleation protein. FEMS Microbiology Letters 299, 44-52. https://doi.org/10.1111/j.1574-6968.2009.01724.x

Li, X., Wang, S., An, H., Dong, G., Feng, J., Wei, T., Ren, Y., Ma, J., 2021. Enhanced photocatalytic reduction of nitrate enabled by Fe-doped $LiNbO_3$ materials in water: Performance and mechanism. Applied Surface Science 539, 148257. https://doi.org/10.1016/j.apsusc.2020.148257

Lin, H., Niu, J., Ding, S., Zhang, L., 2012. Electrochemical degradation of perfluorooctanoic acid (PFOA) by Ti/SnO_2–Sb, Ti/SnO_2–Sb/PbO_2 and Ti/SnO_2–Sb/MnO_2 anodes. Water Research, 46, 2281–2289. https://doi.org/10.1016/j.watres.2012.01.053

Liu, T., Xu, S., Lu, S., Qin, P., Bi, B., Ding, H., Liu, Y., Guo, X., Liu, X., 2019. A review on removal of organophosphorus pesticides in constructed wetland: Performance, mechanism and influencing factors. Science of the Total Environment 651, 2247–2268. https://doi.org/10.1016/j.scitotenv.2018.10.087

Lorick, D., Macura, B., Ahlström, M., Grimvall, A., Harder, R., 2020. Effectiveness of struvite precipitation and ammonia stripping for recovery of phosphorus and nitrogen from anaerobic digestate: a systematic review. Environmental Evidence 9, 1–20. https://doi.org/10.1186/S13750-020-00211-X

Luecke, H., Quiocho, F.A., 1990. High specificity of a phosphate transport protein determined by hydrogen bonds. Nature 347, 402–406. https://doi.org/10.1038/347402a0

Luo, Y., Liu, C., Mehmood, T., Zhang, Y., Yu, M., Ren, Y., 2021. Activation of permonosulfate by Co-Fe_3O_4 composite catalyst for amino acid removal: Performance and mechanism of Co-Fe_3O_4 nanoparticles. Journal of Environmental Chemical Engineering 9, 106036. https://doi.org/10.1016/j.jece.2021.106036

Ma, P., Rosen, C., 2021. Land application of sewage sludge incinerator ash for phosphorus recovery: A review. Chemosphere, 274, 129609. https://doi.org/10.1016/j.chemosphere.2021.129609

Madej, T., Lanczycki, C.J., Zhang, D., Thiessen, P.A., Geer, R.C., Marchler-Bauer, A., Bryant, S.H., 2014. MMDB and VAST+: Tracking structural similarities between macromolecular complexes. Nucleic acids research 42, D297–D303. https://doi.org/10.1093/nar/gkt1208

Malliaris, A., Lang, J., Zana, R., 1987. Kinetics and mechanism of the oxidation of allyl alcohol on Ag(110). The Journal of Physical Chemistry 91, 655. https://doi.org/10.1021/j100308a034

Mallick, S. P., Hussein, F. B., Husted, S., Mayer, B. K., 2022. Adsorption of recalcitrant phosphorus compounds using the phosphate-selective binding-protein

PstS. Chemosphere, 304, 135311.
https://doi.org/10.1016/j.chemosphere.2022.135311

Mallick, S.P., Mallick, Z., Mayer, B.K., 2022. Meta-analysis of the prevalence of dissolved organic nitrogen (DON) in water and wastewater and review of DON removal and recovery strategies. Science of the Total Environment 828, 154476. https://doi.org/10.1016/j.scitotenv.2022.154476

Mallick, S.P., Ryan, D.R., Venkiteshwaran, K., McNamara, P.J., Mayer, B.K., 2021. Electro-oxidation to convert dissolved organic nitrogen and soluble non-reactive phosphorus to more readily removable and recoverable forms. Chemosphere 279. https://doi.org/10.1016/j.chemosphere.2021.130876

Mayer, B.K., Baker, L.A., Boyer, T.H., Drechsel, P., Gifford, M., Hanjra, M.A., Parameswaran, P., Stoltzfus, J., Westerhoff, P., Rittmann, B.E., 2016. Total value of phosphorus recovery. Environmental Science & Technology, 50, 6606-6620. https://doi.org/10.1021/acs.est.6b01239

Mayer, B.K., Gerrity, D., Rittmann, B.E., Reisinger, D., Brandt-Williams, S., 2013. Innovative strategies to achieve low total phosphorus concentrations in high water flows. Critical Reviews in Environmental Science and Technology, 43, 409-441, https://doi.org/10.1080/10643389.2011.604262

Mesfioui, R., Love, N.G., Bronk, D.A., Mulholland, M.R., Hatcher, P.G., 2012. Reactivity and chemical characterization of effluent organic nitrogen from wastewater treatment plants determined by Fourier transform ion cyclotron resonance mass spectrometry. Water Research 46, 622–634. https://doi.org/10.1016/j.watres.2011.11.022

Miklos, D.B., Remy, C., Jekel, M., Linden, K.G., Drewes, J.E., Hübner, U., 2018. Evaluation of advanced oxidation processes for water and wastewater treatment – A critical review. Water Research, 139, 118-131, https://doi.org/10.1016/j.watres.2018.03.042.

Mohammadi, R., Tang, W., Sillanpää, M., 2021. A systematic review and statistical analysis of nutrient recovery from municipal wastewater by electrodialysis. Desalination 498, 114626. https://doi.org/10.1016/j.desal.2020.114626

Monbet, P., McKelvie, I.D., Worsfold, P.J., 2009. Dissolved organic phosphorus speciation in the waters of the Tamar estuary (SW England). Geochimica et Cosmochimica Acta 73, 1027–1038. https://doi.org/10.1016/j.gca.2008.11.024

Moreira, F.C., Boaventura, R.A.R., Brillas, E., Vilar, V.J.P., 2017. Electrochemical advanced oxidation processes: A review on their application to synthetic and real wastewaters. Applied Catalysis B: Environmental 202, 217–261. https://doi.org/10.1016/j.apcatb.2016.08.037

Morse, G.K., Brett, S.W., Guy, J.A., Lester, J.N., 1998. Review: Phosphorus removal and recovery technologies. Science of the Total Environment 212, 69–81. https://doi.org/10.1016/s0048-9697(97)00332-x

Müller, W.E.G., Schröder, H.C., Wang, X., 2019. The phosphoanhydride bond: one cornerstone of life. The Biochemist (Lond), 41, 22-27. https://doi.org/10.1042/bio04104022

Murthy, S., Kimberly, J., Baidoo, S., Pagilla, K., 2006. Biodegradability of dissolved organic nitrogen: Adaptation of the BOD test. Proceedings of the Water Environment Federation. 1550-1559. https://doi.org/10.2175/193864706783750529.

Nagarajan, D., Lee, D.J., Chen, C.Y., Chang, J.S., 2020. Resource recovery from wastewaters using microalgae-based approaches: A circular bioeconomy perspective. Bioresource Technology 302, 122817. https://doi.org/10.1016/j.biortech.2020.122817

Nangan, S., Ding, Y., Alhakemy, A.Z., Liu, Y., Wen, Z., 2021. Hybrid alkali-acid urea-nitrate fuel cell for degrading nitrogen-rich wastewater. Applied Catalysis B: Environmental 286, 119892. https://doi.org/10.1016/j.apcatb.2021.119892

National Academy of Engineering, 2019. Grand challenges - Manage the nitrogen cycle [WWW Document]. URL http://www.engineeringchallenges.org/9132.aspx (accessed 11.8.21).

National Center for Biotechnology Information, 2022. PubChem compound summary for CID 90472028, Humic acid. Retrieved January 7, 2022 from https://pubchem.ncbi.nlm.nih.gov/compound/Humic-acid

Neta, P., Madhavan, V., Zemel, H., Fessenden, R.W., 1976. Rate constants and mechanism of reaction of $SO_4 \cdot^-$ with aromatic compounds. Journal of the American Chemical Society, 99, 163–164. https://doi.org/10.1021/ja00443a030

Neznansky, A., Blus-Kadosh, I., Yerushalmi, G., Banin, E., Opatowsky, Y., 2014. The Pseudomonas aeruginosa phosphate transport protein PstS plays a phosphate-independent role in biofilm formation. FASEB journal: Official publication of the Federation of American Societies for Experimental Biology 28, 5223–5233. https://doi.org/10.1096/fj.14-258293

Nitoi, I., Oancea, P., Raileanu, M., Crisan, M., Constantin, L., Cristea, I., 2015. UV–VIS photocatalytic degradation of nitrobenzene from water using heavy metal doped titania. Journal of Industrial and Engineering Chemistry 21, 677–682. https://doi.org/10.1016/j.jiec.2014.03.036

Ohtake, H., Kato, J., Kuroda, A., Wu H., Ikeda, T., 1998. Regulation of bacterial phosphate taxis and polyphosphate accumulation in response to phosphate

starvation stress. Journal of Biosciences 23, 491–499.
https://doi.org/10.1007/bf02936143

Parkin, G.F., McCarty, P.L., 1981. A comparison of the characteristics of soluble organic nitrogen in untreated and activated sludge treated wastewaters. Water Research 15, 139–149. https://doi.org/10.1016/0043-1354(81)90194-9

Pastor, E., Schmidt, V.M., Iwasita, T., Arévalo, M.C., González, S., Arvia, A.J., 1993. The reactivity of primary C_3-alcohols on gold electrodes in acid media. A comparative study based on dems data. Electrochimica Acta 38, 1337–1344. https://doi.org/10.1016/0013-4686(93)80067-A

Pehlivanoglu-Mantas, E., Sedlak, D.L., 2006. Wastewater-derived dissolved organic nitrogen: Analytical methods, characterization, and effects-A review. Critical Reviews in Environmental Science and Technology 36, 261–285. https://doi.org/10.1080/10643380500542780

Pehlivanoglu-Mantas, E., Sedlak, D.L., 2008. Measurement of dissolved organic nitrogen forms in wastewater effluents: Concentrations, size distribution and NDMA formation potential. Water Research 42, 3890–3898. https://doi.org/10.1016/j.watres.2008.05.017

Peters, R.J.B., de Leer, E.W.B., de Galan, L., 1990. Dihaloacetonitriles in dutch drinking waters. Water Research 24, 797–800. https://doi.org/10.1016/0043-1354(90)90038-8

Pishnamazi, M., Koushkbaghi, S., Hosseini, S.S., Darabi, M., Yousefi, A., Irani, M., 2020. Metal organic framework nanoparticles loaded- PVDF/chitosan nanofibrous ultrafiltration membranes for the removal of BSA protein and Cr(VI) ions. Journal of Molecular Liquids 317, 113934. https://doi.org/10.1016/j.molliq.2020.113934

Plazinski, W., Dziuba, J., Rudzinski, W., 2013. Modeling of sorption kinetics: The pseudo-second order equation and the sorbate intraparticle diffusivity. Adsorption 19, 1055–1064. https://doi.org/10.1007/s10450-013-9529-0

Plewa, M.J., Simmons, J.E., Richardson, S.D., Wagner, E.D., 2010. Mammalian cell cytotoxicity and genotoxicity of the haloacetic acids, a major class of drinking water disinfection by-products. Environmental and Molecular Mutagenesis 51, 871–878. https://doi.org/10.1002/em.20585

Poole, K., Hancock, R.E.W., 1984. Phosphate transport in *Pseudomonas aeruginosa*. European Journal of Biochemistry 144, 607-612. https://doi.org/10.1111/j.1432-1033.1984.tb08508.x

Porter, C.K., Putnam, S.D., Hunting, K.L., Riddle, M.R., 2005. The effect of trihalomethane and haloacetic acid exposure on fetal growth in a Maryland county. American Journal of Epidemiology 162, 334–344. https://doi.org/10.1093/aje/kwi211

Qian, W., Peng, Y., Li, X., Zhang, Q., Ma, B., 2017. The inhibitory effects of free ammonia on ammonia oxidizing bacteria and nitrite oxidizing bacteria under anaerobic condition. Bioresource Technology 243, 1247–1250. https://doi.org/10.1016/j.biortech.2017.07.119

Qin, C., Liu, H., Liu, L., Smith, S., Sedlak, D.L., Gu, A.Z., 2015. Bioavailability and characterization of dissolved organic nitrogen and dissolved organic phosphorus in wastewater effluents. Science of the Total Environment 511, 47–53. https://doi.org/10.1016/j.scitotenv.2014.11.005

Rabaey, K., Bützer, S., Brown, S., Keller, J., Rozendal, R.A., 2010. High current generation coupled to caustic production using a lamellar bioelectrochemical system. Environmental Science & Technology 44, 4315–4321. https://doi.org/10.1021/es9037963

Rahmani, A.R., Godini, K., Nematollahi, D., Azarian, G., 2015. Electrochemical oxidation of activated sludge by using direct and indirect anodic oxidation. Desalination and Water Treatment, 56, 2234–2245. https://doi.org/10.1080/19443994.2014.958761

Reijnders, L., 2014. Phosphorus resources, their depletion and conservation, a review. Resources, Conservation and Recycling, 93, 32-49. https://doi.org/10.1016/j.resconrec.2014.09.006

Revellame, E.D., Fortela, D.L., Sharp, W., Hernandez, R., Zappi, M.E., 2020. Adsorption kinetic modeling using pseudo-first order and pseudo-second order rate laws: A review. Cleaner Engineering and Technology 1, 100032. https://doi.org/10.1016/j.clet.2020.100032

Ribeiro, D.M., Roncaratti, L.F., Possa, G.C., Garcia, L.C., Cançado, L.J., Williams, T.C.R., Brasil, B. dos S. A. F., 2020. A low-cost approach for *Chlorella sorokiniana* production through combined use of urea, ammonia and nitrate based fertilizers. Bioresource Technology Reports, 9, 100354. https://doi.org/10.1016/j.biteb.2019.100354

Ryther, J.H., Dunstan, W.M., 1971. Nitrogen, phosphorus, and eutrophication in the coastal marine environment. Science 171, 1008–1013. https://doi.org/10.1126/science.171.3975.1008

Saadi, R., Saadi, Z., Fazaeli, R., Fard, N.E., 2015. Monolayer and multilayer adsorption isotherm models for sorption from aqueous media. Korean Journal of Chemical Engineering 32, 787–799. https://doi.org/10.1007/s11814-015-0053-7

Saarela, T., Lafdani, E.K., Laurén, A., Pumpanen, J., Palviainen, M., 2020. Biochar as adsorbent in purification of clear-cut forest runoff water: Adsorption rate and adsorption capacity. Biochar 2020 2, 227–237. https://doi.org/10.1007/s42773-020-00049-z

Saerens, B., Geerts, S., Weemaes, M., 2021., Phosphorus recovery as struvite from digested sludge – experience from the full scale. Journal of Environmental Management 280, 111743. https://doi.org/10.1016/j.jenvman.2020.111743

Santos-Beneit, F., Rodríguez-García, A., Franco-Domínguez, E., Martín, J.F., 2008. Phosphate-dependent regulation of the low- and high-affinity transport systems in the model actinomycete *Streptomyces coelicolor*. Microbiology 154, 2356–2370. https://doi.org/10.1099/mic.0.2008/019539-0

Sañudo-Wilhelmy, S.A., 2006. A phosphate alternative. Nature 439, 25–26. https://doi.org/10.1038/439025a

Sattayatewa, C., Pagilla, K., Sharp, R., Pitt, P., 2010. Fate of organic nitrogen in four biological nutrient removal wastewater treatment plants. Water Environment Research 82, 2306–2315. https://doi.org/10.2175/106143010x12609736966324

Sayed, E.T., Eisa, T., Mohamed, H.O., Abdelkareem, M.A., Allagui, A., Alawadhi, H., Chae, K.J., 2019. Direct urea fuel cells: Challenges and opportunities. Journal of Power Sources 417, 159–175. https://doi.org/10.1016/j.jpowsour.2018.12.024

Schmitz, U., Behrens, S., Freymann, D.M., Keenan, R.J., Lukavsky, P., Walter, P., James, T.L., 1999. Structure of the phylogenetically most conserved domain of SRP RNA. RNA 5, 1419–1429. https://doi.org/10.1017/S1355838299991458

Schranck, A., Doudrick, K., 2020. Effect of reactor configuration on the kinetics and nitrogen byproduct selectivity of urea electrolysis using a boron doped diamond electrode. Water Research 168, 115130. https://doi.org/10.1016/j.watres.2019.115130

Sehnal, D., Bittrich, S., Deshpande, M., Svobodová, R., Berka, K., Bazgier, V., Velankar, S., Burley, S.K., Koča, J., Rose, A.S., 2021. Mol* Viewer: modern web app for 3D visualization and analysis of large biomolecular structures. Nucleic Acids Research 49, W431–W437. https://doi.org/10.1093/nar/gkab314

Seitzinger, S.P., Kroeze, C., Bouwman, A.F., Caraco, N., Dentener, F., Styles, R.V., 2002. Global patterns of dissolved inorganic and particulate nitrogen inputs to coastal systems: Recent conditions and future projections. Estuarine 25, 640–655. https://doi.org/10.1007/bf02804897

Sharma, L., Kakkar, R., 2017. Hierarchical porous magnesium oxide (Hr-MgO) microspheres for adsorption of an organophosphate pesticide: Kinetics, isotherm, thermodynamics, and DFT studies. ACS Applied Materials & Interfaces 9, 38629-38642.https://doi.org/10.1021/acsami.7b14370

Shetye, S.S., Kurian, S., Naik, H., Gauns, M., Chndrasekhararao, A.V., Kumar, A., Naik, B., 2019. Variability of organic nitrogen and its role in regulating phytoplankton in the eastern Arabian Sea. Marine Pollution Bulletin 141, 550–560. https://doi.org/10.1016/j.marpolbul.2019.02.036

Shin, Y.U., Yoo, H.Y., Ahn, Y.Y., Kim, M.S., Lee, K., Yu, S., Lee, C., Cho, K., Kim, H., Lee, J., 2019. Electrochemical oxidation of organics in sulfate solutions on boron-doped diamond electrode: Multiple pathways for sulfate radical generation. Applied Catalysis B: Environmental, 254, 156–165. https://doi.org/10.1016/j.apcatb.2019.04.060

Sindelar, H.R., Lloyd, J., Brown, M.T., Boyer, T.H., 2016. Transformation of dissolved organic phosphorus to phosphate using UV/H_2O_2. Environmental Progress and Sustainable Energy 35, 680–691. https://doi.org/10.1002/ep.12272

Sipler, R.E., Bronk, D.A., 2015. Dynamics of dissolved organic nitrogen, in: Biogeochemistry of Marine Dissolved Organic Matter: 2nd Edition. Elsevier Inc., pp. 127–232. https://doi.org/10.1016/B978-0-12-405940-5.00004-2

Soriano, A., Gorri, D., Urtiaga, A., 2017. Efficient treatment of perfluorohexanoic acid by nanofiltration followed by electrochemical degradation of the NF concentrate. Water Research, 112, 147–156. https://doi.org/10.1016/j.watres.2017.01.043

Sun, H., Mohammed, A.N., Liu, Y., 2020. Phosphorus recovery from source-diverted blackwater through struvite precipitation. Science of the Total Environment 743, 140747. https://doi.org/10.1016/j.scitotenv.2020.140747.

Sun, J., Cao, H., Wang, Z., 2020. Progress in nitrogen removal in bioelectrochemical systems. Processes 8, 831. https://doi.org/10.3390/pr8070831

Tang, Y., Chen, Z., Wen, Q., Yang, B., Pan, Y., 2021. Evaluation of a hybrid process of magnetic ion-exchange resin treatment followed by ozonation in secondary effluent organic matter removal. Science of the Total Environment 754, 142361. https://doi.org/10.1016/j.scitotenv.2020.142361

Thompson, S.K., Cotner, J.B., 2018. bioavailability of dissolved organic phosphorus in temperate lakes. Frontiers in Environmental Science 6, 62. https://doi.org/10.3389/fenvs.2018.00062/bibtex

Tong, Y., McNamara, P.J., Mayer, B.K., 2017. Fate and impacts of triclosan, sulfamethoxazole, and 17β-estradiol during nutrient recovery via ion exchange and struvite precipitation. Environmental Science: Water Research & Technology 3, 1109–1119. https://doi.org/10.1039/c7ew00280g

Trebše, P., Arčon, I., 2003. Degradation of organophosphorus compounds by X-ray irradiation. Radiation Physics and Chemistry 67, 527–530. https://doi.org/10.1016/S0969-806X(03)00099-9

Trebše, P., Franko, M., 2002. Laser-induced degradation of organophosphorus compounds. International Journal of Photoenergy 4. https://doi.org/10.1155/S1110662X02000077

Urgun-Demirtas, M., Sattayatewa, C., Pagilla, K.R., 2008. Bioavailability of dissolved organic nitrogen in treated effluents. Water Environment Research 80, 397–406. https://doi.org/10.2175/106143007x221454

Vähätalo, A.V., 2009. Light, photolytic reactivity and chemical products, in: Encyclopedia of Inland Waters. Elsevier Inc., pp. 761–773. https://doi.org/10.1016/B978-012370626-3.00110-1

van der Hoek, J.P., Duijff, R., Reinstra, O., 2018. Nitrogen recovery from wastewater: possibilities, competition with other resources, and adaptation pathways. Sustainability 10, 4605. https://doi.org/10.3390/SU10124605

Vanderford, B.J., Rosario-Ortiz, F.L., Snyder, S.A., 2007. Analysis of p-chlorobenzoic acid in water by liquid chromatography–tandem mass spectrometry. Journal of Chromatography A, 1164, 219-223. https://doi.org/10.1016/j.chroma.2007.07.035.

Venkiteshwaran, K., Kennedy, E., Graeber, C., Mallick, S.P., McNamara, P.J., Mayer, B.K., 2021a. Conversion of soluble recalcitrant phosphorus to recoverable orthophosphate form using UV/H_2O_2. Chemosphere 278, 130391. https://doi.org/10.1016/j.chemosphere.2021.130391

Venkiteshwaran, K., McNamara, P.J., Mayer, B.K., 2018a. Meta-analysis of non-reactive phosphorus in water, wastewater, and sludge, and strategies to convert it for enhanced phosphorus removal and recovery. Science of the Total Environment 644, 661-674. https://doi.org/10.1016/j.scitotenv.2018.06.369

Venkiteshwaran, K., Pokhrel, N., Hussein, F., Antony, E., Mayer, B.K., 2018b. Phosphate removal and recovery using immobilized phosphate binding proteins. Water Research X 1, 100003. https://doi.org/10.1016/j.wroa.2018.09.003

Venkiteshwaran, K., Wells, E., Mayer, B.K., 2020. Kinetics, affinity, thermodynamics, and selectivity of phosphate removal using immobilized phosphate-binding proteins. Environmental Science & Technology 54, 10885–10894. https://doi.org/10.1021/ACS.EST.0C02272

Venkiteshwaran, K., Wells, E., Mayer, B.K., 2021b. Immobilized phosphate-binding protein can effectively discriminate against arsenate during phosphate adsorption and recovery. Water Environment Research 93, 1173–1178. https://doi.org/10.1002/WER.1498

Wang, D., Mueses, M.A., Márquez, J.A.C., Machuca-Martínez, F., Grčić, I., Moreira, R.P.M., Puma, G.L., 2021. Engineering and modeling perspectives on photocatalytic reactors for water treatment. Water Research 117421. https://doi.org/10.1016/J.WATRES.2021.117421

Wang, S., Chew, J.W., Liu, Y., 2020. Development of an integrated aerobic granular sludge MBR and reverse osmosis process for municipal wastewater reclamation.

Science of the Total Environment 748, 141309. https://doi.org/10.1016/J.SCITOTENV.2020.141309

Wang, W., Deng, S., Li, D., Ren, L., Shan, D., Wang, B., Huang, J., Wang, Y., Yu, G., 2018a. Sorption behavior and mechanism of organophosphate flame retardants on activated carbons. Chemical Engineering Journal 332, 286–292. https://doi.org/10.1016/J.CEJ.2017.09.085

Wang, W., Deng, S., Li, D., Ren, L., Wang, B., Huang, J., Wang, Y., Yu, G., 2018b. Adsorptive removal of organophosphate flame retardants from water by non-ionic resins. Chemical Engineering Journal 354, 105–112. https://doi.org/10.1016/J.CEJ.2018.08.002

Wang, Z., Choudhary, A., Ledvina, P.S., Quiocho, F.A., 1994. Fine tuning the specificity of the periplasmic phosphate transport receptor. Site-directed mutagenesis, ligand binding, and crystallographic studies. Journal of Biological Chemistry 269, 25091–25094. https://doi.org/10.1016/S0021-9258(17)31503-X

Wang, Z., Luecke, H., Quiocho, F.A., 1996. Phosphate-binding protein (PBP) complexed with phosphate. http://dx.doi.org/10.2210/pdb1ixh/pdb

Wang, Z., Luecke, H., Yao, N., Quiocho, F.A., 1997. A low energy short hydrogen bond in very high resolution structures of protein receptor-phosphate complexes. Nature Structural Biology 1997 4, 519–522. https://doi.org/10.1038/nsb0797-519

Wanner B.L., 1993. Gene regulation by phosphate in enteric bacteria. Journal of Cellular Biochemistry 51, 47-54. https://doi.org/10.1002/jcb.240510110

Ward, A.J., Arola, K., Brewster, E.T., Mehta, C.M., Batstone, D.J., 2018. Nutrient recovery from wastewater through pilot scale electrodialysis. Water Research 135, 57–65. https://doi.org/10.1016/j.watres.2018.02.021

Westerhoff, P., Mash, H., 2002. Dissolved organic nitrogen in drinking water supplies: a review. Journal of Water Supply: Research and Technology-Aqua 51, 415–448. https://doi.org/10.2166/aqua.2002.0038

Xu, R., Lyu, T., Zhang, M., Cooper, M., Pan, G., 2020. Molecular-level investigations of effective biogenic phosphorus adsorption by a lanthanum/aluminum-hydroxide composite. Science of the Total Environment 725, 138424. https://doi.org/10.1016/j.scitotenv.2020.138424

Xu, Y., Ding, Y., Wang, J., Zhu, M., Yang, M., Qian, G., Sun, Y., 2020. In-situ synthesis of calcium aluminum layered double hydroxides for advanced treatment of leachate biochemical tail water. Science of the Total Environment 701, 134891. https://doi.org/10.1016/j.scitotenv.2019.134891

Yang, Y., Ballent, W., Mayer, B.K., 2016. High-affinity phosphate-binding protein (PBP) for phosphorous recovery: Proof of concept using recombinant Escherichia coli. FEMS Microbiology Letters 363, fnw240. https://doi.org/10.1093/femsle/fnw240

Yoshimura, T., Nishioka, J., Saito, H., Takeda, S., Tsuda, A., Wells, M.L., 2007. Distributions of particulate and dissolved organic and inorganic phosphorus in North Pacific surface waters. Marine Chemistry 103, 112–121. https://doi.org/10.1016/j.marchem.2006.06.011

Yu, D., 2012. Evaluation of effluent organic nitrogen and its impacts on receiving water bodies. Thesis, University of Massachusetts Amherst, Amherst, MA. https://doi.org/10.7275/5rvr-6a55

Zhang, M., Song, G., Gelardi, D.L., Huang, L., Khan, E., Mašek, O., Parikh, S.J., Ok, Y.S., 2020. Evaluating biochar and its modifications for the removal of ammonium, nitrate, and phosphate in water. Water Research 186, 116303. https://doi.org/10.1016/j.watres.2020.116303

Zheng, F., Wang, J., Xiao, R., Chai, W., Xing, D., Lu, H., 2021. Dissolved organic nitrogen in wastewater treatment processes: Transformation, biosynthesis and ecological impacts. Environmental Pollution 273, 116436. https://doi.org/10.1016/j.envpol.2021.116436

Zhu, J., Qu, B., Li, M., 2017. Phosphorus mobilization in the Yeyahu Wetland: Phosphatase enzyme activities and organic phosphorus fractions in the rhizosphere soils. International Biodeterioration & Biodegradation 124, 304–313. https://doi.org/10.1016/j.ibiod.2017.05.010

Ziegler, T., Tschinke, V., Versluis, L., Baerends, E.J., Ravenek, W., 1988. A theoretical study of metal-ligand bond strengths (M□L: L = OH, OCH$_3$, SH, NH$_2$, PH$_2$, CH$_3$, SiH$_3$, CN and H) in the early transition metal systems Cl$_3$ML (M = Ti, Zr and Hf) and late transition metal systems LCo(CO)$_4$. Polyhedron, 7, 1625-1637. https://doi.org/10.1016/s0277-5387(00)81788-x

Zuo, F., Sui, Q., Zheng, R., Ren, J., Wei, Y., 2020. In situ startup of a full-scale combined partial nitritation and anammox process treating swine digestate by regulation of nitrite and dissolved oxygen. Bioresource Technology 315, 123837. https://doi.org/10.1016/J.BIORTECH.2020.123837

**APPENDICES**

A. SUPPORTING INFORMATION FOR CHAPTER 2

A1. Meta-analysis of nitrogen (N) species in surface waters across the United States (US)

A meta-analysis was employed in this study to analyze the occurrence of dissolved organic nitrogen (DON) in groundwater, surface water, and wastewater effluent matrices. The data analysis is described in the main text; additional details about the dataset and results are provided here. Included in this data set were 106 groundwater samples from 75 sites, 11,803 surface water samples from 1,599 sites, and 163 wastewater effluent samples from 163 sites across the United States (US) for the year 2019 (which avoided disruption in sample collecting and reporting due to COVID-related protocols).

Spatial variability in the DON:TDN ratio was observed, as shown in Figure 2.1 in the main text. Further analysis of the variability in DON and TDN concentrations among the states is shown in Figure A.1and Figure A.2, respectively. Notably, even if the level of DON is high at a certain location, the ratio of DON to TDN may still be low if TDN is also high. The figures show wide variability in the quantity of data available at each location, where some states are far more represented in the data set than others, which inherently skews the analysis toward overrepresented locations (for example, Florida alone accounted for over 3,000 data points). The heat map in Figure A.3 shows the variability in reporting DON and TDN measurements across the US.
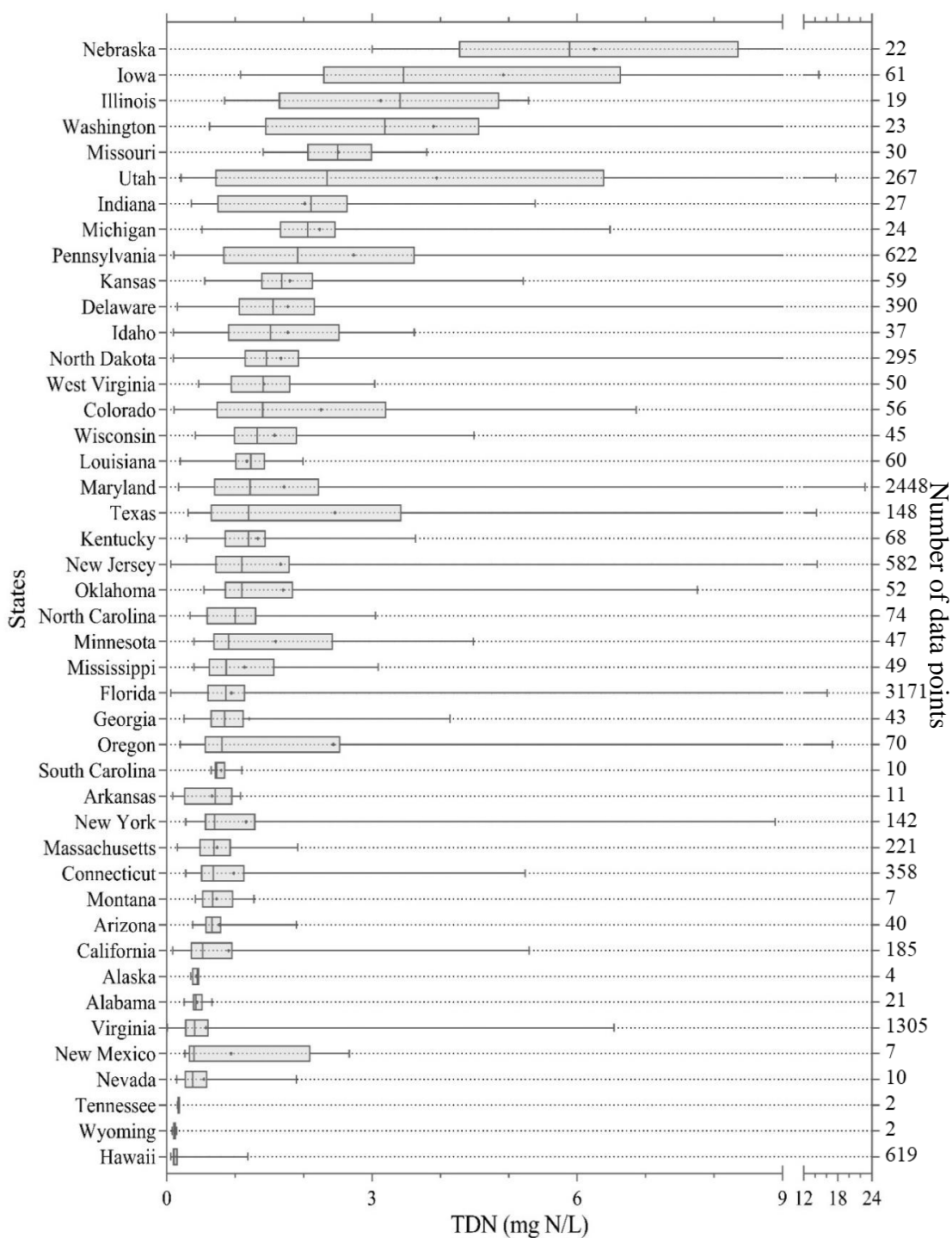
Figure A.1. Variability of total dissolved nitrogen (TDN) in surface water among 44 different states in the US in 2019. Surface water data for these analyses were downloaded from the Water Quality Portal. Data for six states – South Dakota, Ohio, Maine, New Hampshire, Vermont, Rhodes Island – was not available. The whiskers represent the minimum and maximum values in the data set, the boxes represent the 25th and 75th percentile values with a median line inside the box, and the mean is shown with a "•" sign. States are arranged from high to low median TDN.
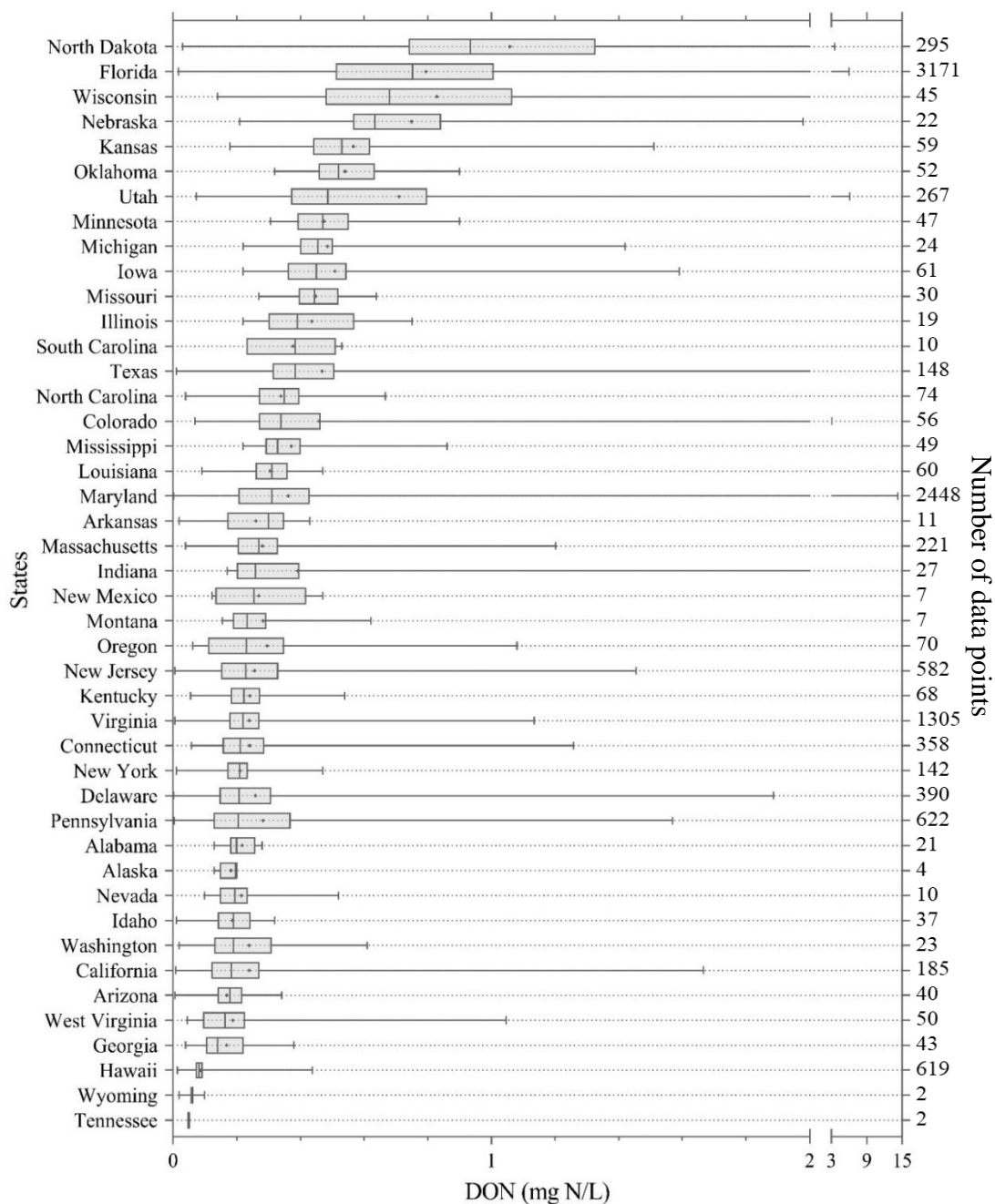
Figure A.2. Variability of dissolved organic nitrogen (DON) in surface water among 44 different states in the US in 2019. Surface water data for these analyses were downloaded from the Water Quality Portal. Data for six states – South Dakota, Ohio, Maine, New Hampshire, Vermont, Rhodes Island – was not available. The whiskers represent the minimum and maximum values in the data set, the boxes represent the 25th and 75th percentile values with a median line inside the box, and the mean is shown with a "•" sign. States are arranged from high to low median DON.
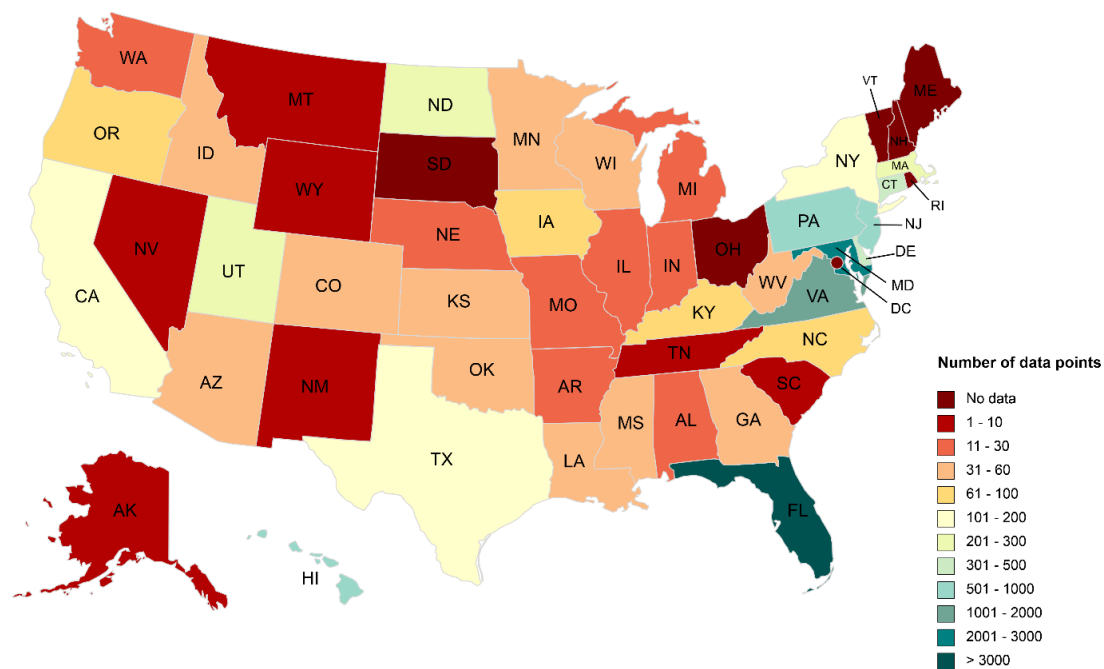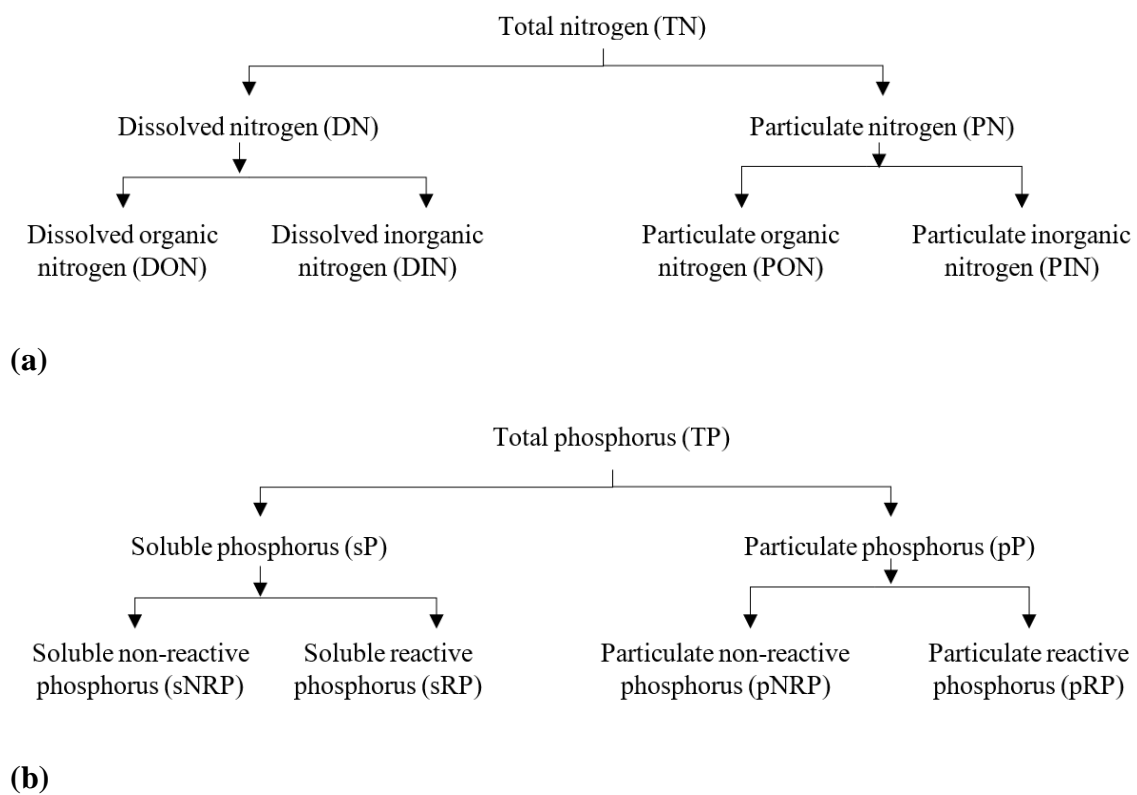
Figure A.3. Heat map showing number of data points per state (no data was available for Washington D.C.). The map was drawn using the online drawing tool provided by Mapchart.net.

B. SUPPORTING INFORMATION FOR CHAPTER 4

B1. Different fractions of N and P

Nitrogen (N) and phosphorus (P) fractionation is shown in Figure B.1.

Total nitrogen (TN)

Dissolved nitrogen (DN) Particulate nitrogen (PN)

Dissolved organic nitrogen (DON) Dissolved inorganic nitrogen (DIN) Particulate organic nitrogen (PON) Particulate inorganic nitrogen (PIN)

(a)

Total phosphorus (TP)

Soluble phosphorus (sP) Particulate phosphorus (pP)

Soluble non-reactive phosphorus (sNRP) Soluble reactive phosphorus (sRP) Particulate non-reactive phosphorus (pNRP) Particulate reactive phosphorus (pRP)

(b)

Figure B.1. Fractions of **(a)** total nitrogen and **(b)** total phosphorus in wastewater.

B2. Wastewater sample characteristics

Wastewater effluent characteristics of the sample collected from the South Shore

Water Reclamation Facility through one time sampling (Oak Creek, WI) are listed in

Table B.1. Wastewater effluent sample was collected on one single day and all

experiments were conducted within seven days of collection. All parameters listed in

Table B.1. were measured while DON and sNRP was calculated as follows: DON = TDN

– (NH_3-N + NO_3-N + NO_2-N); sNRP = soluble P (sP) – sRP.

Table B.1. Wastewater characteristics. All concentrations are reported as the means of n = 3 measurements ± 1 standard deviation.

Parameter	Concentration	Unit
Dissolved organic carbon (DOC)	11.5 ± 0.17	mg/L
Chemical oxygen demand (COD)	101 ± 6.43	mg/L
Alkalinity	160 ± 0.00	mg/L as $CaCO_3$
Chloride (Cl^-)	320 ± 0.00	mg/L
Sulfate (SO_4^{2-})	57.9 ± 0.11	mg/L
Total dissolved nitrogen (TDN)	17.9 ± 0.24	mg N/L
NH_3-N	1.17 ± 0.01	mg N/L
NO_3-N	12.8 ± 0.02	mg N/L
NO_2-N	0.00	mg N/L
Dissolved organic nitrogen (DON)	3.93 ± 0.26	mg N/L
Total phosphorus	0.46 ± 0.005	mg P/L
Soluble phosphorus (sP)	0.39 ± 0.0001	mg P/L
Soluble non-reactive phosphorus (sNRP)	0.11 ± 0.01	mg P/L
Soluble reactive phosphorus (sRP)	0.29 ± 0.002	mg P/L

B3. Electrolyte concentrations

Electrolytes were added to the synthetic test solutions with a target conductivity of 650 – 700 µS/cm. Concentrations of each electrolyte and the corresponding oxidizing species are listed in Table B.2.

Table B.2. Concentration of electrolyte and the corresponding oxidizing species in the test solutions.

Electrolyte	Corresponding oxidizing species	Concentration (mM)
Na_2SO_4	SO_4^{2-}	2.60
NaCl	Cl^-	10.27
$NaHCO_3$	HCO_3^-	4.76
$NaClO_4$	ClO_4^-	3.68

B4. Change in pH after EO-based DON and sNRP transformation

The change in solution pH was monitored in all experiments, as shown in Table B.3.

Table B.3. Final pH after EO-based DON and sNRP transformation. (Met = methionine, BSA = bovine serum albumin, HCT = hydrochlorothiazide, PA = phytic acid, BGP = beta-glycerol phosphate, HMP = hexa-meta phosphate, TrP = sodium triphosphate, TEP = triethyl phosphate).

Compound		Current density[a]	Mixing speed[a]	Experiment							
				Electrolyte[a]				pH[b]			
				Na_2SO_4	NaCl	$NaClO_4$	$NaHCO_3$	3	5	7	9
DON	Urea	6.6 - 8.8	6.8 - 7.9	9	7.2	7.4	7.4	3.1	8.1	9	9
	Met	6.6 - 7.1	6.5 - 7	7	6.7	7.4	7.2	3	7	7	8.6
	HCT	4.1 - 4.6	4.3 - 4.7	4.4	7	7.4	7.6	2.9	4.2	4.4	5
	BSA	8.1 - 8.9	7.5 - 8.8	9.6	9	7.4	7.3	3	9.6	9.6	9.7
sNRP	PA	6 - 6.1	6 - 6.2	6.2	8.3	8.2	9.3	4.7	6.1	6.2	6.1
	BGP	6 - 6.5	6.1 - 6.4	6.3	8.1	8.5	8.2	6.1	6.1	6.3	7.2
	HMP	6.4 - 6.6	6.3 - 6.6	6.7	8.3	8.1	8.5	6.3	6.6	6.7	7.3
	TrP	6.5 - 6.8	6.4 - 6.6	6.6	8.4	8.6	8.4	4.6	6.3	6.6	8.3
	TEP	5.5 - 6.1	5 - 5.5	6.4	8.2	8.1	8.6	6.2	6.7	6.4	7.3

[a] The initial pH for the current density, mixing speed, and electrolyte experiments was pH 7.
[b] Heading denotes initial pH of the solution.

**B5. Wastewater effluent DON and sNRP transformation**

Transformation of wastewater effluent DON and sNRP using EO was tested and compared to DON and sNRP transformation in synthetic water at the same test conditions (Table B.4).

Table B.4. Transformation of dissolved organic nitrogen (DON) and soluble non-reactive phosphorus (sNRP) species in secondary wastewater effluent versus synthetic water matrices under the same operating conditions (current density = 7.41 mA/cm^2, mixing speed = 50 rpm, wastewater pH = 7.07, and synthetic water pH = 7).

Nutrient	Water matrices	Initial concentration (mg L^{-1})	Transformation (%)
DON	Secondary effluent un-spiked	3.93 ± 0.26	8.33 ± 1.10
	Urea in synthetic water	2.0	11.7 ± 0.09
sNRP	Secondary effluent un-spiked	0.11 ± 0.01	32.7 ± 3.3
	Secondary effluent spiked with BGP	1.0	10.8 ± 0.1
	BGP in synthetic water	1.0	30.1 ± 3.0

B6. Temperature change over time at varying current density

The change in temperature of the bulk solution was monitored at varying current density (Figure B.2). The lowest applied current density (0.74 mA/cm^2) was selected for kinetic studies as the least temperature change was observed at this applied current.
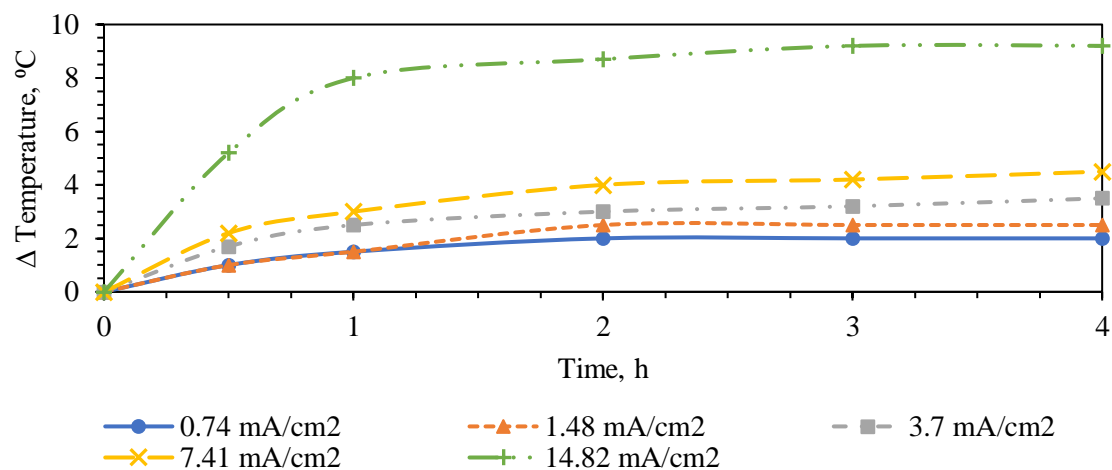
Figure B.2. Change in temperature over time at varying current density. The y-axis shows the change in temperature relative to the initial temperature (ΔT). All points are single experimental results.

B7. Kinetic parameters for DON and sNRP transformation

The transformation of DON and sNRP using EO followed zero order kinetics, as shown in Figure 4.6 in the main text. The kinetic parameters are shown in Table B.5.

Table B.5. Zero order transformation kinetic parameters for dissolved organic nitrogen (DON) and soluble non-reactive phosphorus (sNRP) transformation using electrooxidation to treat synthetic water matrices.

Nutrient	Compound	Rate constant ($mg\ L^{-1}\ h^{-1}$)	Half-life, $t_{1/2}$ (hr)	R^2
DON	Urea	0.0406	24.6	0.96
	Met (methionine)	0.0100	100	0.94
	BSA (bovine serum albumin)	0.0020	500	0.79
	HCT (hydrochlorothiazide)	0.0137	73.0	0.90
sNRP	BGP (beta-glycerol	0.0893	5.6	0.99
	PA (phytic acid)	0.0956	5.2	0.99
	TEP (triethyl phosphate)	0.0771	6.5	0.99
	HMP (sodium	0.0085	58.8	0.05
	TrP (sodium triphosphate)	0.0088	56.8	0.19

B8. Energy consumption for EO-based DON and sNRP transformation

Energy consumption as electric energy per mass (E_{EM}) for DON and sNRP

transformation using EO and UV/H_2O_2 is reported in Table B.6. Comparing the E_{EM}

values between the two processes, EO was generally more energy efficient for DON and

sNRP transformation.

Table B.6. Comparison of electrooxidation (EO) and UV/H_2O_2 energy consumption (E_{EM}) for dissolved organic nitrogen (DON) transformation to dissolved inorganic nitrogen (DIN) and soluble non-reactive phosphorus (sNRP) transformation to soluble reactive phosphorus (sRP) in synthetic water matrices.

| Nutrient	Compound	$E_{EM,EO}$ (kWh/kg)	$E_{EM,UV/H_2O_2}$ (kWh/kg)	$E_{EM,UV/H_2O_2}$ /$E_{EM,EO}$
DON	Urea	7.7×10^6	N/A[a]	N/A[a]
	Met (methionine)	3.1×10^7	N/A[a]	N/A[a]
	BSA (bovine serum albumin)	1.2×10^8	N/A[a]	N/A[a]
	HCT (hydrochlorothiazide)	2.1×10^7	N/A[a]	N/A[a]
sNRP	BGP (beta-glycerol phosphate)	5.1×10^6	4.2×10^6 [b]	0.8
	PA (phytic acid)	8.5×10^6	2.0×10^7 [b]	2.3
	TEP (triethyl phosphate)	1.7×10^7	N/A[a, b]	N/A[a]
	HMP (sodium hexametaphosphate)	3.3×10^7	6.3×10^7 [b]	1.4
	TrP (sodium triphosphate)	3.7×10^7	5.4×10^7 [b]	1.4
[a] Not applicable as UV/H_2O_2 did not effectively transform DON or TEP. [b] $E_{EM,UV/H_2O_2}$ values for sNRP were calculated from Venkiteshwaran et al. (2021a).				

C. SUPPORTING INFORMATION FOR CHAPTER 5

C1. Quenchers for sorbed and dissolved oxidant tests

To investigate the role of sorbed and dissolved oxidants in electrooxidation (EO)-based transformation of soluble non-reactive phosphorus (sNRP) to soluble reactive phosphorus (sRP), allyl alcohol (quenches sorbed oxidants) and tertiary butanol (quenches dissolved oxidants) were used in separate experiments. The results are shown in main text. Both quencher and sNRP compound structures are shown in Figure C.1.
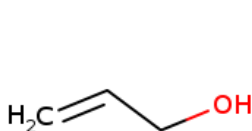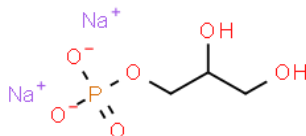

(a) Allyl alcohol
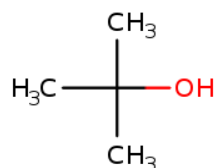
(b) Tertiary butanol
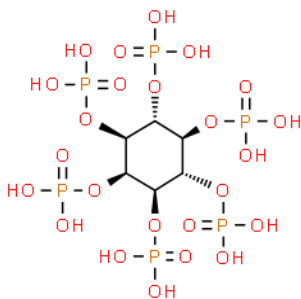
(c) Phytic acid

(d) Beta-glycerol phosphate

Figure C.1. Molecular structure of **(a)** allyl alcohol and **(b)** tertiary butanol (images from the National Institute of Health (NIH) National Medical Library database, https://www.nlm.nih.gov/). Molecular structure of **(c)** phytic acid and **(b)** beta-glycerol phosphate (images from Chemspider).

Transformation of sNRP compounds with or without quenchers followed zero order kinetics, as discussed in the main text. Table C.1 lists the rate constants corresponding to sNRP transformation using EO with or without using quenchers.

Table C.1. Zero order rate constants (mg/L-hr) for soluble non-reactive phosphorus (sNRP) compounds with or without quenchers
.

| Quenching condition	Soluble non-reactive compound	
	Phytic acid	Beta-glycerol phosphate
No quenching	0.0956 ± 0.0015	0.0893 ± 0.0039
Quenching with allyl alcohol	0.0424 ± 0.008	0.02 ± 0.0038
Quenching with tertiary butanol	0.0299 ± 0.0248	$0.303 \ .0021$

C2. Direct electron transfer tests for soluble non-reactive phosphorus transformation

Among the potential pathways for phosphorus (P) transformation during EO, i.e., direct electron transfer (DET) and oxidation utilizing in-situ generated oxidants, DET was reported as the likely dominant mechanism for sNRP transformation to sRP (Mallick et al., 2021 [Chapter 4]). To directly confirm DET of sNRP compounds, chronoamperometry tests were conducted here, where an increase in current after spiking the test solution with the sNRP compound would indicate DET of the compound. In EO, oxidants generated in-situ ($S_2O_8^{2-}$, $C_2O_6^{2-}$, Cl_2, ClO_4^-, $SO_4\bullet^-$, $Cl\bullet$, $CO_3\bullet^-$ etc.) from the electrolytes can compete with the target sNRP compound for DET on the anode. Depending on the oxidation state of the oxidants, the degree of competition might vary. Therefore, DET of sNRP compounds might or might not be affected by the presence of different electrolytes. Accordingly, three electrolytes were tested in separate DET probe experiments to confirm DET of the sNRP compound beta-glycerol phosphate (BGP). The three electrolytes were sodium sulfate (Na_2SO_4), sodium bicarbonate ($NaHCO_3$), and sodium chloride (NaCl). Concentrations of the electrolyte salts (Table C.2) were chosen to have the same degree of conductivity (650 µS/cm) in the test solution.

Table C.2. Concentration of electrolyte used in the direct electron transfer (DET) experiments. All electrolytes were tested at 650 µS/cm.

Electrolyte	Electrolyte concentration (mg/L)
Na_2SO_4	2.60
NaCl	10.27
$NaHCO_3$	4.76

In all three sets of experiments, an increase in current was observed when the test solution was spiked with BGP. The chronoamperometry experiments in Na_2SO_4 are shown in Figure 5.2 of main text, while the experiments in $NaHCO_3$ and NaCl are shown in Figure C.2.
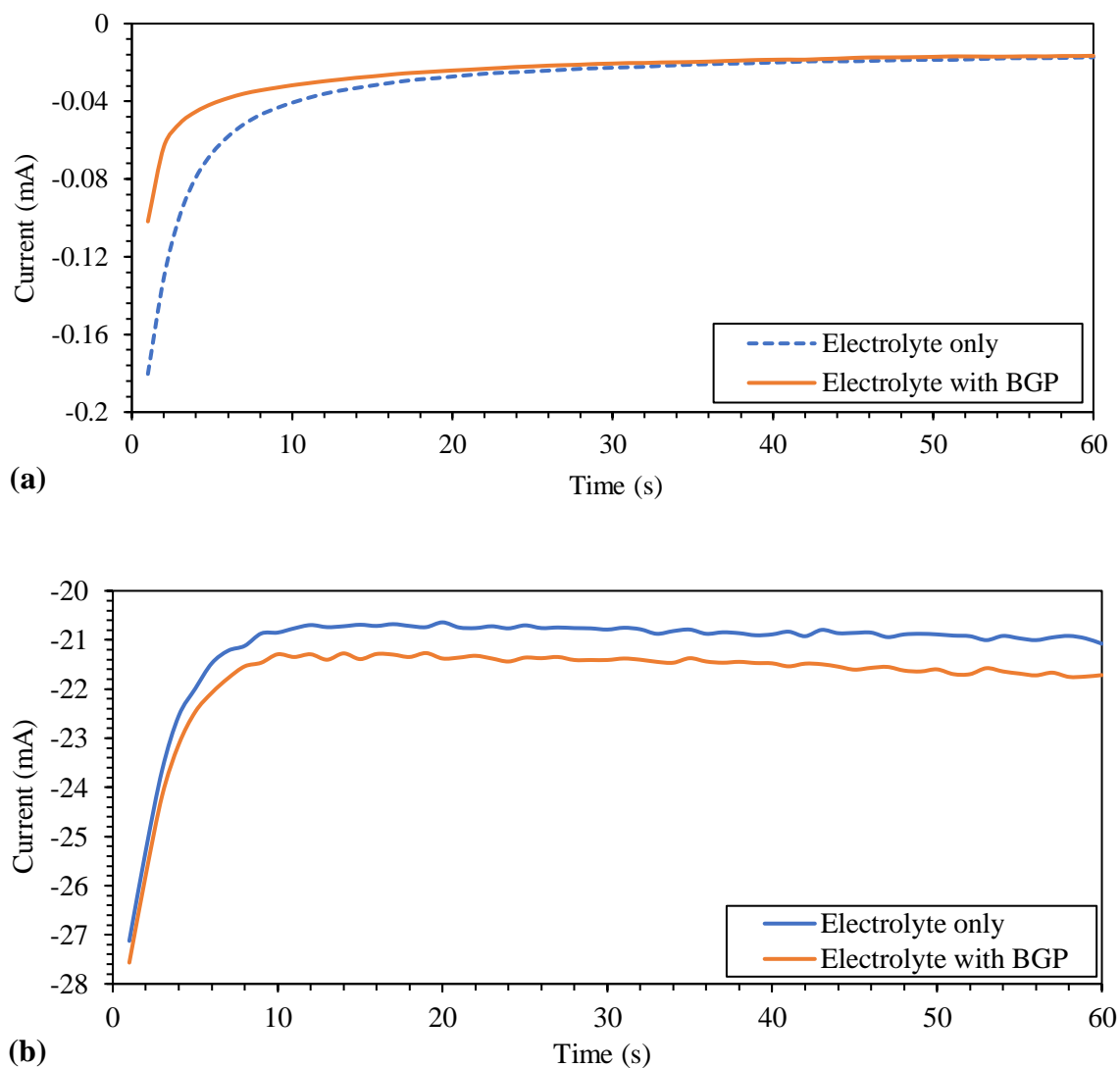
Figure C.2. Direct electron transfer tests using chronoamperometry in synthetic water matrices using **(a)** $NaHCO_3$ and **(b)** NaCl as the electrolyte. One set of experiments was conducted using only the test water matrix (containing no beta-glycerol phosphate [BGP]) and another set of experiments was conducted by spiking the water matrix with 1 mg P/L BGP. An increase in current indicates DET of BGP in the electrooxidation reactor.

C3. Centrate characterization

The wastewater centrate samples were characterized for solids, organics, alkalinity, and hardness (Table C.3).

Table C.3. Municipal wastewater centrate characteristics, shown as averages ± 1 standard deviation of triplicate analyses (single measurements for alkalinity and hardness)

Solids	
TS (mg/L)	1653 ± 95
VS (mg/L)	530 ± 72
TSS (mg/L)	182 ± 11
VSS (mg/L)	144 ± 7
TDS (mg/L)	1471 ± 96
Organics	
TCOD (mg/L)	783 ± 45
SCOD (mg/L)	548 ± 24
DOC (mg/L)	112 ± 3
TCOD/DOC	7.0 ± 0.4
SCOD/DOC	4.9 ± 0.3
Alkalinity	
Phenolphthalein alkalinity (mg/L as $CaCO_3$)	0
Total alkalinity (mg/L as $CaCO_3$)	2800
Hardness	
Total hardness (mg/L as $CaCO_3$)	380
Calcium hardness (mg/L as $CaCO_3$)	240

C4. Precipitate phosphorus analysis

After electrooxidation of the centrate, a white precipitate was observed on the cathode surface. The precipitate was analyzed using EDX and ICP-MS, results of which are discussed in main text. Figure C.3 shows magnification backscatter electron image of the precipitate while Figure C.4 shows results from EDX analysis.
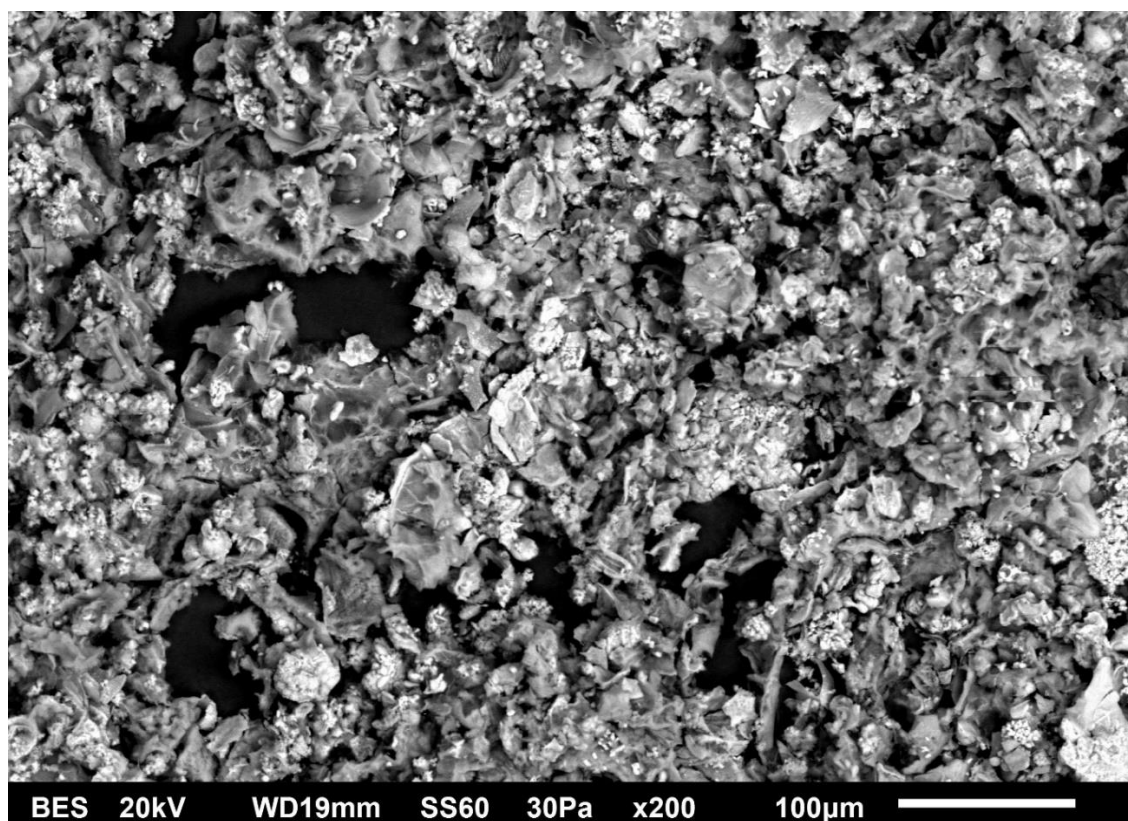
Figure C.3. High magnification backscatter electron image of the precipitates deposited on the cathode.
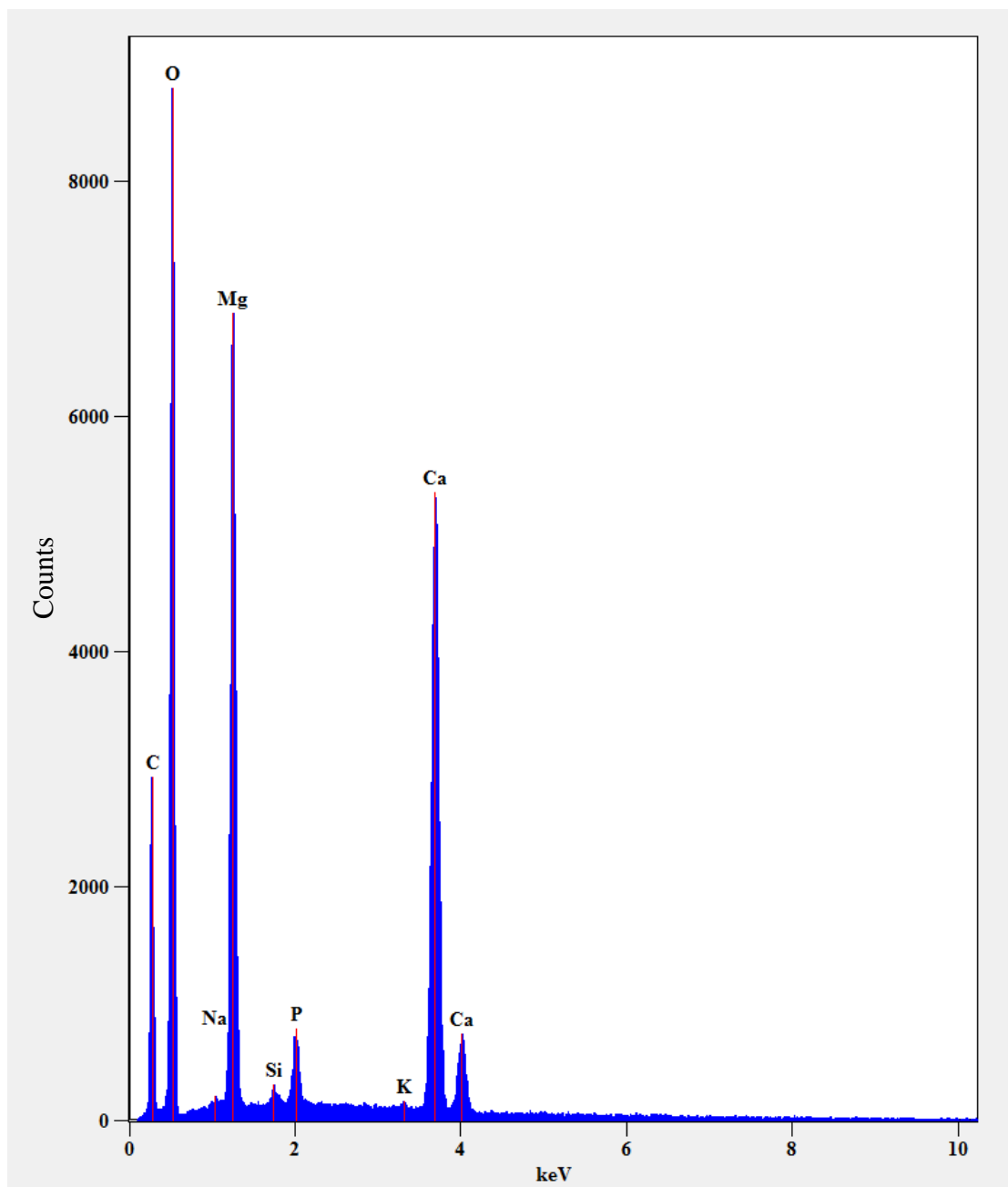
Figure C.4. Energy dispersive X-ray spectrum obtained from the precipitate shown in Figure C.3.

Chemical precipitation of phosphate was confirmed by analyzing the precipitate for reactive phosphorus (P). The summation of precipitated reactive P and bulk solution reactive P in the EO-treated centrate was statistically similar (Figure C.5, $p = 0.7730$) to

the bulk solution reactive P prior to EO treatment, indicating that the precipitate effectively closed the mass balance on the change in P partitioning as a result of EO treatment.
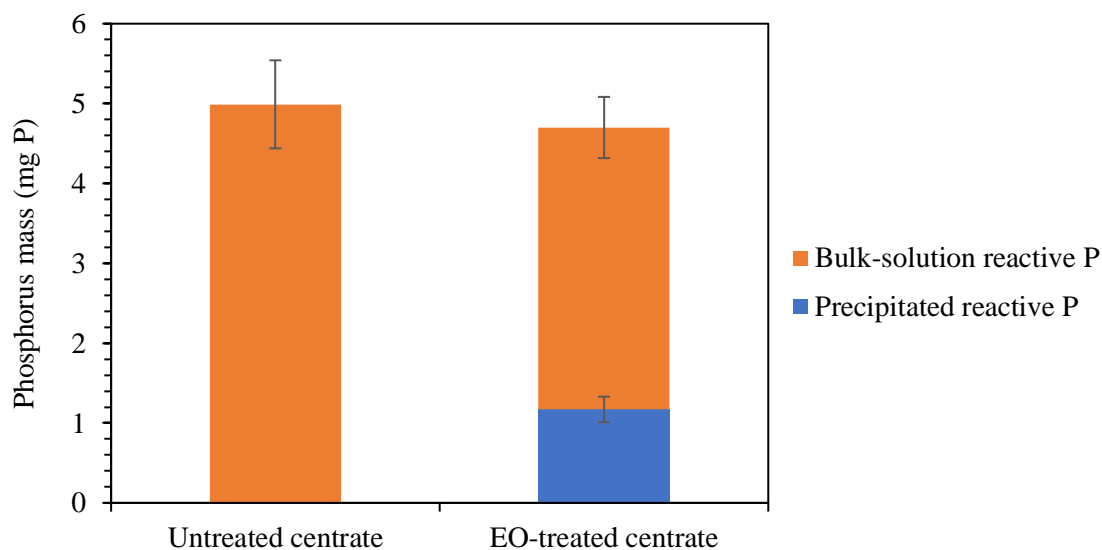
Figure C.5. Bulk-solution and precipitated reactive phosphorus (P) in untreated and electrooxidation (EO)-treated municipal wastewater centrate. Bars represent average of triplicate analyses while the error bars represent ±1 standard error.

## C5. Change in UV absorbance of organics after electrooxidation

Since phosphorus transformation was not achieved with EO, the process effectiveness was confirmed by testing for changes in organics (carbon mineralization and change in UV absorbance). Carbon mineralization is shown in main text while the UV-VIS spectroscopy scan is shown in Figure C.6. Changes in UV absorbance confirms that organics were being removed or transformed with increasing extent of EO treatment.
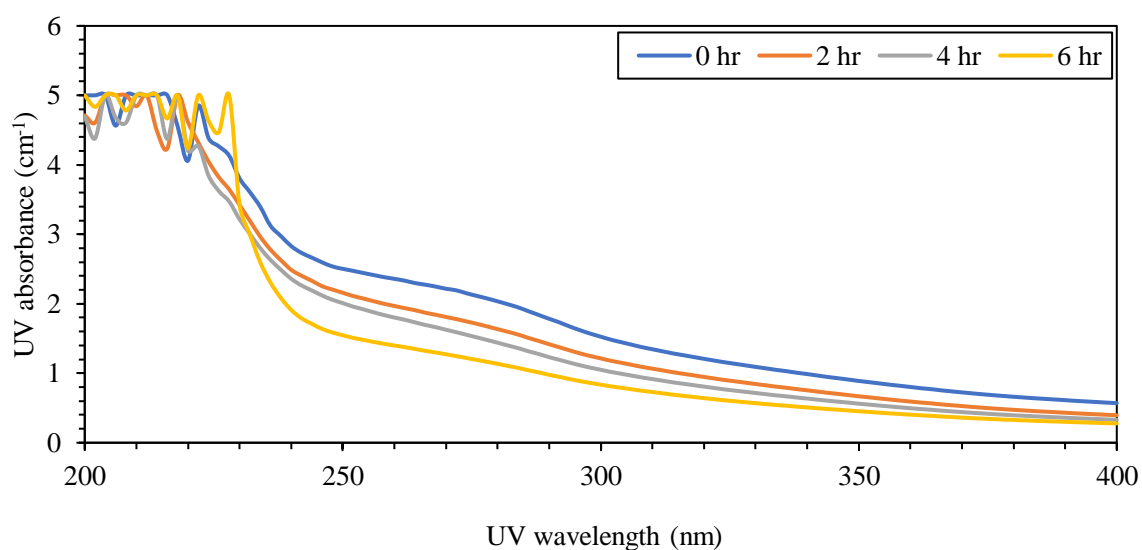
Figure C.6. UV-VIS absorbance scan before and after electrooxidation (EO) treatment for 0, 2, 4, or 6 hr. The treatment condition for EO treatment were 7.41 mA/cm^2 current density and 50 rpm mixing speed.

## C6. Linear kinetic models of centrate soluble non-reactive phosphorus removal using LayneRT^{TM}

Removal of centrate sNRP using EO followed by LayneRT^{TM} ion exchange was evaluated for pseudo-first order and pseudo-second order kinetic models. The linear models are shown in Figure C.7.
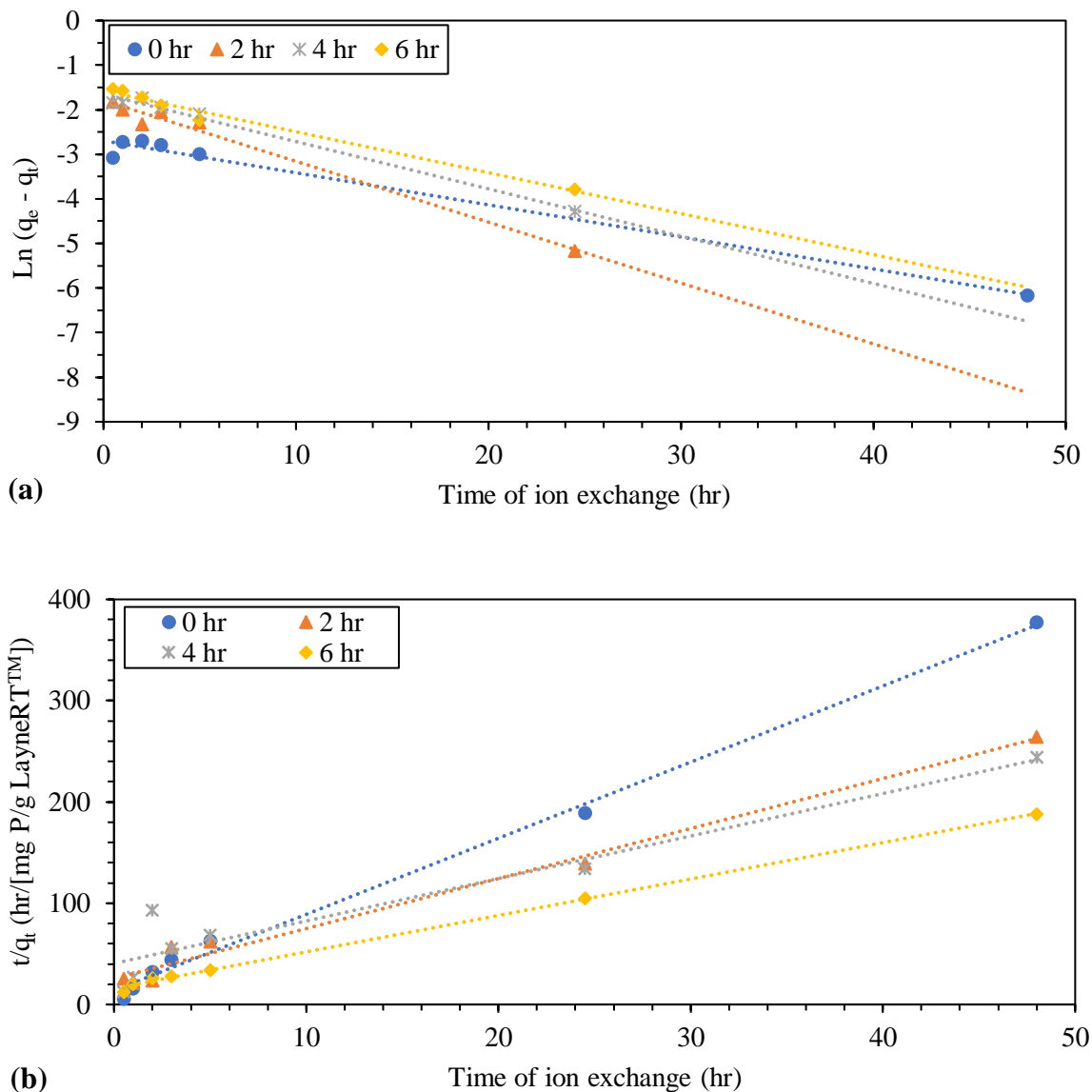
Figure C.7. Linear **(a)** pseudo-first order and **(b)** pseudo-second order isotherm models for centrate sNRP removal using LayneRT[TM] after electrooxidation (EO) treatment. EO treatment was operated at 7.41 mA/cm^2 current density and 50 rpm mixing speed. EO treatment was conducted for 2, 4, or 6 hr. The ion exchange kinetics were conducted in batch experiments at 20 rpm mixing speed dosing 10 mL of centrate with 250 mg LayneRT[TM].

C7. Linear isotherm models of centrate soluble non-reactive phosphorus removal using LayneRT^{TM}

Removal of centrate sNRP using EO followed by LayneRT^{TM} ion exchange was evaluated using Langmuir and Freundlich isotherm models. The Langmuir linear model provided a better fit ($R^2 \geq 0.85$) compared to Freundlich model, as shown in the linear models in Figure C.8. Therefore, the Freundlich model was not modeled using the nonlinear form. The nonlinear Langmuir isotherm model for sNRP removal using LayneRT^{TM} is shown in the main text.
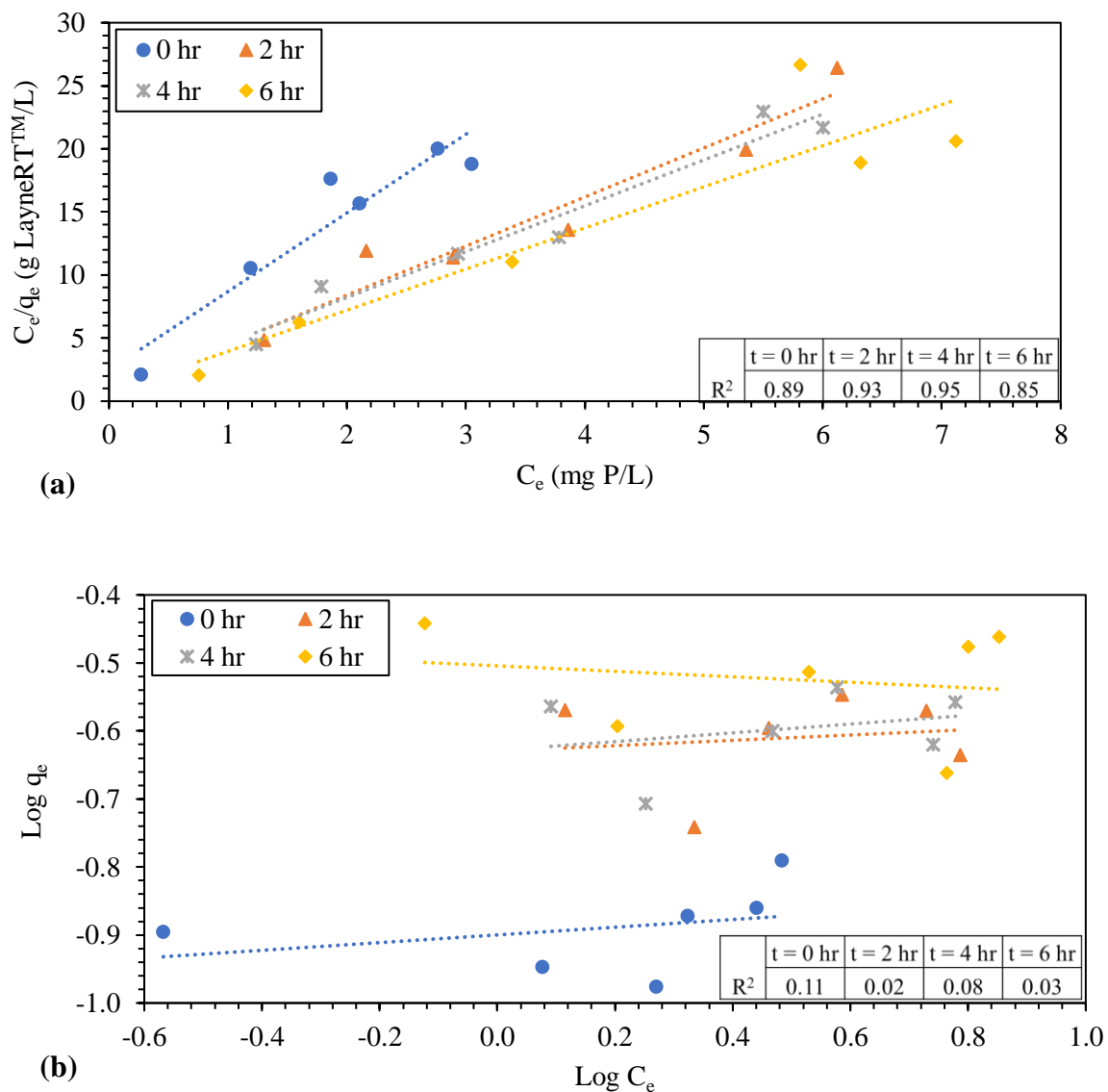
Figure C.8. Linear **(a)** Langmuir and **(b)** Freundlich isotherm models for centrate sNRP removal using LayneRT[TM] after electrooxidation (EO) treatment. EO treatment was operated at 7.41 mA/cm^{2} current density and 50 rpm mixing speed. EO treatment was conducted for 2, 4, or 6 hr. Isotherm experiments were conducted for 5 days, which was sufficient to achieve equilibrium.

D. SUPPORTING INFORMATION FOR CHAPTER 6

D1. Reaction kinetics for sNRP adsorption on PBP resin

The kinetic data were modeled using linear pseudo-first order (PFO) and pseudo-second order (PSO) reaction kinetics, as shown in Equations D.1 and D.2, respectively (Figure D.1).

$$ln(q_e - q_t) = ln\, q_e - K_{PFO}\, t \qquad\qquad \text{Equation D.1}$$

$$\frac{t}{q_t} = \frac{1}{K_{PSO}\, q_e^2} + \frac{1}{q_e} t \qquad\qquad \text{Equation D.2}$$

where, q_e = adsorption of sNRP at equilibrium (nmol P/ nmol PBP),

q_t = adsorption capacity of sNRP at time t in min (nmol P/ nmol PBP),

K_{PFO} = pseudo-first order rate constant (1/min), and

K_{PSO} = pseudo-second order rate constant (nmol PBP/ nmol P-min).

As the pseudo-second order (PSO) linear model offered a better fit, non-linear PFO modeling was not performed. The non-linear PSO model is shown in Figure 6.2a in the main text.
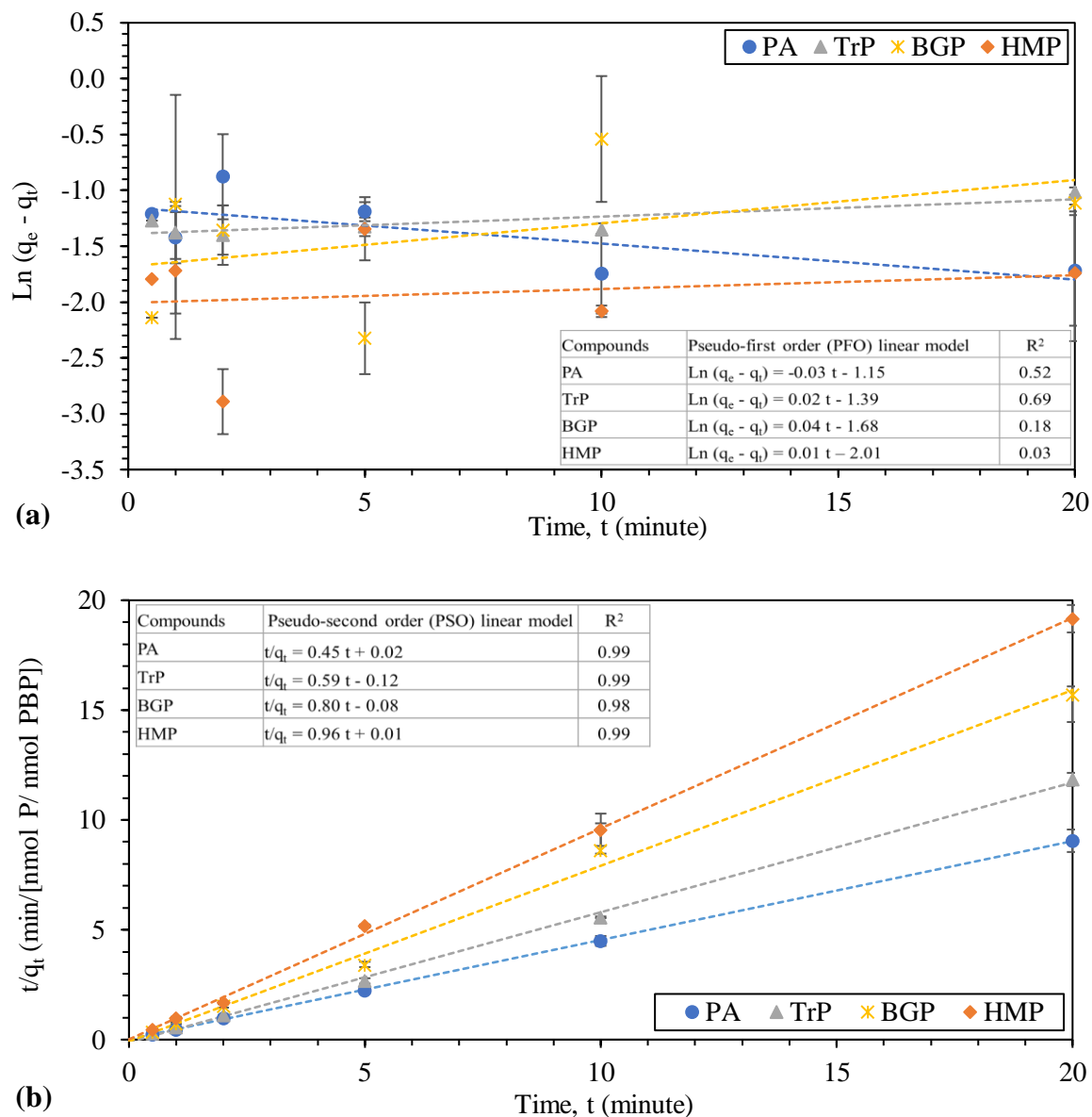
Figure D.1. Linear **(a)** pseudo-first order (PFO) kinetic model and **(b)** pseudo-second order (PSO) kinetic model for adsorption of soluble non-reactive phosphorus (sNRP), including phytic acid (PA), sodium triphosphate (TrP), beta-glycerol phosphate (BGP), and sodium hexametaphosphate (HMP), on phosphate-binding protein (PBP) resin. Tests were run at 25 ℃ for different time periods under neutral pH conditions. Error bars represent ±1 standard error for triplicate experiments.

D2. Isotherms for sNRP adsorption on PBP resin

Linear Langmuir (Equation D.3) and Freundlich (Equation D.4) isotherms were used to model the experimental data (Figure D.2).

$$\frac{C_e}{q_e} = \frac{1}{K_L \, q_{max}} + \frac{C_e}{q_{max}}$$
Equation D.3

$$log q_e = log K_F + \frac{1}{n} log C_e$$
Equation D.4

where, C_e = concentration of sNRP in equilibrium (µM P),

q_{max} = maximum sNRP adsorption capacity (nmol P/nmol PBP),

K_L = Langmuir constant (1/µM P),

K_F = Freundlich constant ([nmol P/nmol PBP]*[L/µmol P]$^{1/n}$), and

n = unitless empirical constant in the Freundlich isotherm model.

The linear Langmuir model provided a better fit; therefore, non-linear Freundlich isotherm modeling was not performed. The nonlinear Langmuir model is shown in Figure 5.7a in the main text.
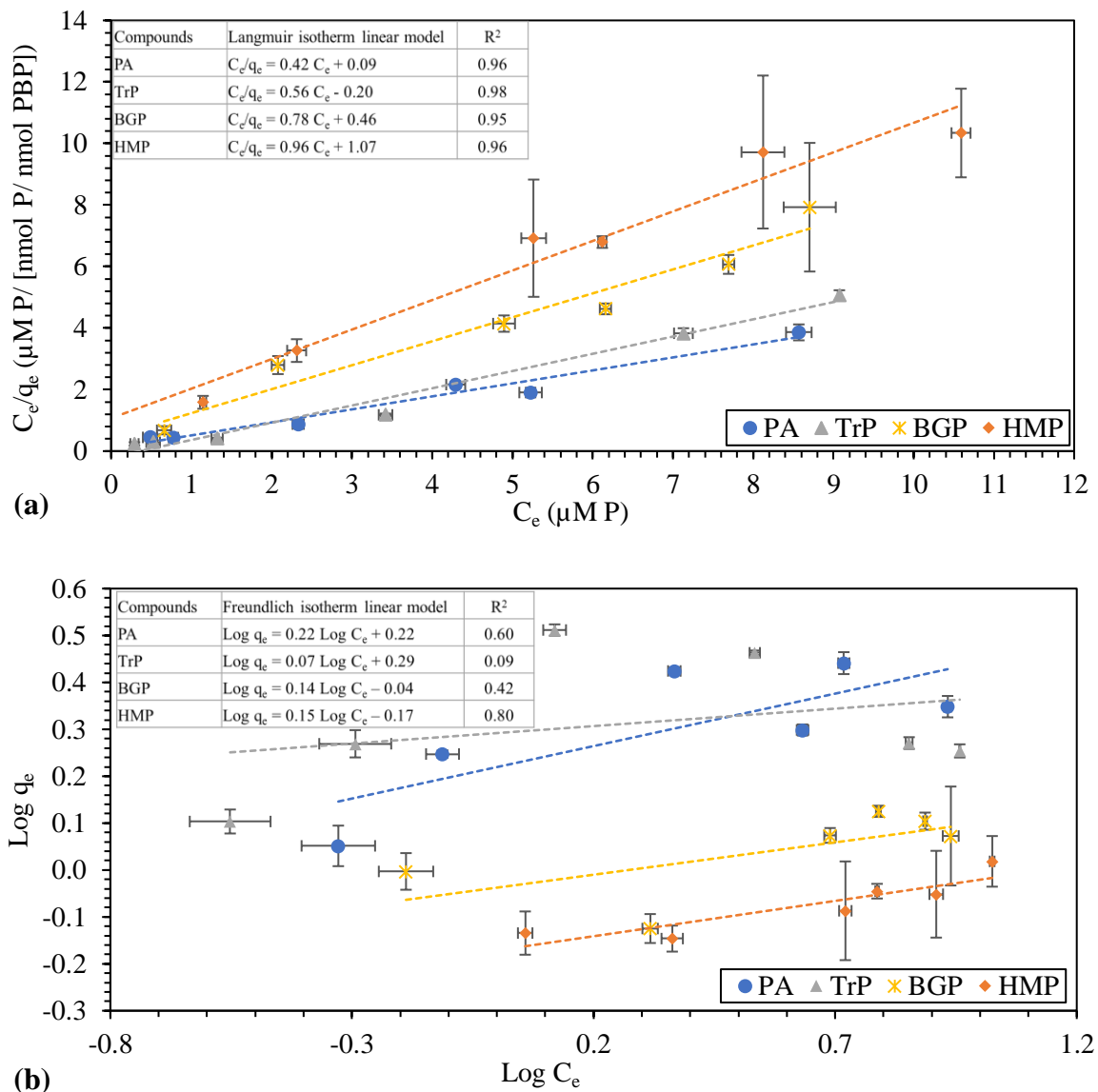
Figure D.2. Linear **(a)** Langmuir and **(b)** Freundlich isotherm models for adsorption of soluble non-reactive phosphorus (sNRP), including phytic acid (PA), sodium triphosphate (TrP), beta-glycerol phosphate (BGP), and sodium hexametaphosphate (HMP), on phosphate-binding protein (PBP) resin. Tests were run at 25 ℃ for 10 minutes under neutral pH conditions. Error bars represent ±1 standard error for triplicate experiments.